N80-13028

NASA Contractor Report 159139

Analysis and Correlation with Theory of Rotor Lift-Limit Test Data

Marc Sheffler

Boeing Vertol Company
Philadelphia, Pennsylvania 19142

Contract NAS 1-14317

November 1979

NASA
National Aeronautics and
Space Administration

Langley Research Center
Hampton, Virginia 23665
AC 804 827-3966

NASA CR 159139

NASA

Analysis and Correlation with Theory of Rotor Lift-Limit Test Data

Prepared by Marc Sheffler
Approved by Frank McHugh

November 1979

Prepared Under Contract No. NAS 1-14317
for
National Aeronautics and Space Administration
Langley Research Center
by

BOEING VERTOL COMPANY
A DIVISION OF THE BOEING COMPANY
PHILADELPHIA, PENNSYLVANIA 19142

D210-11525-1

TABLE OF CONTENTS

LIST OF FIGURES AND TABLES

LIST OF FIGURES AND TABLES

LIST OF FIGURES AND TABLES

LIST OF FIGURES AND TABLES

LIST OF FIGURES AND TABLES

NOMENCLATURE

SYMBOL		UNITS
A	Rotor Area (πR^2)	m^2 (ft^2)
c	Blade Chord	m (ft)
C_d	Section Drag Coefficient	
C_l	Section Lift Coefficient	
C_m	Section Pitching Moment Coefficient	
C_p/σ	Rotor Power Coefficient = $Q/\rho AV_{TIP}^2 R\sigma$	
C_T'/σ	Rotor Lift Coefficient = $L/\rho AV_{TIP}^2\sigma$	
D_e	Effective Drag	N(lb)
d	Rotor Diameter (2R)	m(ft)
EI_β	Flapwise Stiffness	Nm^2($lb\text{-}in^2$)
GJ	Torsional Rigidity	Nm^2($lb\text{-}in^2$)
H	Force in Disc Plane	N (lb)
i_S	Shaft Angle of Attack	rad(deg)
L	Lift Force	N(lb)
M	Mach Number	
$M_l(90)$	Advancing Blade Tip Mach Number	
Q	Rotor Torque	Nm(lb-ft)
q	Dynamic Pressure ($\frac{1}{2}\rho V^2$)	N/m^2(lb/ft^2)
t	Blade Thickness	m(ft)
V	Free Stream Velocity	m/Sec(ft/sec)
V_{TIP}	Rotor Tipspeed	m/Sec(ft/sec)
X	Rotor Propulsive Force	N (lb)
$\bar{x}$	Propulsive Force Coefficient = $X/qd^2\sigma$	

NOMENCLATURE

SYMBOL		UNITS
α	Two-Dimensional Lift Curve Slope	1/rad
β_{1c}	Once Per Rev Cosine Flap Angle	rad(deg)
Δ	Increment (ΔC_D = Additional Drag)	
θ_o	Collective Pitch at Blade Root	rad(deg)
θ_{1S}	Once Per Rev Longitudinal Cyclic Pitch Angle	rad(deg)
θ_t	Blade Twist from Root to 75% Radius	rad(deg)
ψ	Azimuth Position	rad(deg)
ρ	Atmospheric Density	Kg/m^3 ($lb\text{-}sec^2/ft^4$)
σ	Solidity ($bc/\pi R$)	
μ	Advance Ratio (V/V_{TIP})	

CENTER OF AXIS SYSTEMS: HUB CENTER OF GRAVITY
POSITIVE DIRECTIONS SHOWN

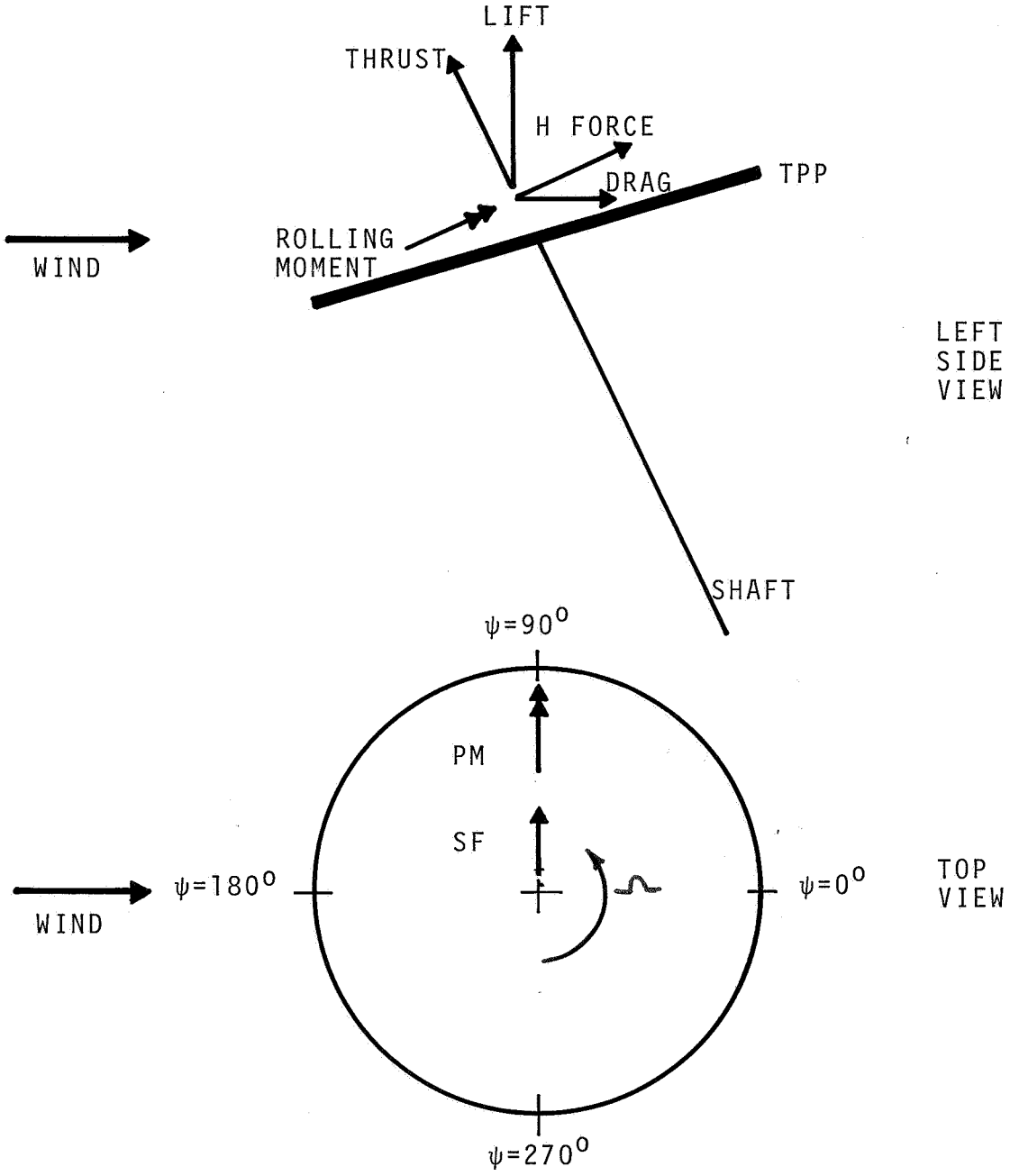

SIGN CONVENTION FOR FORCES AND MOMENTS

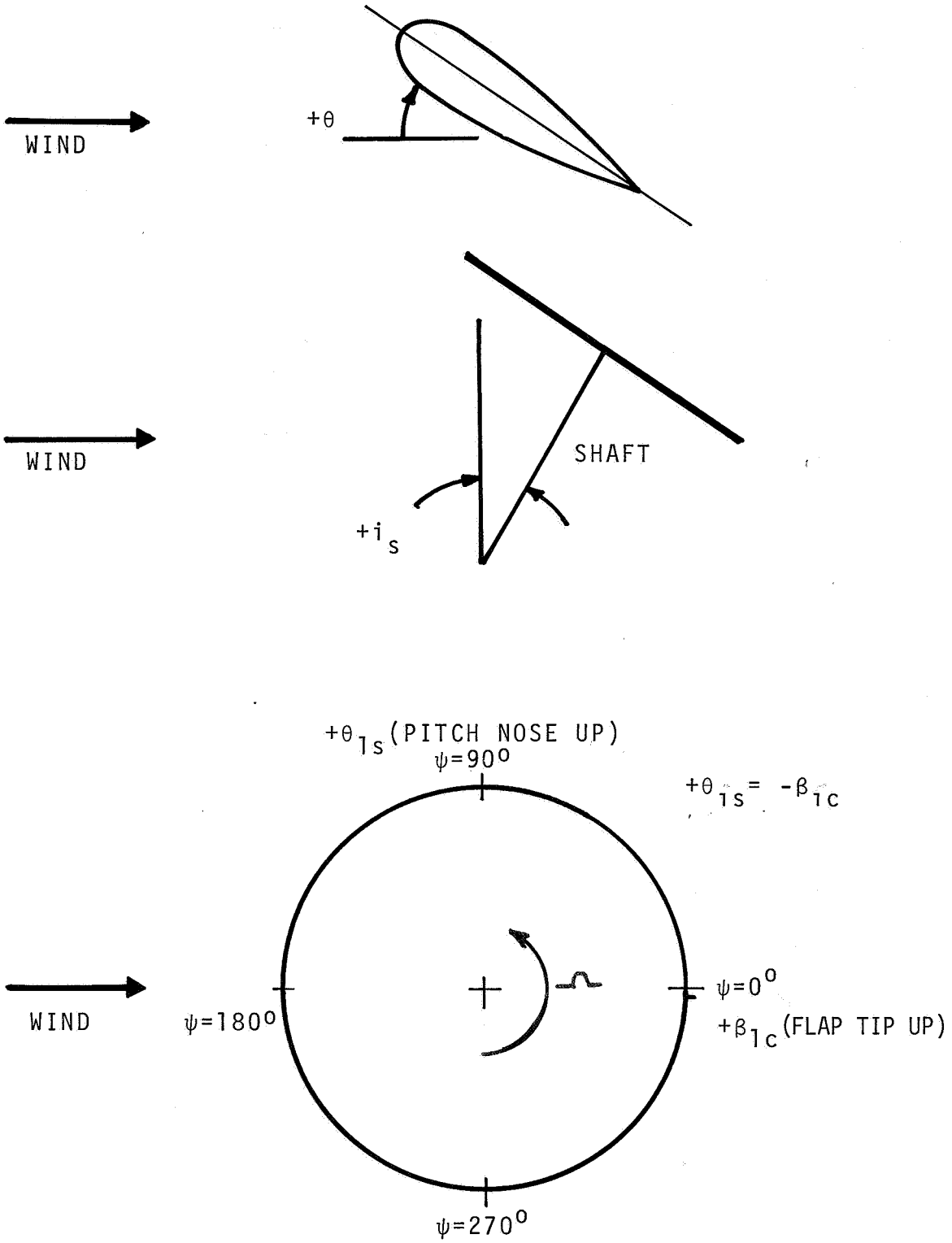

SIGN CONVENTION FOR ANGLES

SUMMARY

In 1977 a wind tunnel test program was conducted to define the cruise performance and determine any limitations to lift and propulsive force of a conventional helicopter rotor. This test was performed on a 2.96 foot radius model rotor in the Boeing Vertol Wind Tunnel. The objectives of this program were as follows:

1. Determine the maximum lift and propulsive force obtainable from an articulated rotor for advance ratios of 0.4 to 0.67.
2. Establish the blade load growth as the lift approaches the limit.
3. Obtain cruise rotor performance for advance ratios of 0.4 to 0.67.
4. Determine the sensitivity of the rotor forces and moments to rotor control inputs as the lift limit is approached.
5. Define the effect of advancing tip Mach number on these limits.
6. Determine the blade flapping response to a step input in cyclic as the lift limit is approached.

A summary of the conditions tested is presented in Table 1.1.

The C-60 Aeroelastic Rotor Analysis Program was used to correlate predictions with the measured performance data from the test described above. At low speeds, $\mu = 0.3$, (Figure 1) the correlation is excellent with the analysis matching the test results at all

thrust levels. At the higher advance ratios, $\mu = 0.53$, (Figure 2) the analysis follows the same trend of lift coefficient versus power coefficient as the test data, but the magnitude of power coefficient required is less for analysis than test for a fixed level of lift coefficient. In general, the lift limit predicted by C-60 is higher than obtained in test. The theoretical trend of limit lift coefficient versus advance ratio, as shown in Figure 3, follows the trend established by test, verifying the capability of the analysis as an effective tool for understanding rotor limits.

The capability of the analysis to predict loads was also investigated. The flap bending waveform correlation is good. At both low speeds (Figure 4) and high speeds (Figure 5), the phase and magnitude of the analytical waveforms compare favorably with the test waveforms. The largest difference is at high speed near the lift coefficient limit where the analysis and test do not agree in the region of $\psi = 0^{o}$. The midspan torsion bending waveform correlation is summarized for low speed in Figure 6 and for high speed in Figure 7. The theory and test agree over much of the azimuth at low lift coefficients and the correlation is fair at the higher lift coefficients throughout the speed range. The analysis in general shows a tendency to stall at a lower coefficient but the test shows a greater degree of stall at the highest rotor lift coefficient levels near the lift limit. The peak-to-peak correlation is very good in most instances and the phases are usually predicted

within 30^{o}. The test does indicate conventional stall occurring at 225^{o} rotor azimuth which is not reflected in the theory at the low advance ratio. At high rotor lift coefficients the rotor is stalling fore and aft as demonstrated by the rapid decrease in root torsion loads at 30^{o} and 180^{o} rotor azimuth, seen in the test data. This agrees with the result that the test shows a lower lift limit than the analysis. Overall the correlation is sufficiently accurate to make the rotor limits investigation meaningful.

The explanation for the rotor behavior at high thrust levels was found to be related to the aerodynamic loads acting on the elastically deflected blade. The azimuthal variation of thrust per blade is presented in Figure 8. The thrust is developed fore and aft in the disc plane. The stalled region at $\psi = 30^{o}$ for the blade with stallable, fully compressible aerodynamics is symptomatic of the thrust waveforms at high speed near the lift limit. This does not occur when linear aerodynamics are used in the analysis, because the blade does not stall on the retreating side, allowing the rotor to carry more lift laterally, thereby reducing the lift requirement fore and aft. It was shown that the nonlinear aerodynamic loads act on the tip of the blade, which is elastically deflected tip down due to a combination of thrust and centrifugal moment, plus the large nosedown aerodynamic moment, to cause a nosedown twist on the advancing blades at $\psi = 45^{o}$ as the lift approaches the stall limit. The blade becomes unstalled and the lift can increase again. As the blade approaches

$\psi = 90^{o}$, the longitudinal cyclic in conjunction with the increasing inplane velocity reduces the section angle of attack to the point where it is negative resulting in the large negative lift.

The flap bending waveforms reflect a downward deflection at the higher thrusts. The blade pitch motion just described can be seen clearly in the midspan torsion waveforms. The blade begins to stall near $\psi = 45^{o}$, recovers from stall, then shows a large increase in nosedown moment around $\psi = 180^{o}$.

To verify the contribution of blade elastic response during and after stall a comparison of thrust per blade was made for a rigid and elastic blade, shown in Figure 9. It indicates that at 30^{o} and 150^{o} rotor azimuth the lift of the rigid blade is higher as a result of the blade not being able to twist more nosedown when subjected to the large nosedown aerodynamic moment. For the elastic blade, flapwise deflection and drag combine to twist the blade further nosedown when subjected to the large nosedown aerodynamic moment.

A comparison of the rapid preliminary design rotor performance analysis with test data is presented in Figure 10 in terms of maximum rotor lift to effective drag ratio. The comparison shows the prediction to be slightly low (a maximum of 8%) at advance ratios below 0.4 and slightly high (a maximum of 15%) at advance ratios between 0.4 and approximately .58. This provides an adequate tool for preliminary design studies with numerous rotor configurations from pure helicopter to compounds.

The contract research effort which led to the results in this report was financially supported by the Structures Laboratory, USARTL (AVRADCOM).

TABLE 1 RUN LOG

TYPE OF TESTING	RUN NO.	ROTOR TIP SPEED V_T	ADVANCE RATIO μ	ROTOR LIFT COEFF. C_T/σ	ROTOR PROPULSIVE FORCE COEFF $X/qd^2\sigma$	TUNNEL SPEED V	COMMENTS
BASELINE ROTOR CHARACTERISTICS	21	Range	0	.06	0	0	Blade Frequency Check
LIFT LIMIT AND CONTROL POWER TESTING	22 23 24	620 FPS	0	Range	- - -	0 0 0	Hover Performance and Lift Limits
	25 27 28 29 30	620 FPS	.10 .20 .20 .30 .40	Range	.05	62 FPS 124 FPS 124 FPS 186 FPS 248 FPS	Cruise Performance and Lift Limits at Baseline Rotor Tip Speed, Control Power Testing at 90% and 70% C_T/σ Max
	32 33 34	620 FPS	.40	Range	.01 .10 .20	248 FPS	
	35 36 37 38	620 FPS	.45	Range	.01 .05 .10 .20	279 FPS	
	39 40 41 42	620 FPS	.50	Range	.05 .025 .10 .20	310 FPS	
	50 51 52 53	620 FPS	.53	Range	.05 .025 .10 .20	329 FPS	
	54	620 FPS	.57	Range	.05	353 FPS	Control System Problem Destroyed the Blades
	55	Range	.30	.06	.05	For μ	Blade Frequency Check
	56 57	620 FPS	.57	Range	.05 .025	353 FPS	New set of blades torsional stiffness approx. 50% of standard blades and twist approx. 10.4°(an increase of 35%) burned out swashplate bearing.

END OF PART 1

TABLE 1 RUN LOG (continued)

TYPE OF TESTING	RUN NO.	ROTOR TIP SPEED V_T	ADVANCE RATIO μ	ROTOR LIFT COEFF. C_T/σ	ROTOR PROPULSIVE FORCE COEFF $X/qd^2\sigma$	TUNNEL SPEED V	COMMENTS
BASELINE ROTOR CHARACTERISTICS	219	Range			0	For μ	Blade Frequency Check
CHECK AND VERIFICATION RUNS	221 222 224 225 226 227	620 FPS	.53 .50 .50 .45	Range	.05 .05 .05 .05 .05 .05	328 310 FPS 310 FPS 279 FPS	These runs were made to verify that the rotor performance or Part 1 and Part 2 were consistent and did not include any model fouling
LIFT LIMIT TESTING	228 245 246 249	620 FPS	.57	Range	.05 .025 .025 .10	353 FPS	Cruise performance and lift limits at baseline rotor tip speed
	229 248	620 FPS	.61	Range	.05 .075	378 FPS	
	250 251 252 253	570 FPS	.40 .45 .50 .53	Range	.05	228 FPS 256 FPS 285 FPS 302 FPS	Cruise performance and lift limits at reduced rotor tip speed to define effect of advancting tip Mach number.
	256 255 254 257 258 259 260	570 FPS	.40 .45 .50 .53 .57 .61 .64	Range	.05	228 FPS 256 FPS 285 FPS 302 FPS 325 FPS 348 FPS 368 FPS	
PROPULSIVE FORCE LIMIT TESTING	230 231	620 FPS	.40	.06 .09	Range	248 FPS	Cruise performance and propulsive force limits at baseline tip speed
	243 244	620 FPS	.45	.06 .076	Range	279 FPS	
	232 233 234 235	620 FPS	.50	.06 .06 .08 .08	Range	311 FPS	

TABLE 1 RUN LOG (continued)

TYPE OF TESTING	RUN NO.	ROTOR TIP SPEED V_T	ADVANCE RATIO μ	ROTOR LIFT COEFF. C_T'/σ	ROTOR PROPULSIVE FORCE COEFF $X/qd^2\sigma$	TUNNEL SPEED V	COMMENTS
PROPULSIVE FORCE LIMIT TESTING	269 270 271 272	620 FPS	.50	.05	Range	311 FPS	Cruise performance and propulsive force limits at baseline tip speed
	268 240 266 241 242 267	620 FPS	.53	.05 .06 .08 .09 .09 .10	Range	328 FPS	
	264 265	620 FPS	.53	.05 .07	Range	328 FPS	
	236 237	620 FPS	.57	.06 .076	Range	353 FPS	
	239 238	620 FPS	.61	.04 .055	Range	378 FPS	
	276 277	665 FPS	.53	.06 .08	Range	352 FPS	Cruise performance and propulsive force limits at increased tip speed
PERFORMANCE SUMMARY	273 274	620 FPS	Range	.08	.05	For μ	Testing to represent a speed sweep for a specific configuration

END OF PART 2

1/10 SCALE CH-47B ROTOR
ROTOR TIP SPEED = 620 FT/SEC

$X/qd^2\sigma = 0.05$

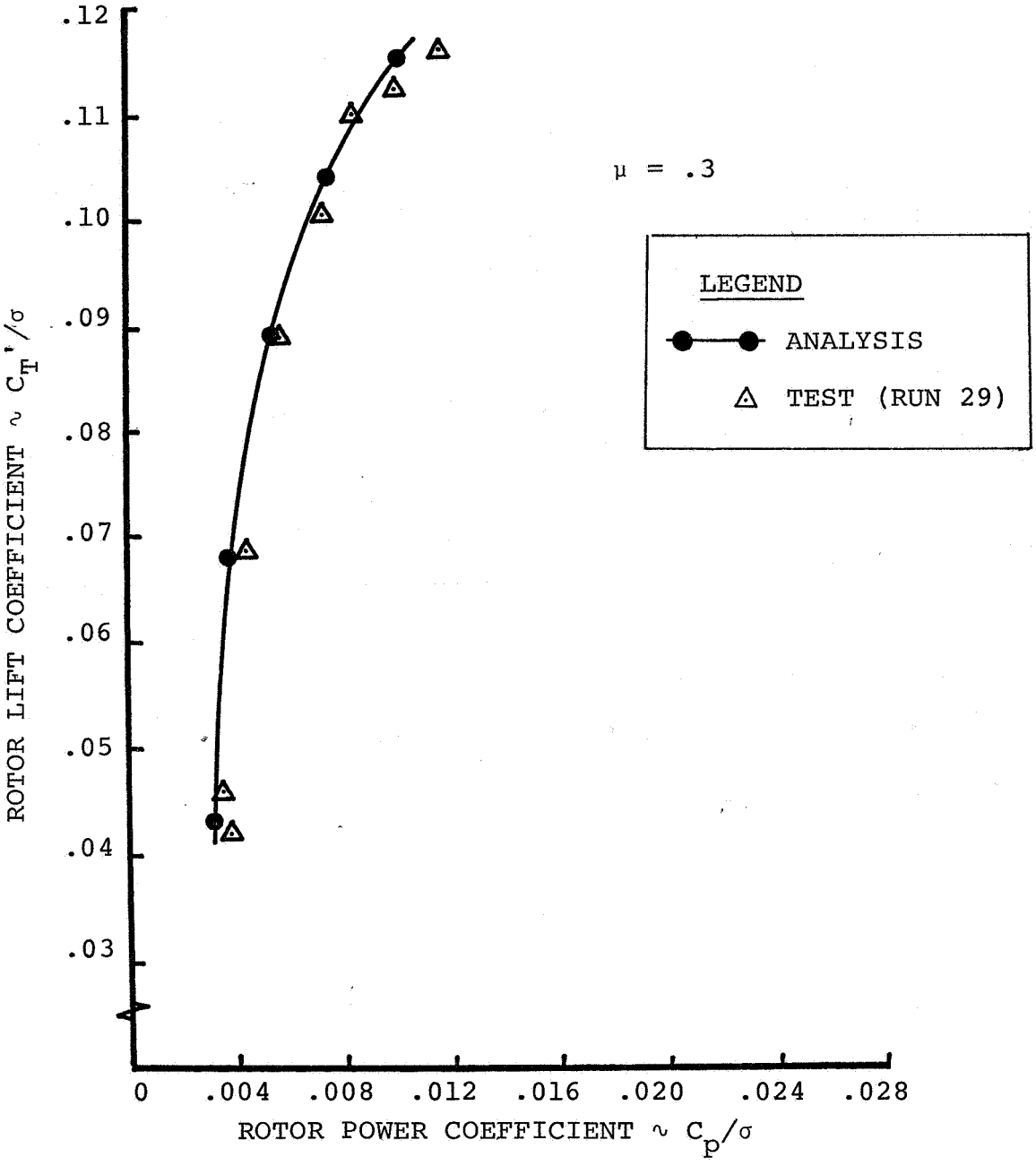

Figure 1 LOW SPEED PERFORMANCE CORRELATION SUMMARY

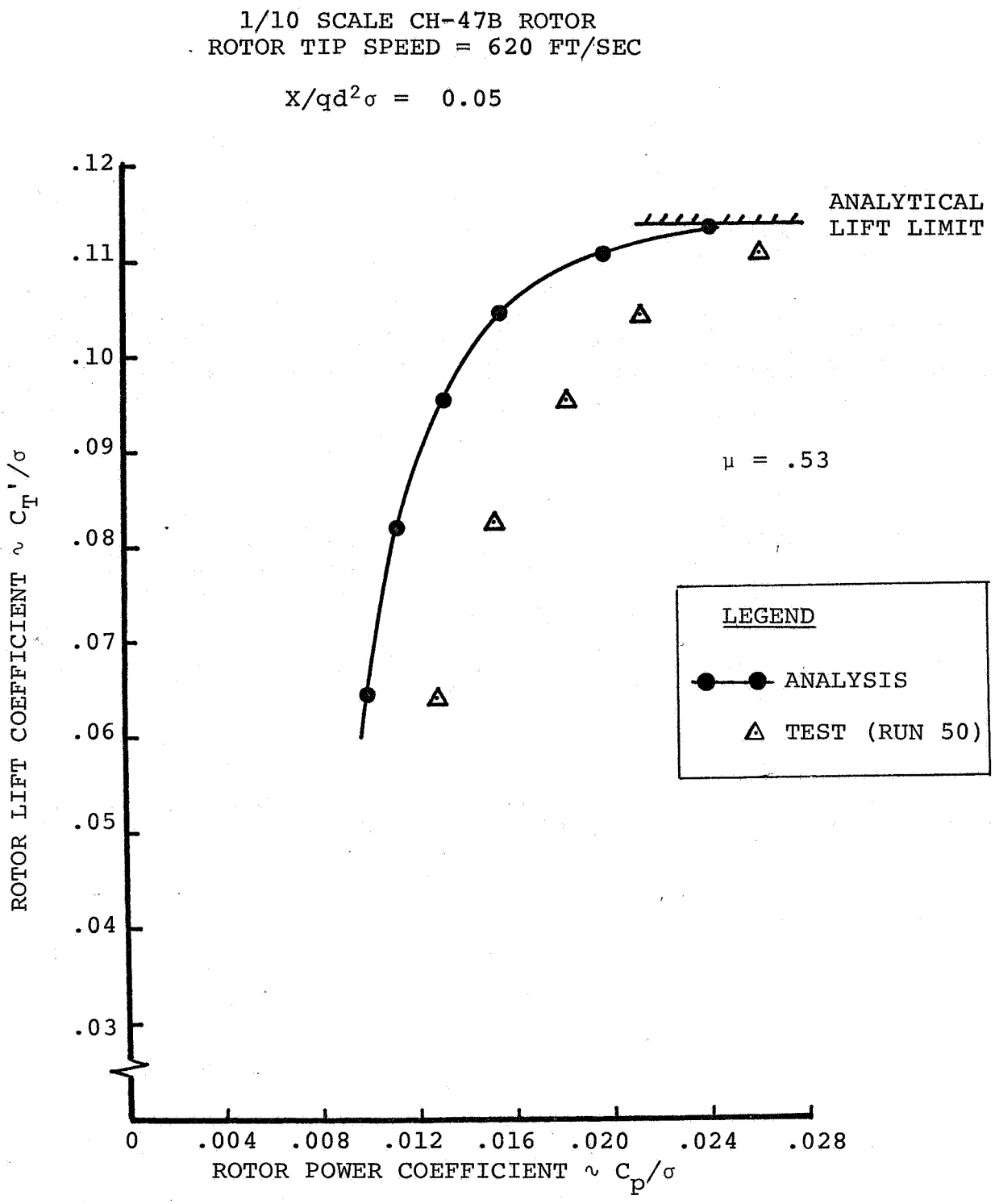

Figure 2 HIGH SPEED PERFORMANCE CORRELATION SUMMARY

1/10 SCALE CH-47B ROTOR
ROTOR TIP SPEED = 620 FT/SEC
$X/qd^2\sigma = 0.05$

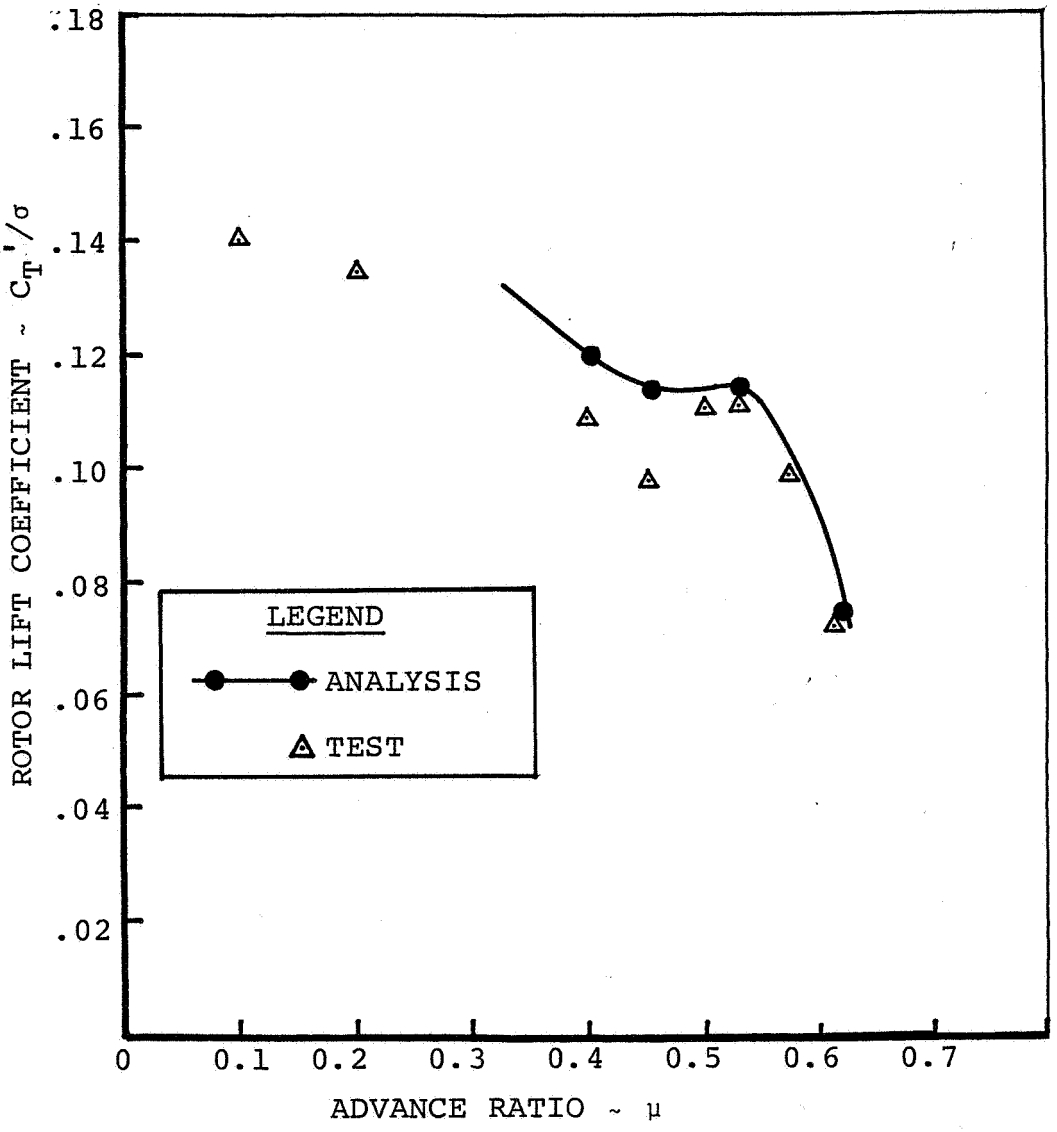

Figure 3 LIMIT LIFT COEFFICIENT VERSUS ADVANCE RATIO

1/10 SCALE CH-47B ROTOR
ROTOR TIP SPEED = 620 FT/SEC

$X/qd^2\sigma = 0.05$

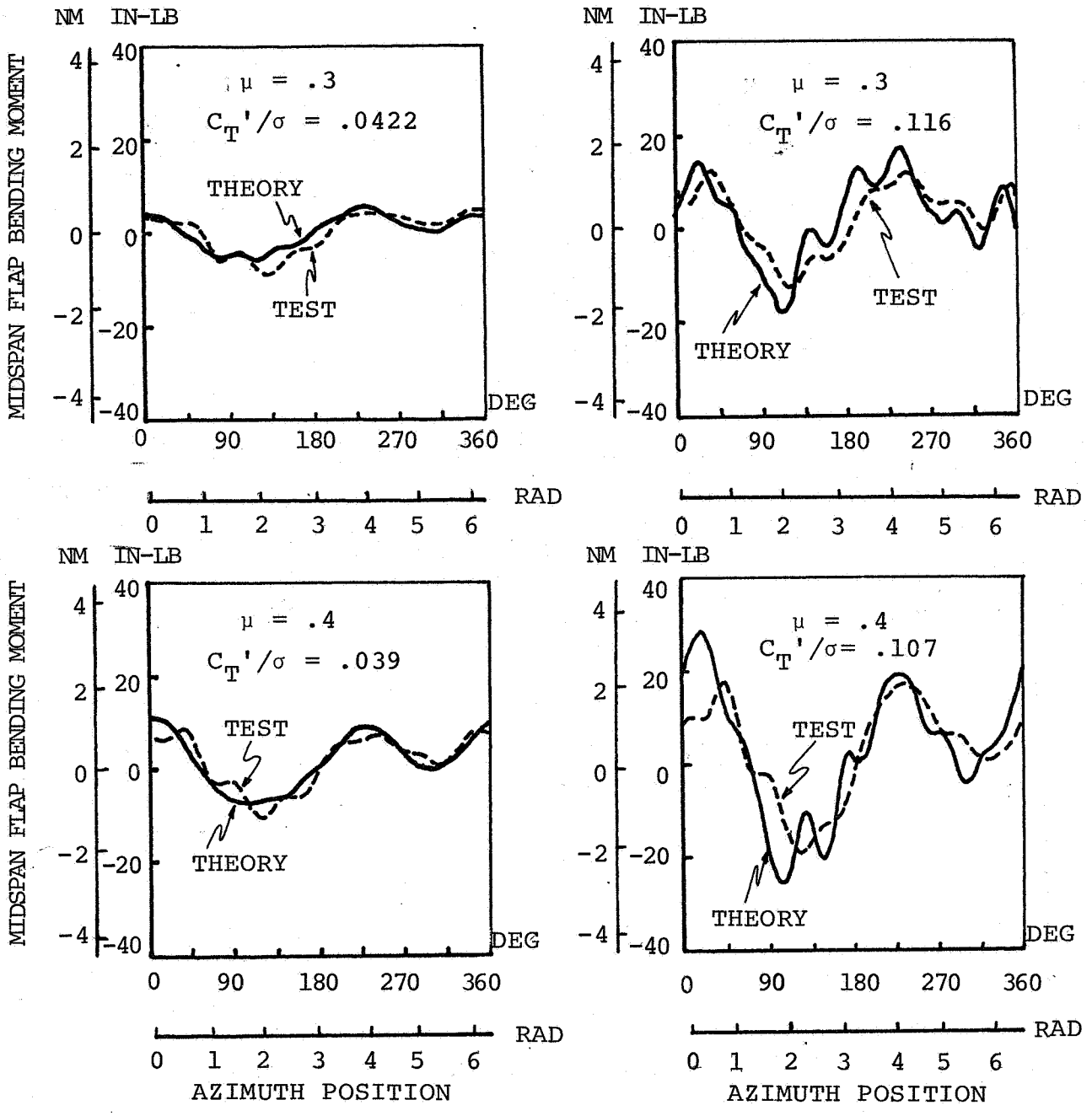

Figure 4 LOW SPEED FLAP BENDING MOMENT WAVEFORM CORRELATION SUMMARY

1/10 SCALE CH-47B ROTOR
ROTOR TIP SPEED = 620 FT/SEC

$X/qd^2\sigma = 0.05$

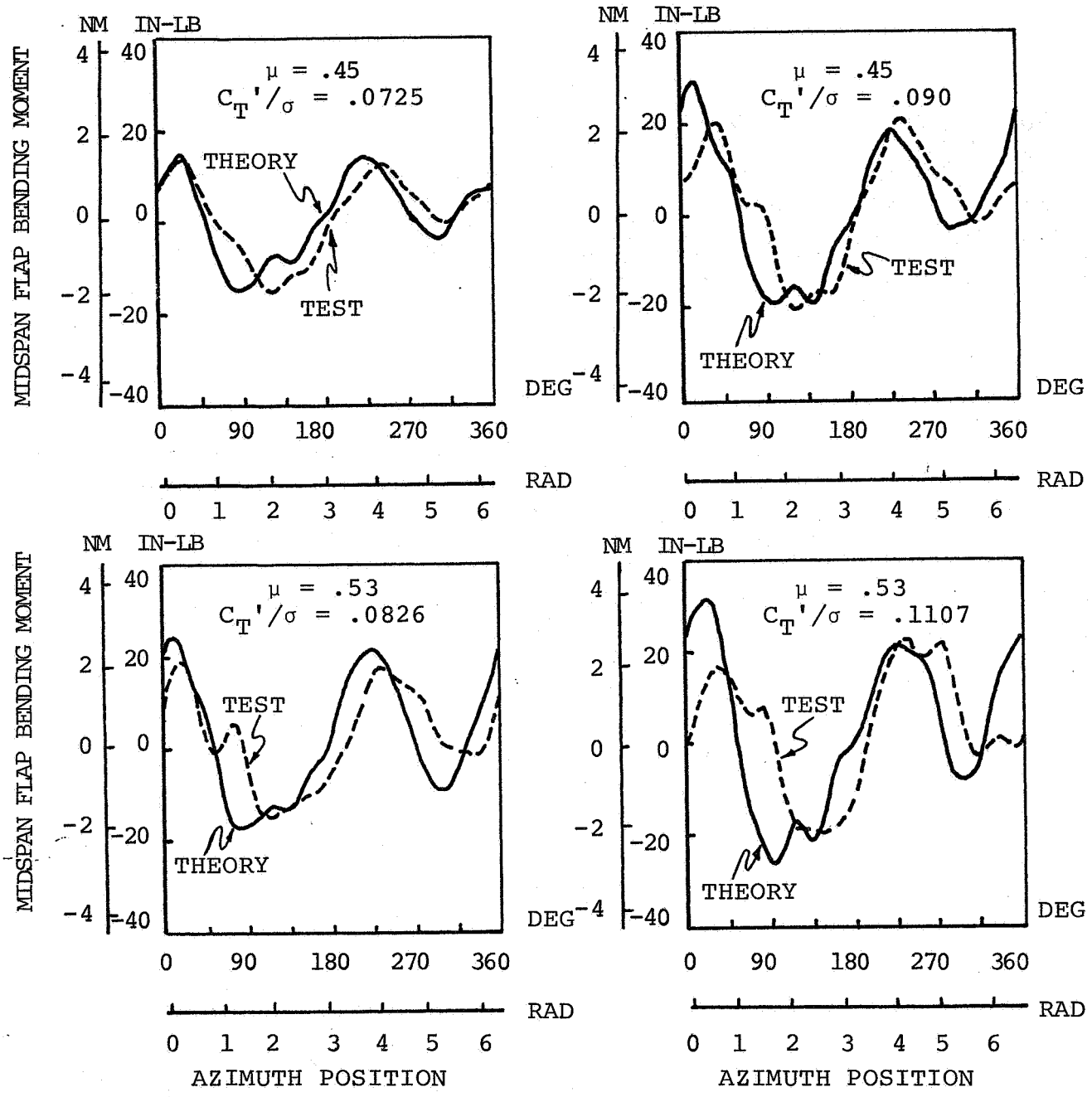

Figure 5 HIGH SPEED FLAP BENDING MOMENT WAVEFORM CORRELATION SUMMARY

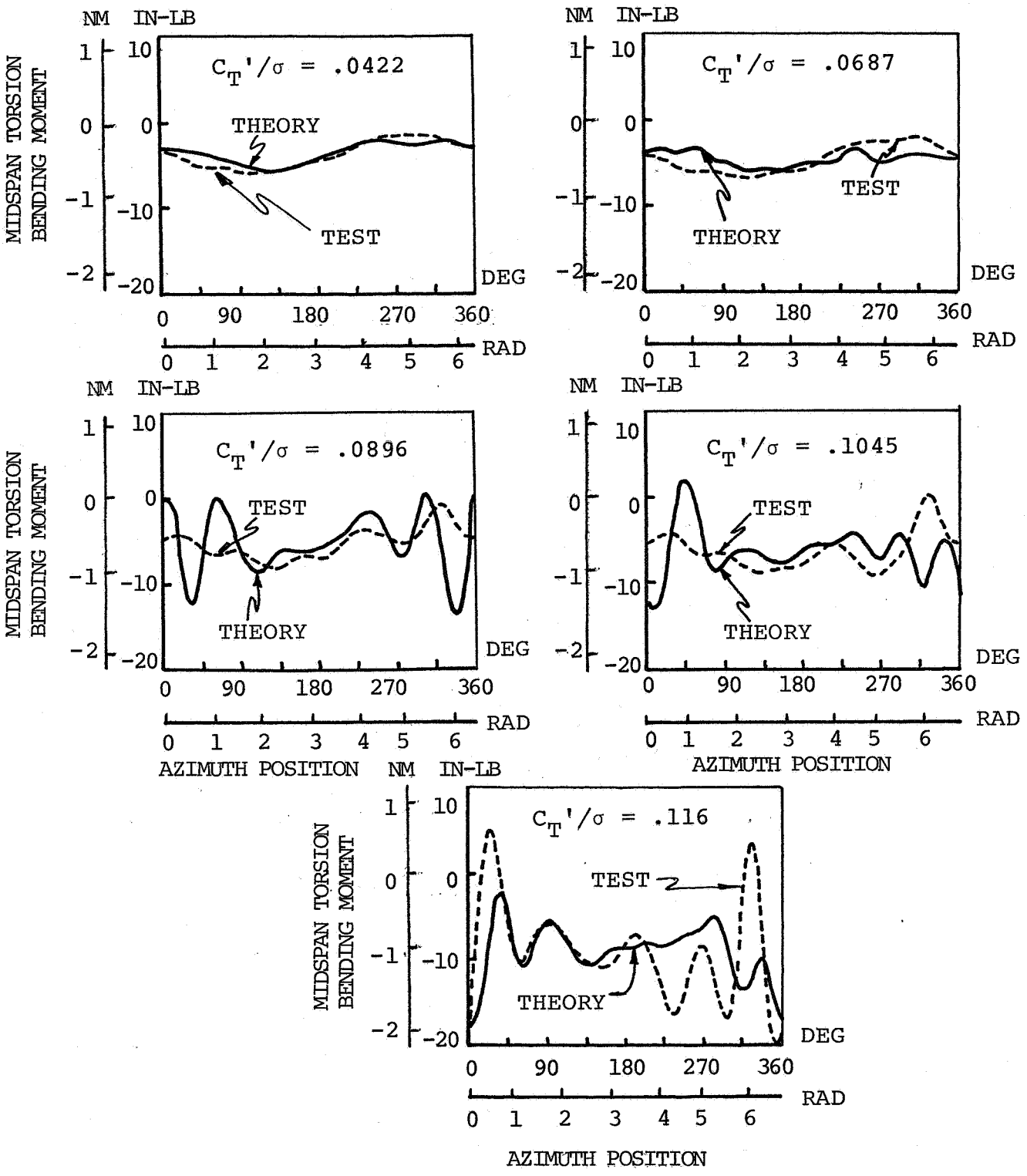

Figure 6 LOW SPEED TORSION MOMENT WAVEFORM CORRELATION SUMMARY

1/10 SCALE CH-47B ROTOR
ROTOR TIP SPEED = 620 FT/SEC

$\mu = 0.53$ $X/qd^2\sigma = 0.05$

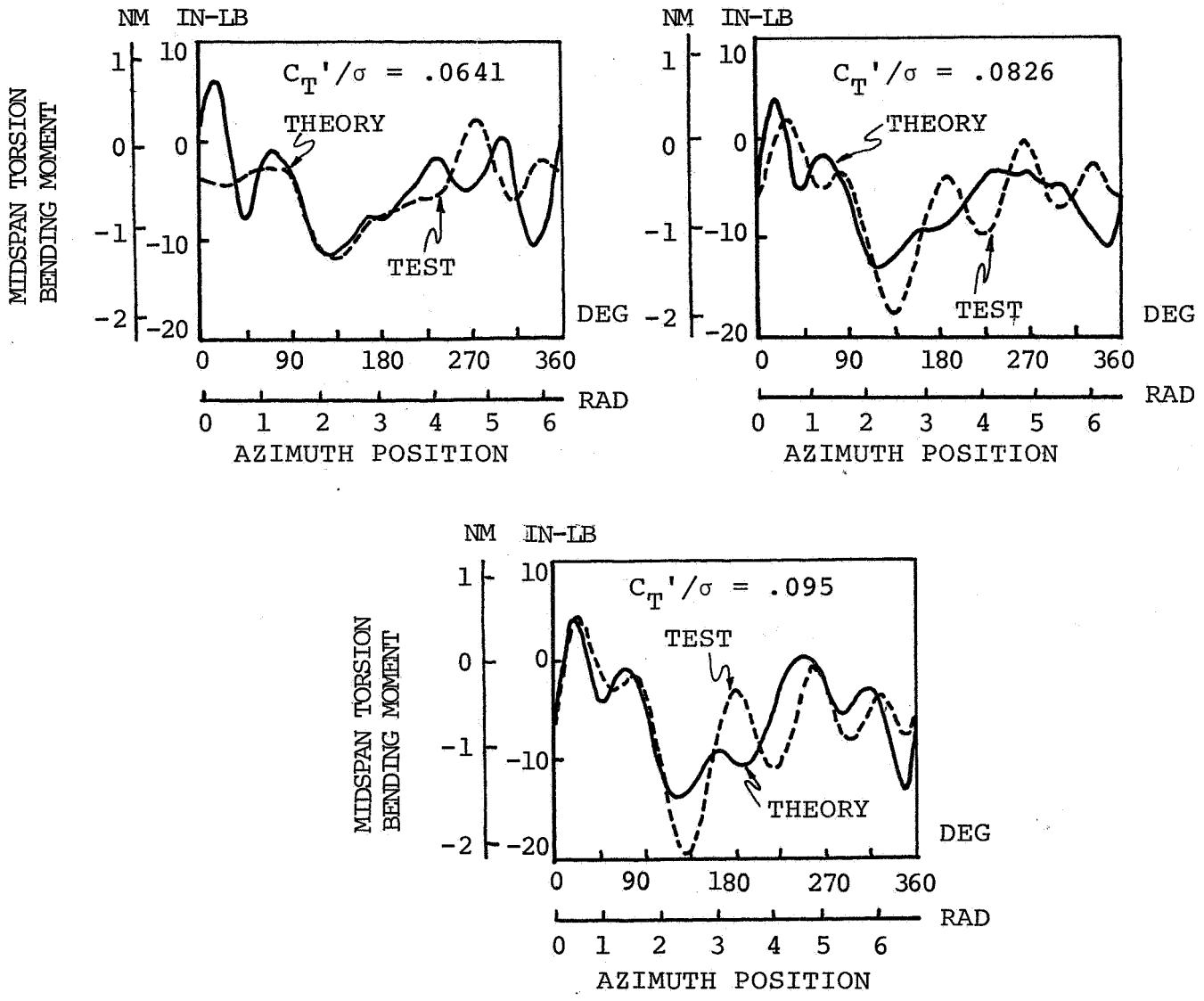

Figure 7 HIGH SPEED TORSION MOMENT WAVEFORM CORRELATION SUMMARY

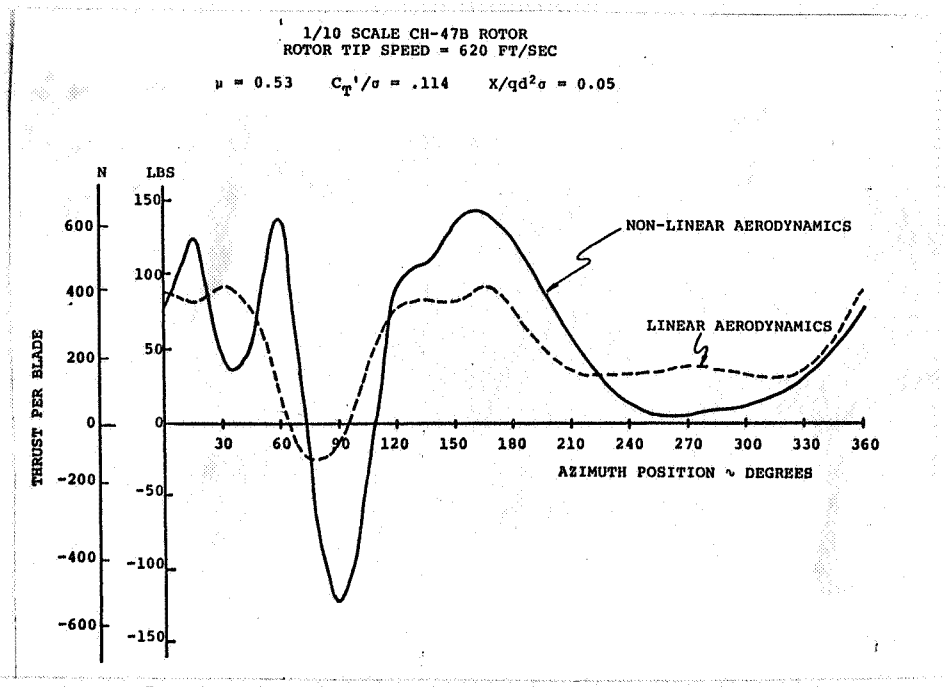

FIGURE 8 COMPARISON OF THRUST WAVEFORMS FOR LINEAR AND NON-LINEAR AERODYNAMIC ANALYSIS

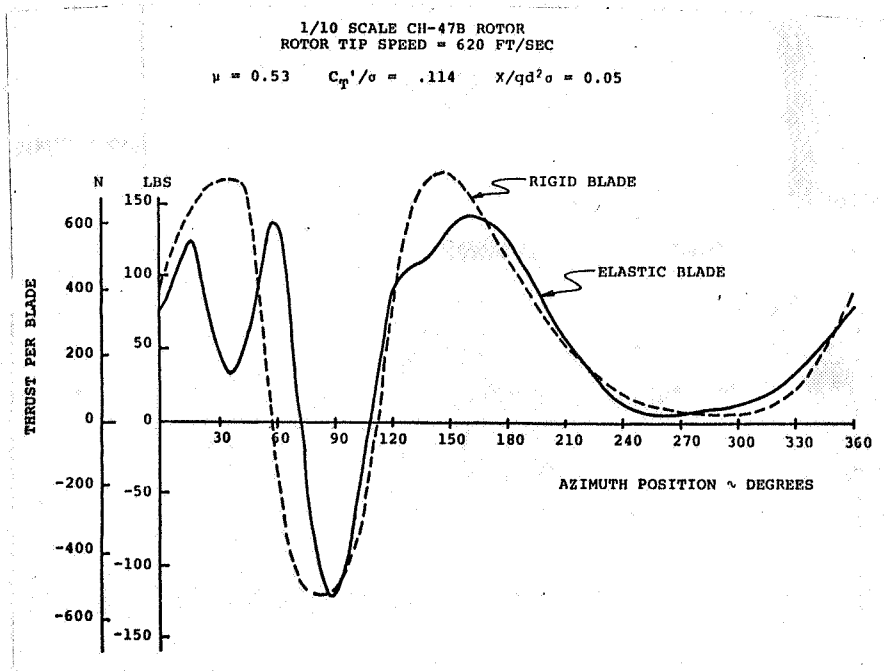

FIGURE 9 COMPARISON OF THRUST WAVEFORMS FOR RIGID AND ELASTIC BLADES

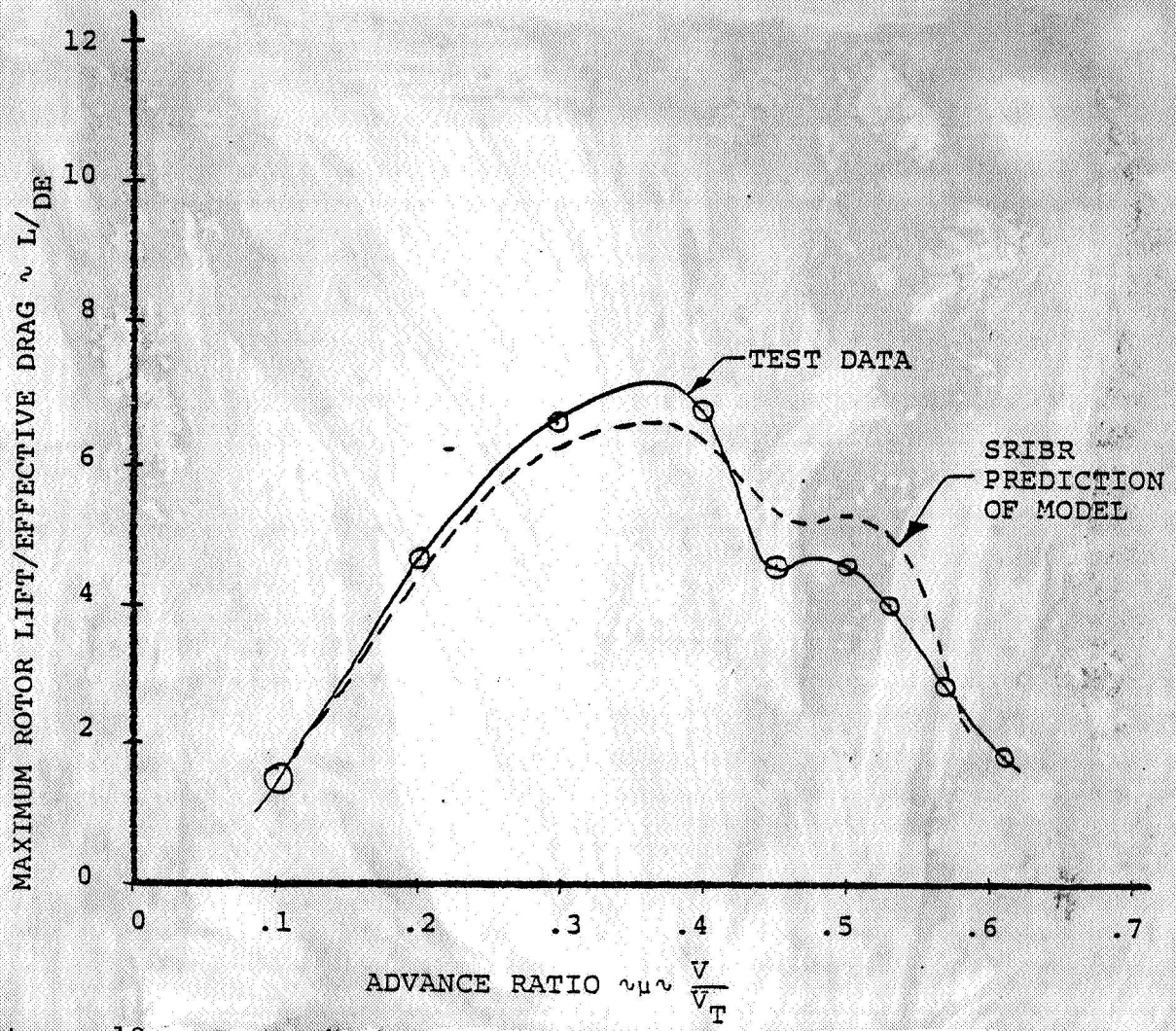

Figure 10. Comparison of SRIBR Prediction with Test Data - Maximum Rotor Lift/Effective Drag Ratio

1.0 STRUCTURAL PROPERTIES AND MODEL DATA

Prior to starting the loads and performance correlation effort, it was necessary to verify that the analytical model of the structural properties was correct. This was done by comparing the distributed parameter model data generated by static testing at the wind tunnel to the theoretical physical properties obtained by computer analysis of the blade cross-sections. Where discrepancies occurred the analytical data was modified as required.

The significant difference between the computed and measured physical properties was in the root torsional stiffness of the blade. In the region of 20% to 40% of the blade span, the measured torsional rigidity was 13% stiffer than calculated. Conversely, over the inboard 10% of the rotor the torsional stiffness of the root end fitting was measured to be 95% of the theoretical value.

Other modifications to the analytical model required were: small changes to the control system stiffness, a reduction in the effective in-plane damping coefficient and the addition of the shear center offset effects to the tabulated properties. The final set of distributed properties were input to the D-01 computer program to generate a set of lumped parameter properties for use in the C-60 loads computer program. The distributed properties which were used in the analysis which follows are shown in Figures 1.1 through 1.2. Additional physical properties data is presented in Table 1.1.

TABLE 2

SUMMARY OF ROTOR BLADE PHYSICAL PROPERTIES

Airfoil Section	V23010-1.58 (t/c = .102)
Rotor I. D. Number	= S.N. 122, 123, 124, 101, 104, 105, 106
Radius	= 0.9017 m (2.9583 FT)
Chord	= 0.0583 m (0.1913 FT)
Flap Hinge Offset	= 0.0538 m (2.12 IN.)
Pitch Axis Location	= 0.0146 m (0.5738 IN.) 25% CHORD
Blade Attachment	= 0.0545 m (2.145 IN.)
Blade Twist	= -0.1222 rad (-7.0 degrees) LINEAR
Disc Area	= 2.554 m^2 (27.4938 FT^2)
Number of Blades	= 3.
Flap Inertia	= 0.0433 kgm^2 (0.0319 $slug\text{-}FT^2$)
Weight Moment	= 0.0713 kgm (0.516 FT-LB)
Lock Number	= 6.7
Solidity	= .06175

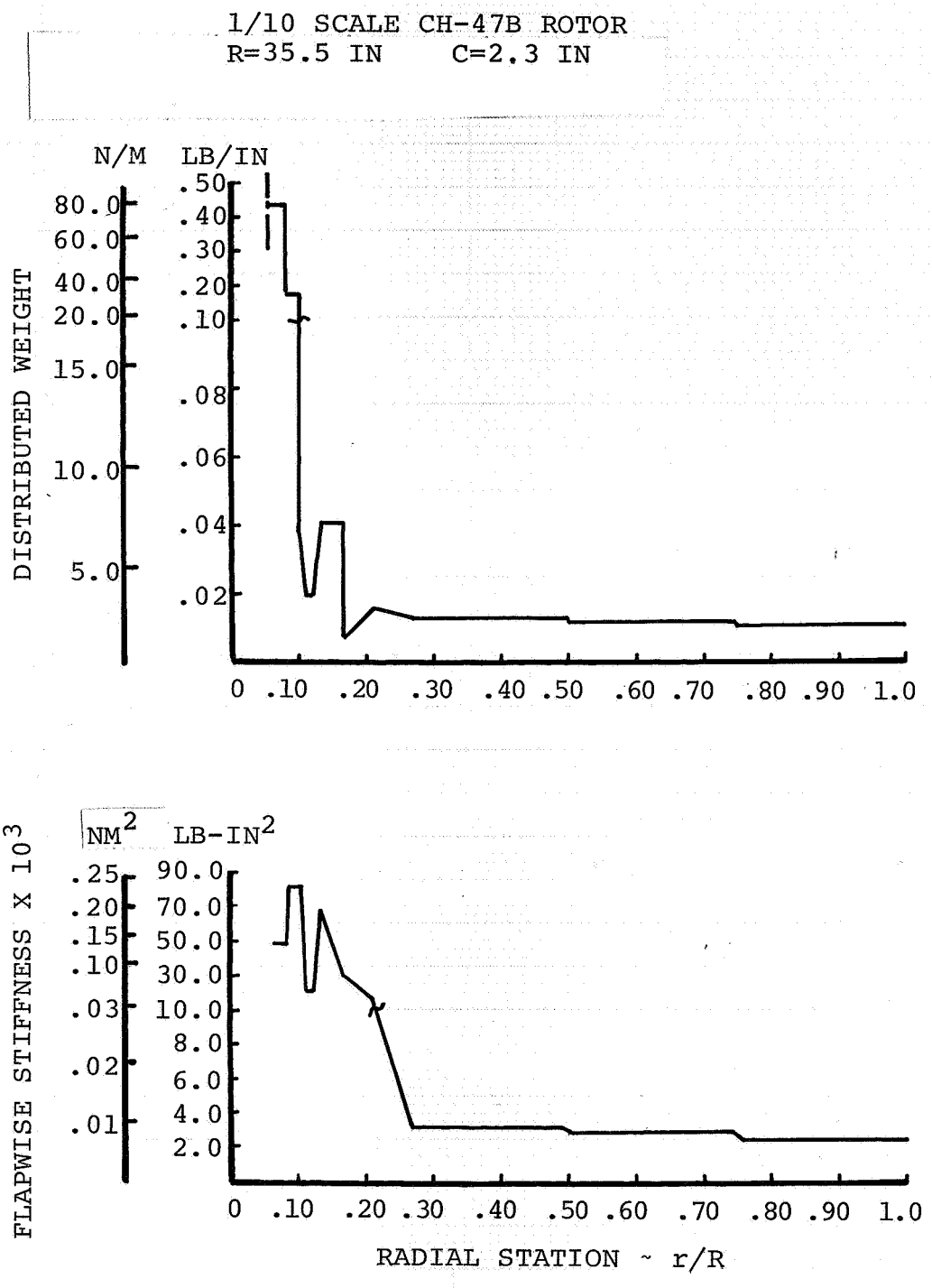

Figure 1.1 BLADE PROPERTIES DISTRIBUTION

1/10 SCALE CH-47B ROTOR
R=35.5 IN C=2.3 IN

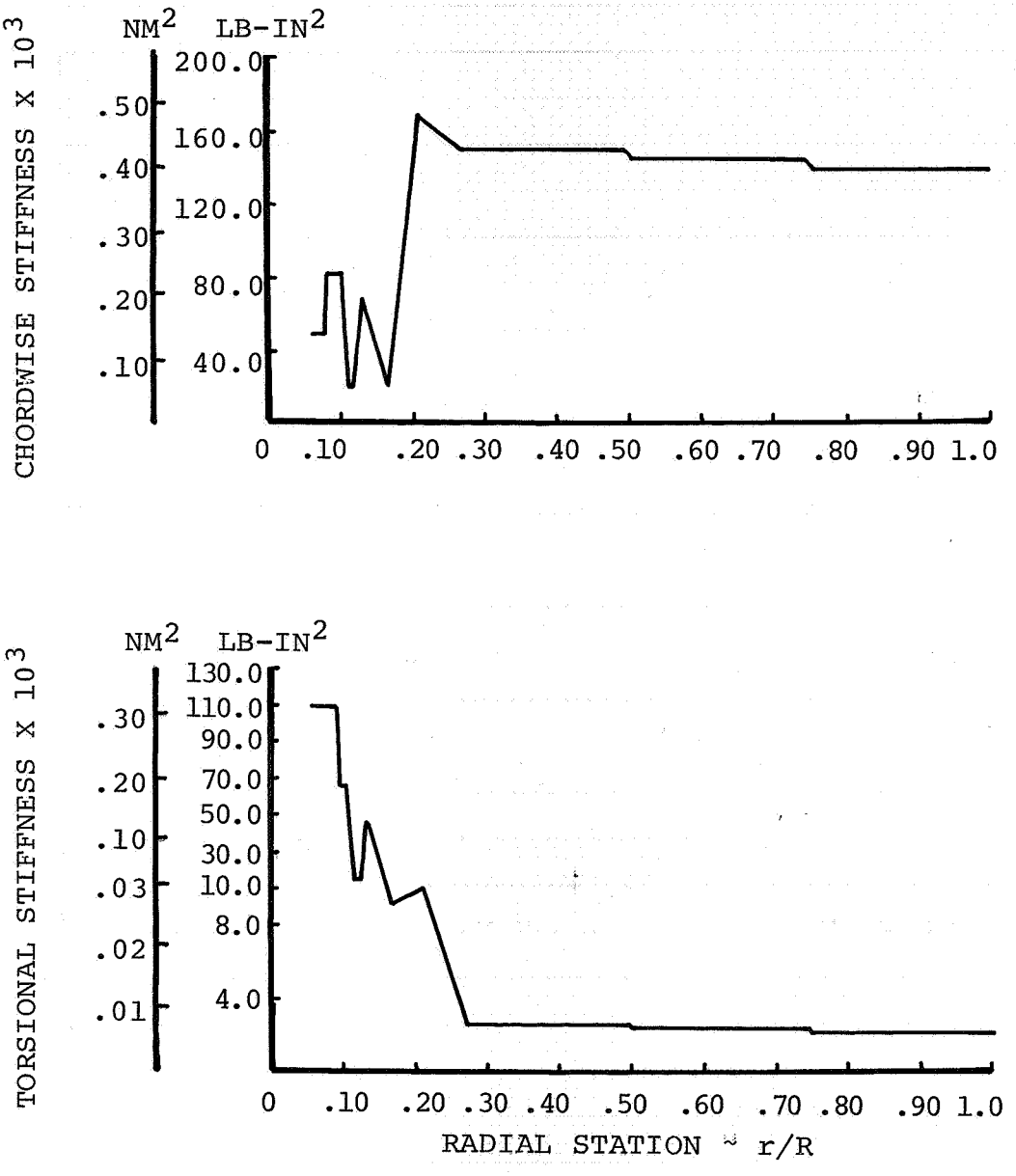

Figure 1.2 BLADE PROPERTIES DISTRIBUTION (Continued)

2.0 ROTOR NATURAL FREQUENCIES

The first step in correlating the analysis and test results required the definition of the natural frequencies of the rotor system. The D-01 coupled flap-pitch, uncoupled lag natural frequency analysis computer program was used to predict the first three flap and first chord elastic modes as well as the first torsion mode. In addition the L-01 uncoupled analysis was used to predict the first torsion mode since it includes the effects of the air spring on torsional frequencies while D-01 predicts the frequencies in a vacuum.

Figure 2.1 illustrates the correlation of the analyses with the measured modal frequencies. Note the correlation is quite good for all flap modes and the first elastic chord mode prediction deviates by less than 5%. The prediction of the first torsion mode using D-01 is considerably lower than the test values, while L-01 shows good correlation with the measured data. This indicates that the air spring effects on the torsional response characteristics are significant. C-60 includes these aeroelastic effects in its analysis.

3.0 ESTABLISH VALIDITY OF LOADS ANALYSIS

3.1 Performance Correlation

To have confidence in the explanation of the trends in rotor loads and performance as the lift limit is approached, it is important to substantiate the predictive capabilities of the analytical tools with regard to loads, trim and performance predictions. The comparison of test data with analysis was performed using the Aeroelastic Rotor Analysis

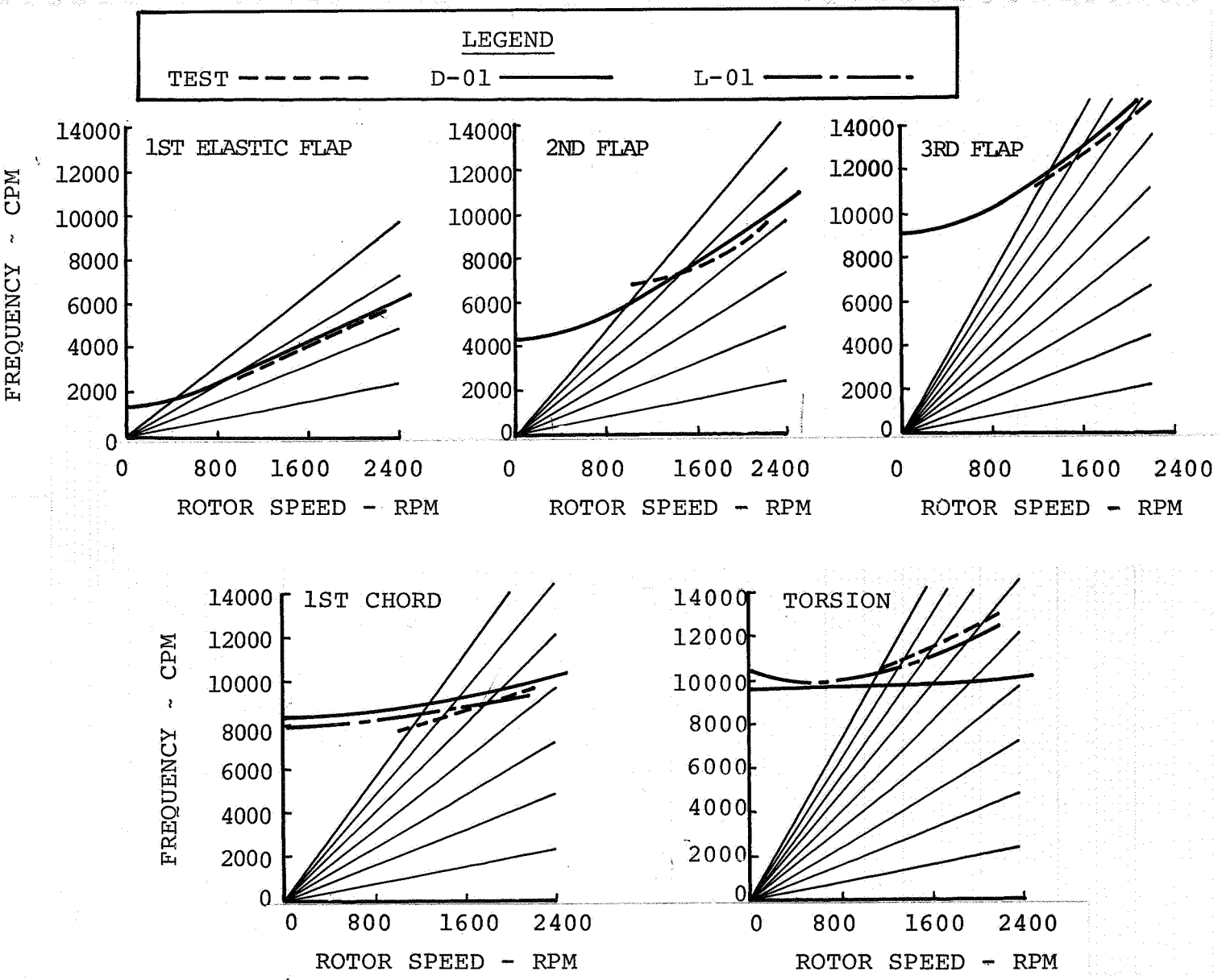

Figure 2.1 FREQUENCY SPECTRUM FOR 1/10 SCALE CH-47B ROTOR

Program, C-60.

The aeroelastic rotor analysis calculates rotor blade flapwise, chordwise and torsional deflections and loads as well as rotor performance, control system forces and vibratory hub loads.

Rotors with blades of arbitrary planform, twist and radial variation in airfoil section are analyzed in steady state forward flight conditions. The analysis incorporates coupled flapwise-torsion deflections and uncoupled chordwise deflections of the rotor blades. The blade is represented by twenty (20) lumped masses, interconnected in series by elastic elements. Boundary conditions for either articulated or hingeless rotors are applied and the solution obtained by expanding the variables in a ten harmonic Fourier series.

Airload calculations include the effects of airfoil section geometry, compressibility, stall, 3-dimensional flow, unsteady aerodynamics and non-uniform inflow. Static airfoil tables are used to account for compressibility, static stall and airfoil shape. The unsteady aerodynamic loads are calculated by modifying the static loads resulting from the airfoil tables to include Theodorsen's shed wake function, dynamic stall effects based on oscillating airfoil data and yawed flow across the blade.

The non-uniform inflow calculations are based on a tip and root vortex trailed from each blade. Through an iterative technique, each trailed

vortex is made compatible with the calculated blade lift distribution, and the lift distribution is compatible with the non-uniform downwash field. The vortex wake is assumed to be rigid and drifts relative to the hub with a constant resultant velocity composed of thrust induced downwash and the aircraft airspeed.

Preliminary predictions of rotor performance, as measured by power requirements for a given thrust, are shown in Figure 3.1.1 for advance ratios of μ = .3 and μ = .53. Both advance ratios are at a propulsive force coefficient of $x/qd^2\sigma$ = .05. The comparison of analysis and test at μ = .3 shows excellent correlation. At μ = .53, however, the analysis underpredicts the power coefficient, Cp/σ, by a constant value of approximately 25%. Therefore it was decided to investigate several possible explanations why the performance predictions were good at low speed but were optimistic in power requirement predictions at higher speeds.

One suggested explanation was that the additional drag due to the instrumentation wire bundles was not accounted for in the airfoil table look-up routine for C_d. An attempt was made to include in the analysis an additional C_d of .015 along the blade due to the straingage wiring. As seen in Figure 3.1.2 this results in greatly improved correlation at μ = .53 but the correlation at μ = .3 is much worse. Since the correlation was obviously degraded at low speed where the flow conditions are better understood than at high speeds, the ΔC_d = .015 modification to the analysis was not used.

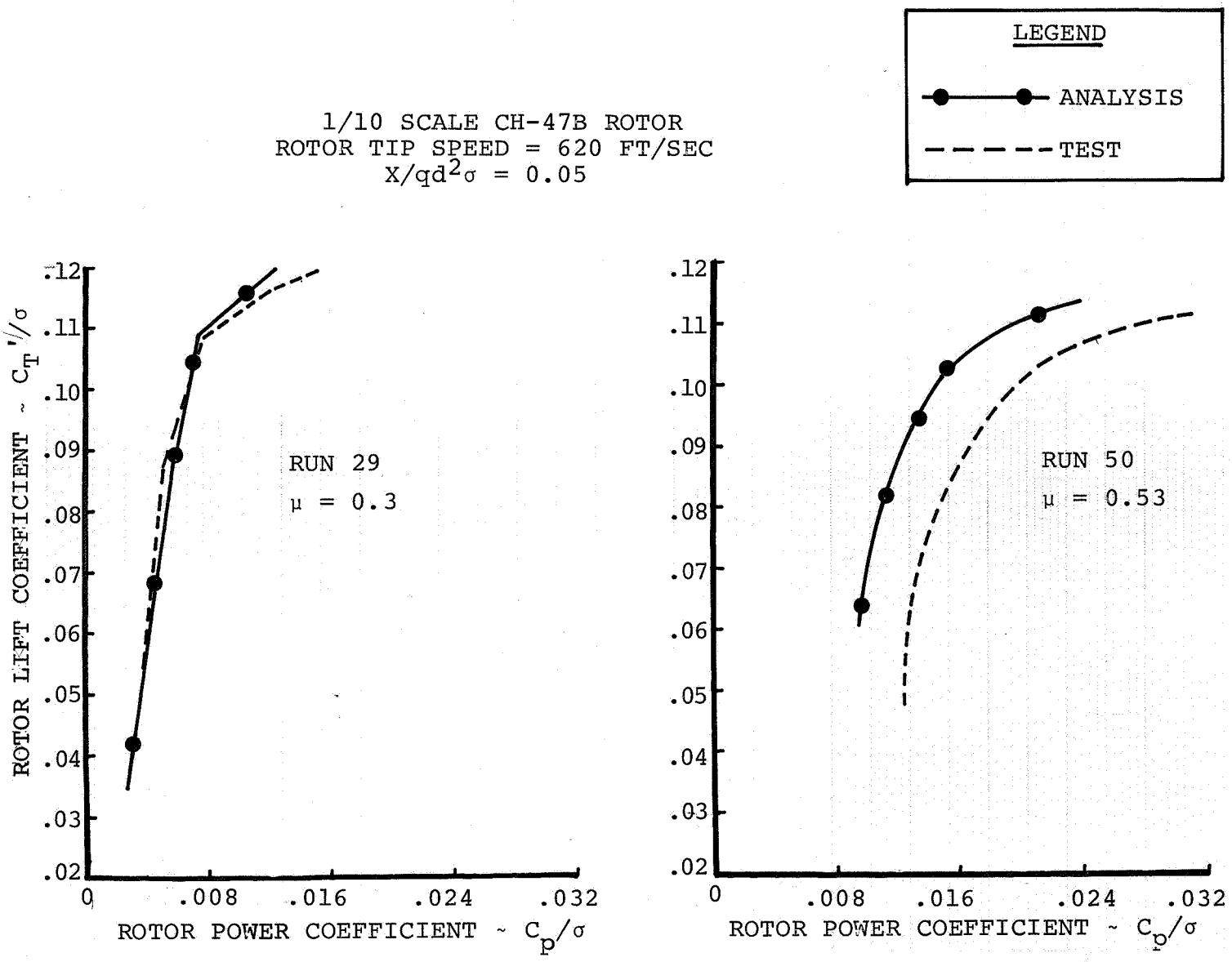

Figure 3.1.1 INITIAL PERFORMANCE CORRELATION SUMMARY

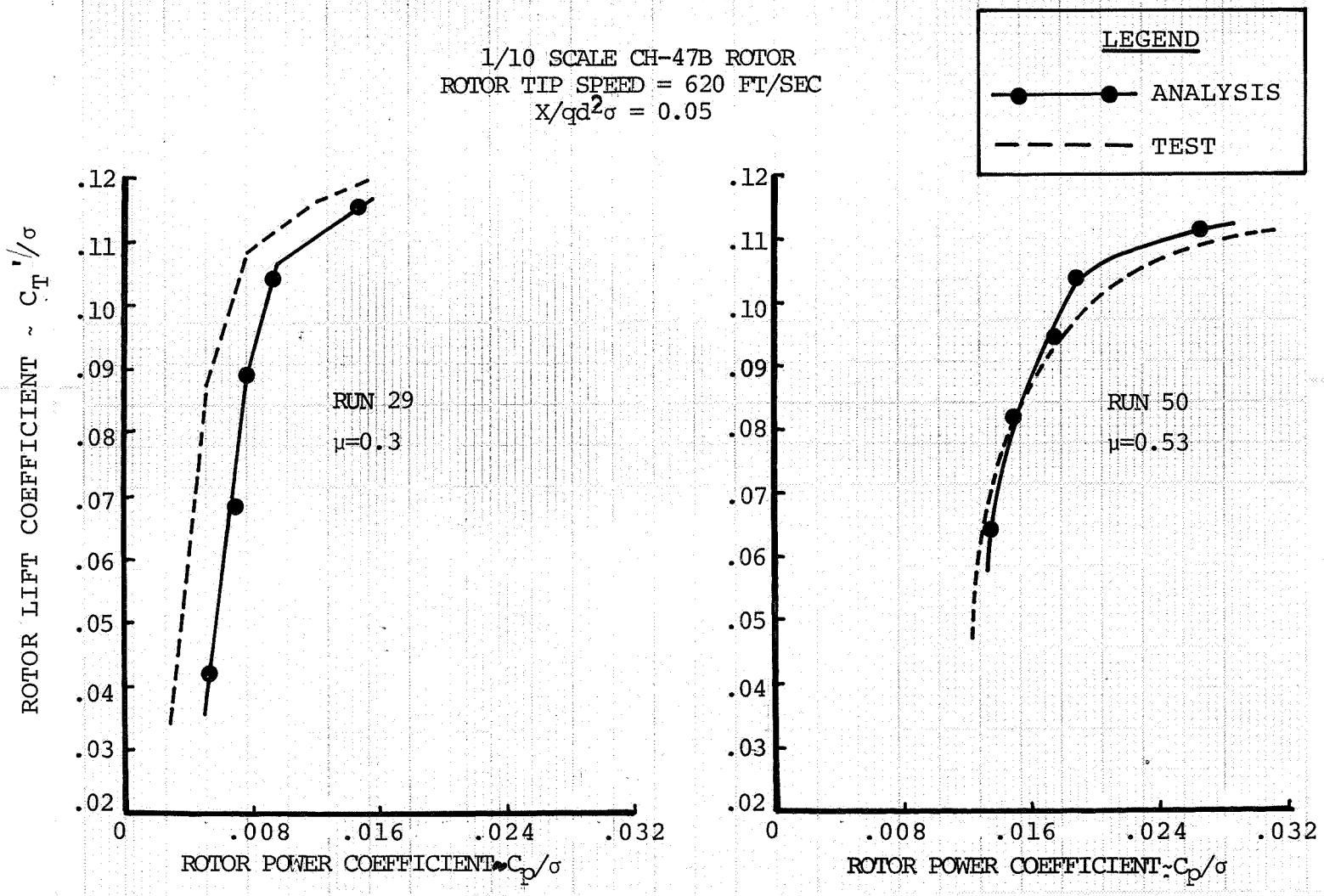

Figure 3.1.2 PERFORMANCE CORRELATION WITH DRAG INCREMENT MODIFICATION

Airfoil test data has indicated that for high angles of attack the lift and pitching moment coefficients, and possibly the drag coefficient, required modification to the existing equations for the 23010 airfoil. These equations represent the airfoil characteristics between 20^{o} and 340^{o} azimuth and are the same for all Mach numbers. The C-60 Aeroelastic Rotor Analysis Program was modified so that the equations for lift, drag and pitching moment coefficients could be adjusted using 19 separate constant coefficients applicable over various angle of attack ranges. However one problem is that these equations are functions of angle of attack only and not Mach number. Thus the constant coefficients which modify the airfoil equations had to be applied at all Mach numbers and not just for the higher Mach numbers.

Using the best estimate of the parameters to modify the airfoil equations the performance predictions were repeated. The correlation of the analysis and test data at $\mu = .3$ and $\mu = .53$ are shown in Figure 3.1.3. As can be seen this attempt to improve the analytical representation of the airfoil characteristics was not successful. At low speeds the analysis now shows an optimistic power requirement at low thrust levels and at higher thrusts the analysis fails to predict the sharp change in the slope of the power required curve. At the higher advance ratio the correlation is generally improved, though only slightly. Again at the higher values of lift the onset of stall is delayed resulting in the correlation actually getting worse. Thus it appears that the current representation of airfoil characteristics at high angles of attack is still the most suitable.

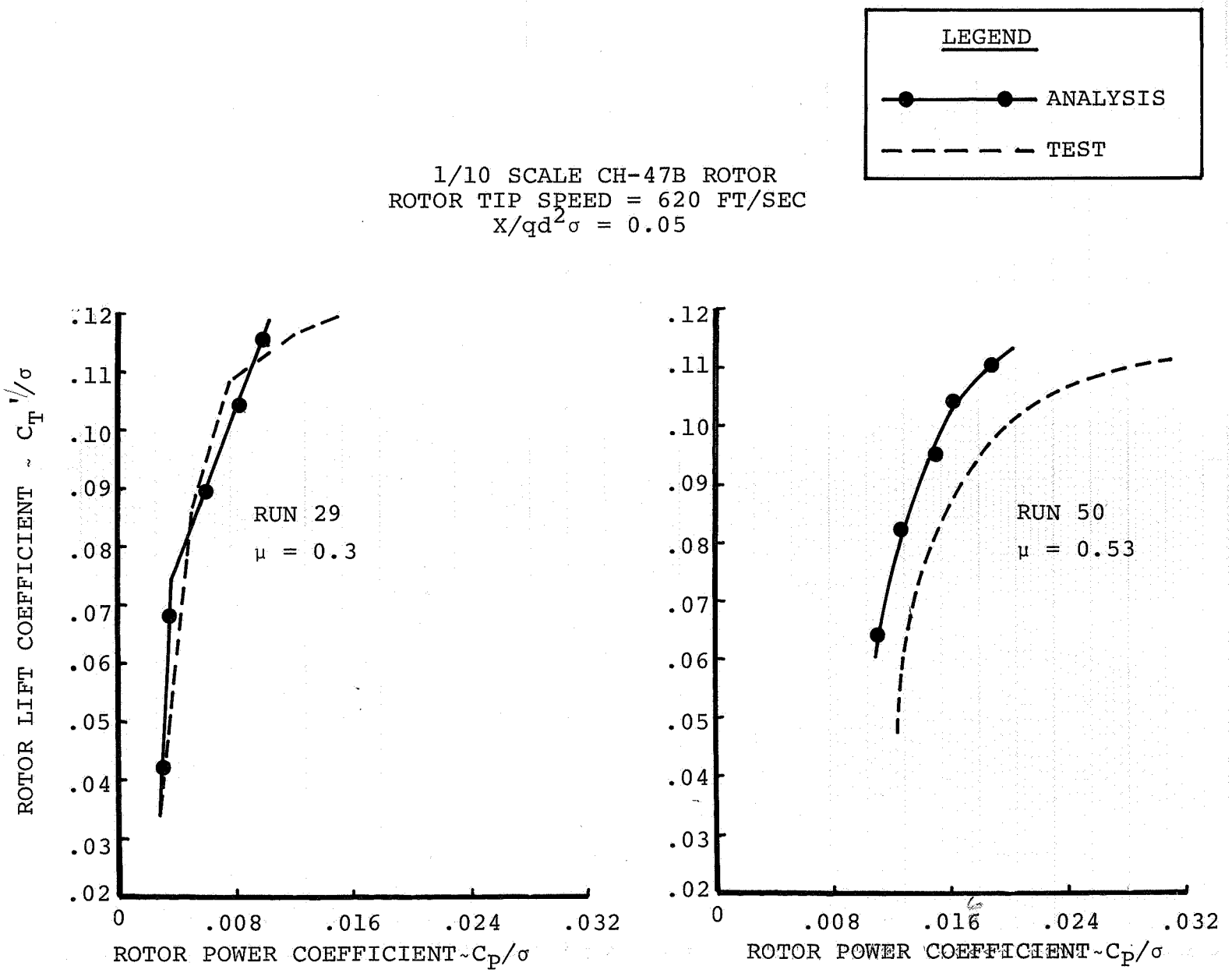

Figure 3.1.3 PERFORMANCE CORRELATION WITH REVISED AERODYNAMIC COEFFICIENTS CALCULATIONS

One further explanation for the variance between analytical performance predictions and test data at high speeds was the method of accounting for the three dimensional compressible flow at the rotor tip and its effect on the lift and drag coefficients. Previously the tip relief effects were included in the airfoil tables by modifying the two-dimensional tables based on wind tunnel data. However, this method does not account for the effects of spanwise changes in the chord length and thickness of the rotor blade. John LeNard and Gabriel Boehler of the USAAMRDL Eustis Directorate have formulated a procedure to directly account for the three-dimensional flow at the tip which can be applied to the two dimensional airfoil tables (Reference 2).

The basic procedure to account for tip relief effects on C_L and C_D is to first determine the difference in flow characteristics between the two- and three-dimensional cases represented by an increment in free stream velocity. This results in a lower local Mach number for the blade element, which in turn results in a change in the dynamic pressure. The new local Mach number and dynamic pressure are used with the original section angle-of-attack to compute the corrected lift and drag coefficients. Due to the nature of the flow corrections for three-dimensional flow at the tip and because of the nature of the normal shape of the C_L and C_D versus Mach number curves, the tip relief corrections are only initially effective around Mach numbers of .65. The real impact of the tip relief corrections is felt at Mach numbers approaching .825 or greater.

The performance predictions for $\mu = .3$ and $\mu = .53$ (both at $\overline{x} = .05$)

were repeated using two-dimensional tables and the LeNard tip relief correction. The differences in performance predictions from the baseline were quite small at both advance ratios. This result was quite surprising and warranted further investigation. It was found that despite forward speeds of up to 225 knots, the primary tip speed was only 620 ft/sec so that the maximum advancing blade Mach number was approximately .88. Thus over most of the blade the local Mach number would be smaller than .85 and at speeds below 225 knots the advancing blade tip Mach number may not even reach .825. Despite the high speed testing which was performed the rotor generally operates outside the regime where the tip relief effects are significant. Therefore, the LeNard correction did not produce the desired benefit of improved performance correlation. The LeNard tip relief three-dimensional correction was used in all subsequent analysis because of its better representation of the tip effects.

The correlation of analytical performance predictions as measured by lift coefficient (C_T'/σ) and power coefficient (C_p/σ) as compared to wind tunnel test results are presented in Figures 3.1.4 through 3.1.8. The correlation effort was performed at advance ratios of .3, .4, .45, .53 and .61 for a propulsive force coefficient of $\bar{x}$ = .05 at several levels of lift. In addition at μ = .4, .45, .53 and .61 for a fixed value of lift the propulsive force coefficient was varied.

The results of the performance correlation at μ = .3 and $\bar{x}$ = .05 are seen in Figure 3.1.4. The analysis and test data agree quite well,

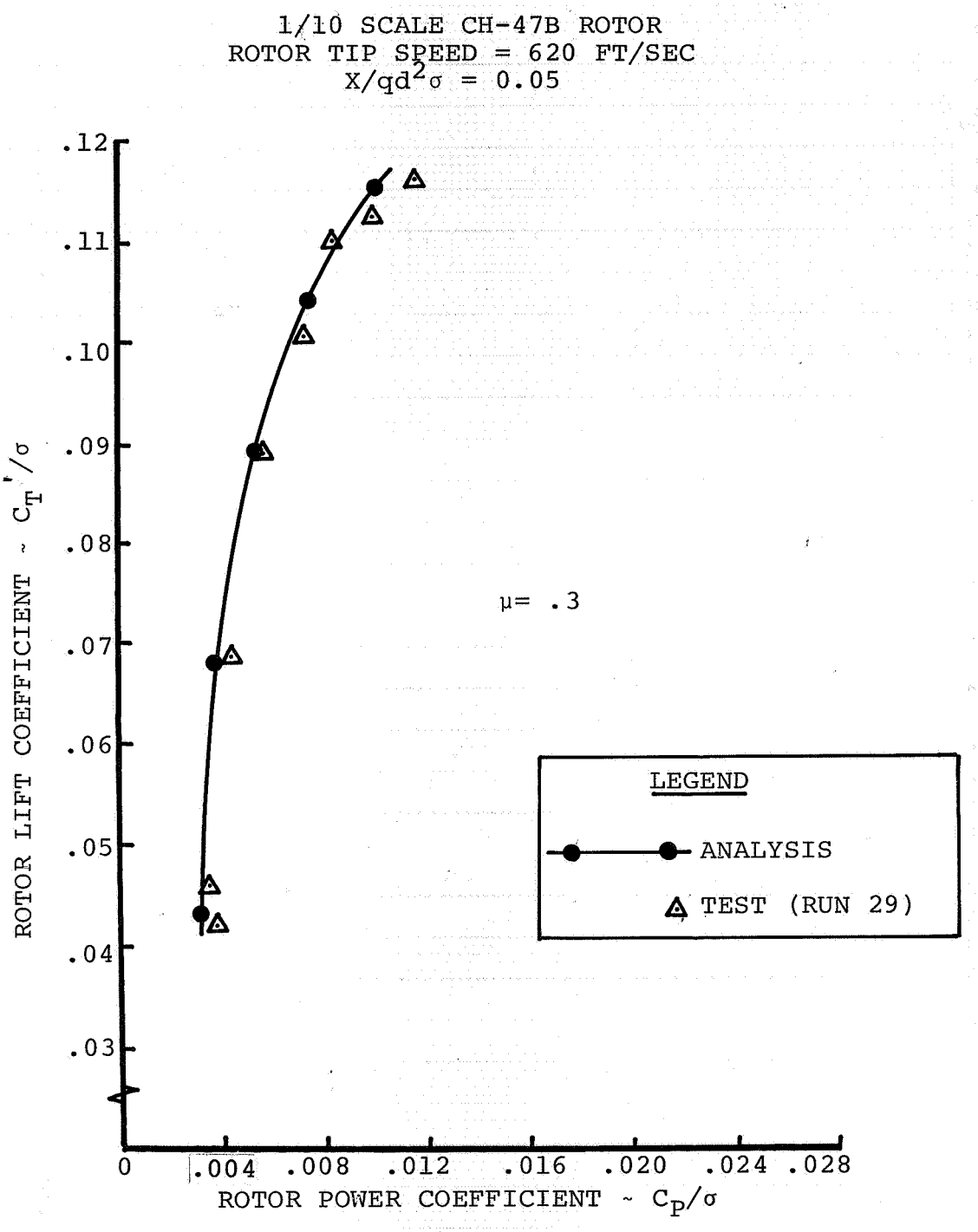

Figure 3.1.4 PERFORMANCE CORRELATION AT 110 KNOTS

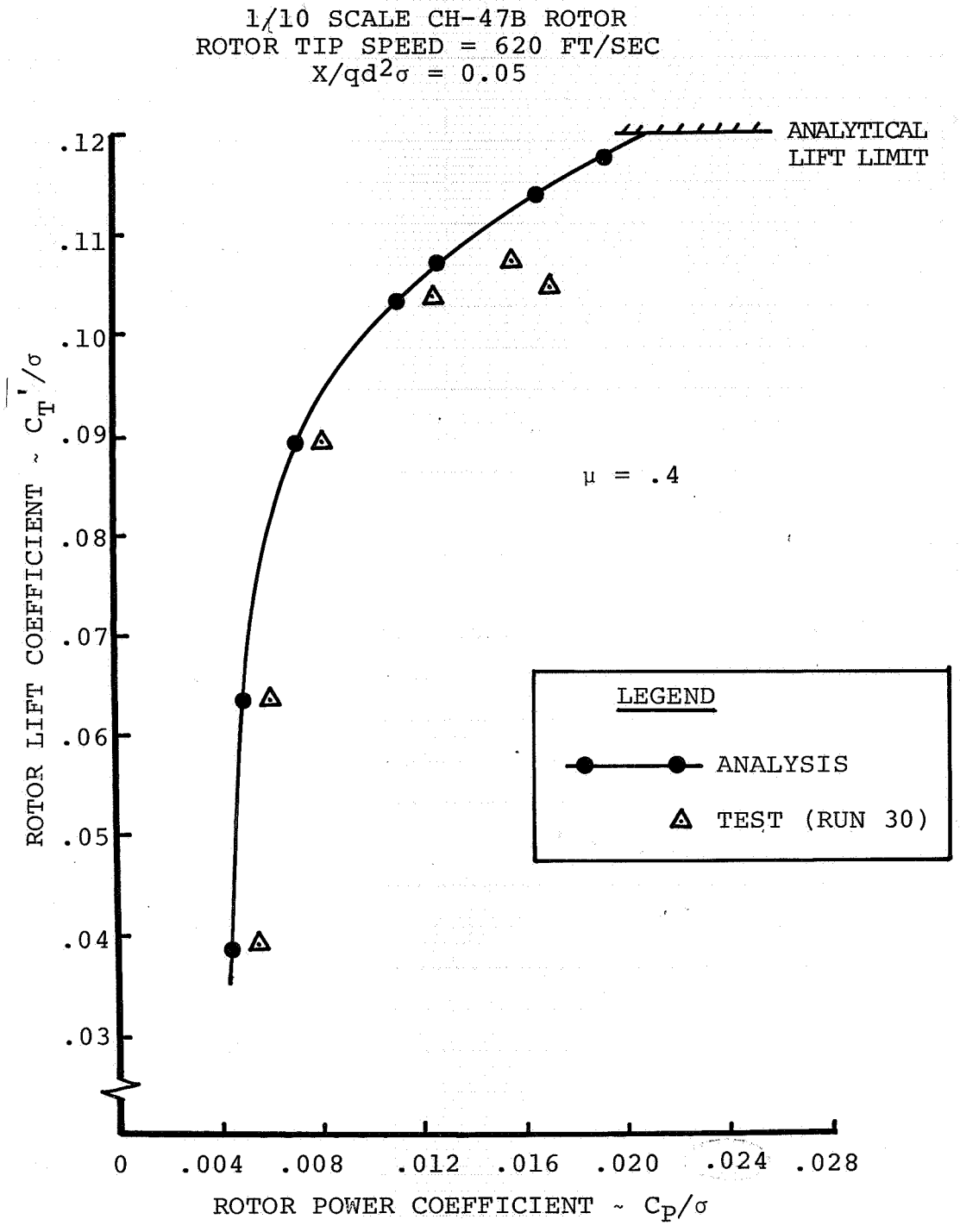

Figure 3.1.5 PERFORMANCE CORRELATION AT 147 KNOTS

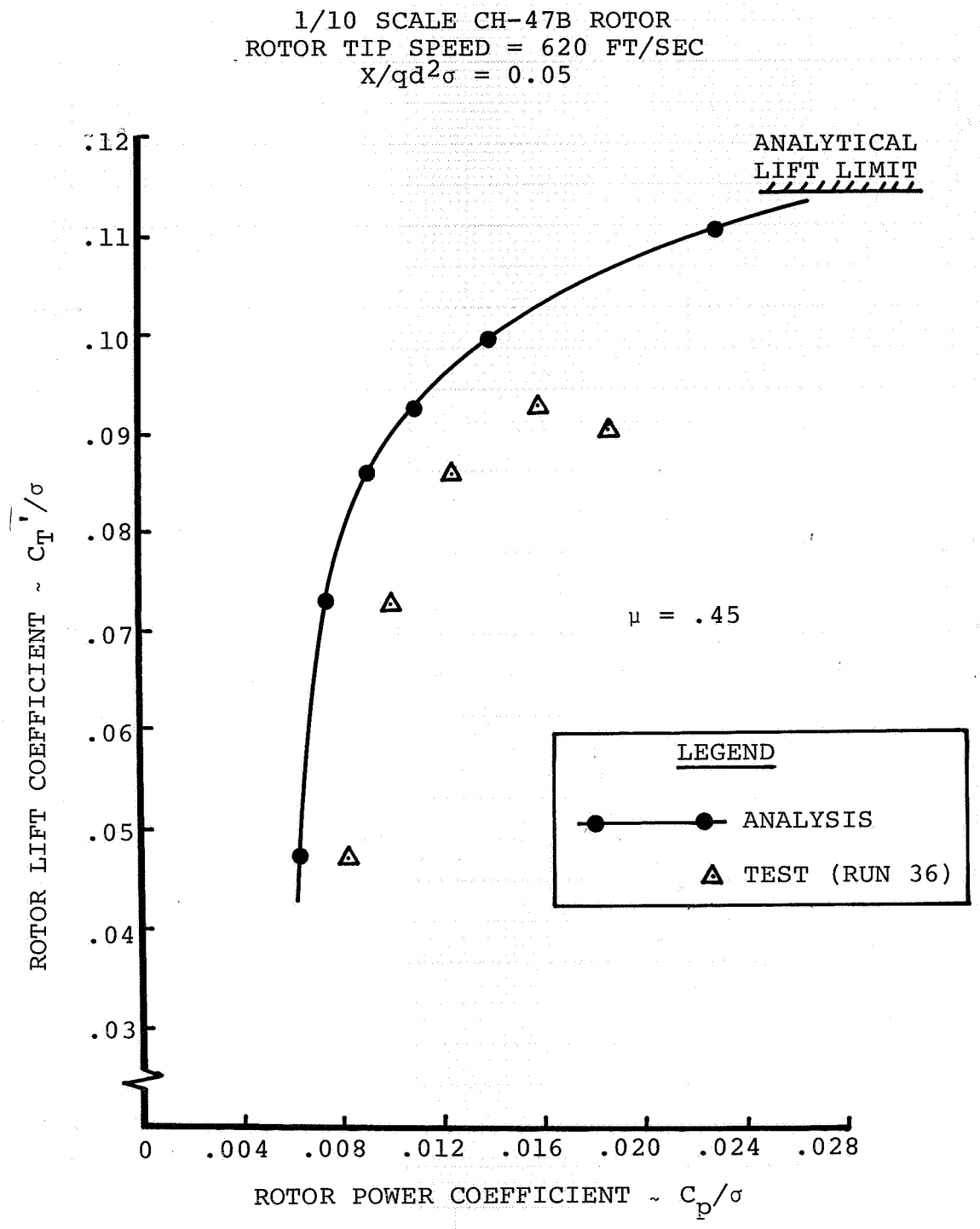

Figure 3.1.6 PERFORMANCE CORRELATION AT 165 KNOTS

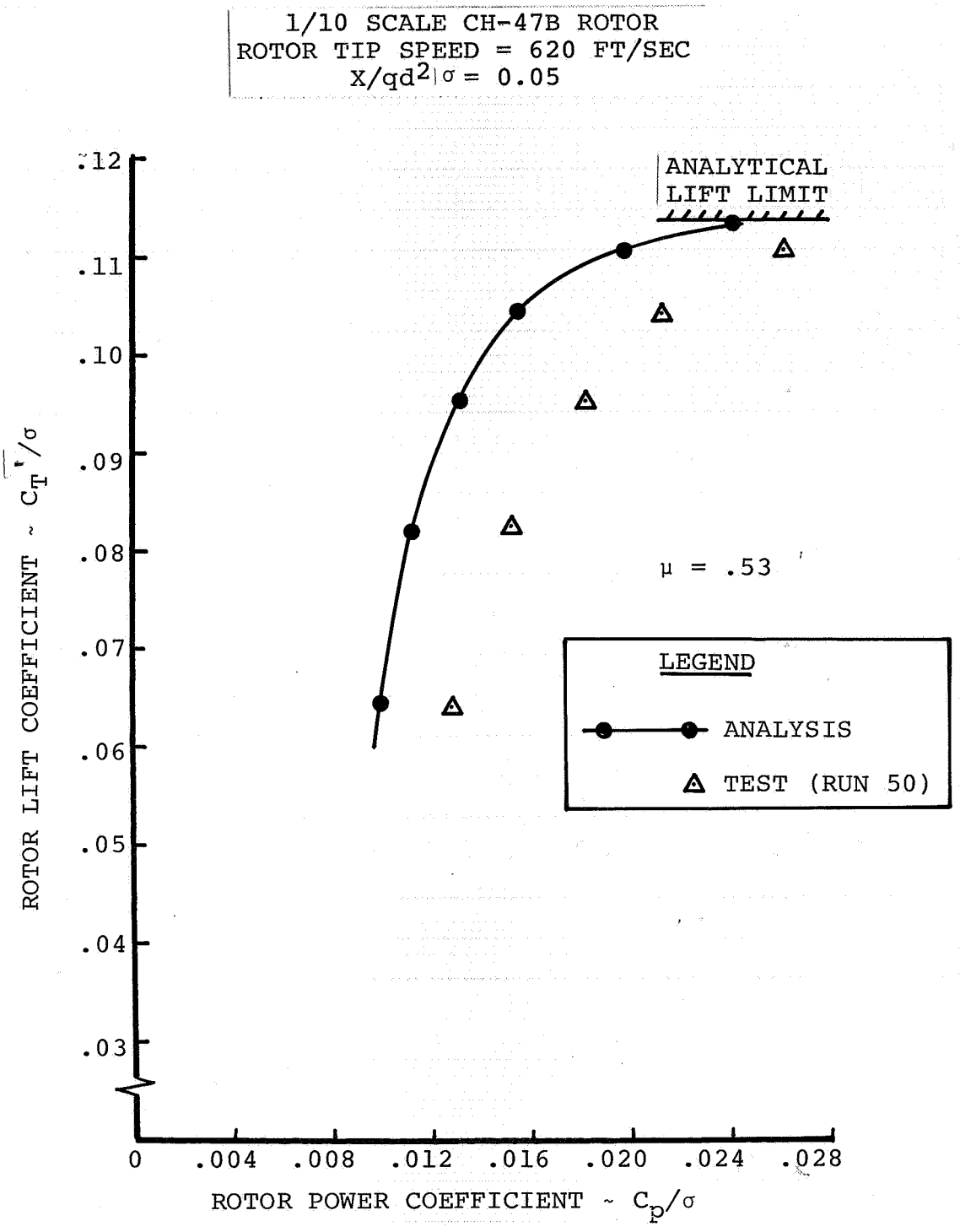

Figure 3.1.7 PERFORMANCE CORRELATION AT 195 KNOTS

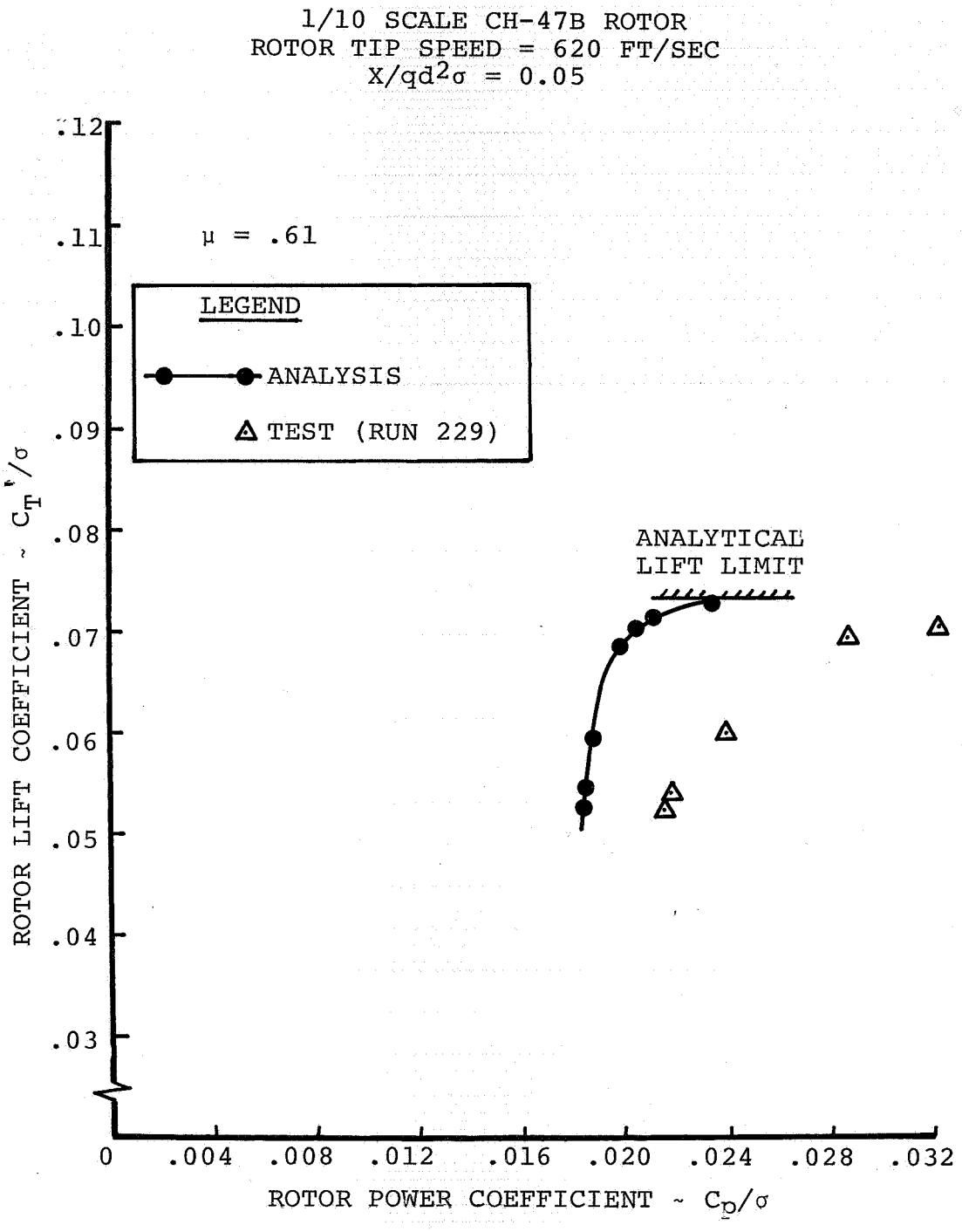

Figure 3.1.8 PERFORMANCE CORRELATION AT 224 KNOTS

as would be expected for this speed range which is typical of a conventional aircraft. Figure 3.1.5 is a similar plot for $\mu = .4$ (147 knots). The analysis follows the test data up to $C_T'/\sigma = .104$. Beyond this point the test shows that increasing collective produces small gains in lift as power requirements continue to rise. The analysis is able to reach a lift coefficient of $C_T'/\sigma = .12$ before a limit is determined. The analytical limit is characterized by a large increase in power required for a small change in lift and simultaneously the analysis is unable to match the required propulsive force and side force trim condition. The analysis indicates a 15% higher lift limit than achieved in the test.

At $\mu = .45$ (Figure 3.1.6) the rotor is approaching the limits of normal high speed flight for the standard tandem articulated rotor (165-170 knots). At this forward speed the analysis is optimistic in the prediction of power required but does follow the trend of the test data up to a lift coefficient of $C_T'/\sigma = .093$. As with the $\mu = .4$ case the test data reaches a lift limit at this point with further increases in collective resulting in higher power requirements with no gain in lift. The analysis predicts the rotor could achieve a lift coefficient of $C_T'/\sigma = .113$ before the rapid increase in power requirement and inability to trim the rotor occur. This is 21% greater than the test indicated for a lift limit.

At 195 knots ($\mu = .53$) and $\bar{x} = .05$, given in Figure 3.1.7, the analysis is more optimistic in predicting power requirements than at

lower speeds although the measured trend with lift is followed closely. In this case the analytical lift limit matches the test defined lift limit very well. A similar conclusion can be drawn for 225 knots (μ = .61) as presented in Figure 3.1.8. The analytical power required is optimistic but the lift limit predicted by the analysis matches the test limit within 4%.

The lift limit as a function of advance ratio for both analysis and test is shown in Figure 3.1.9. The analytical trend versus advance ratio follows the measured lift limit below μ = .4 and above μ = .5. The test does show a sharp drop in lift limit at μ = .45 which is not reflected in the analysis. There is a definite change in slope at this point, however, as the analytical line becomes almost horizontal. Both test and analysis, therefore, indicate a transition region between μ = .4 and μ = .5. The general conclusion is that C-60 can be used to predict the rotor lift limit trend as forward speed is increased. The explanation for the transition region around μ = .45 will be explored further in a later section.

The change in power required (as defined by C_p/σ) as a function of propulsive force for constant lift is shown in Figure 3.1.10 for advance ratios of 0.40 to 0.61. The conclusion can be drawn from these figures that the correlation between analysis and the test is in general not a function of propulsive force. The correlation presented at $\bar{x}$ = .05 is essentially unchanged at other propulsive force coefficients. The exception is at μ = .45 where the correlation

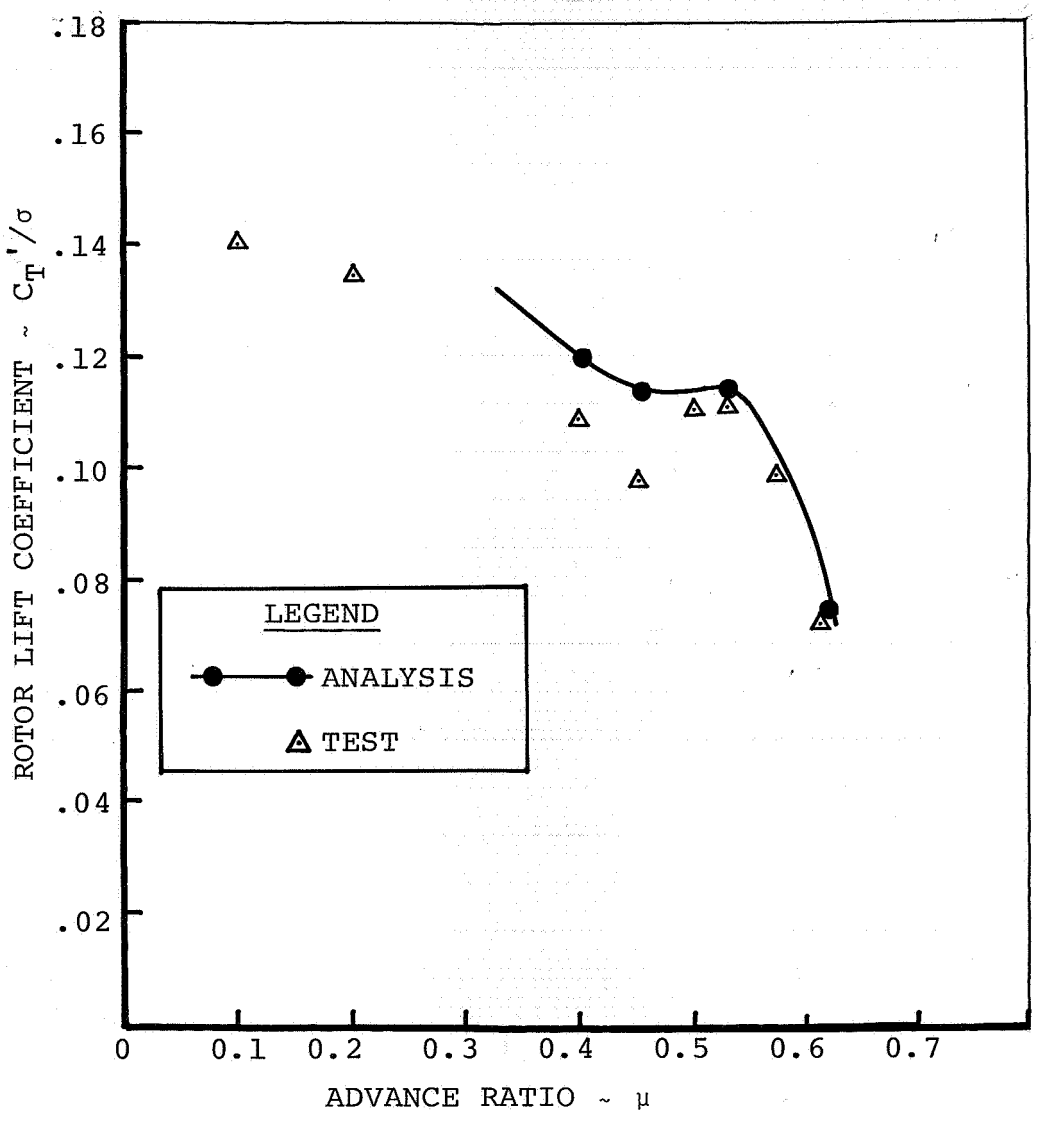

Figure 3.1.9 LIMIT LIFT COEFFICIENT VERSUS ADVANCE RATIO

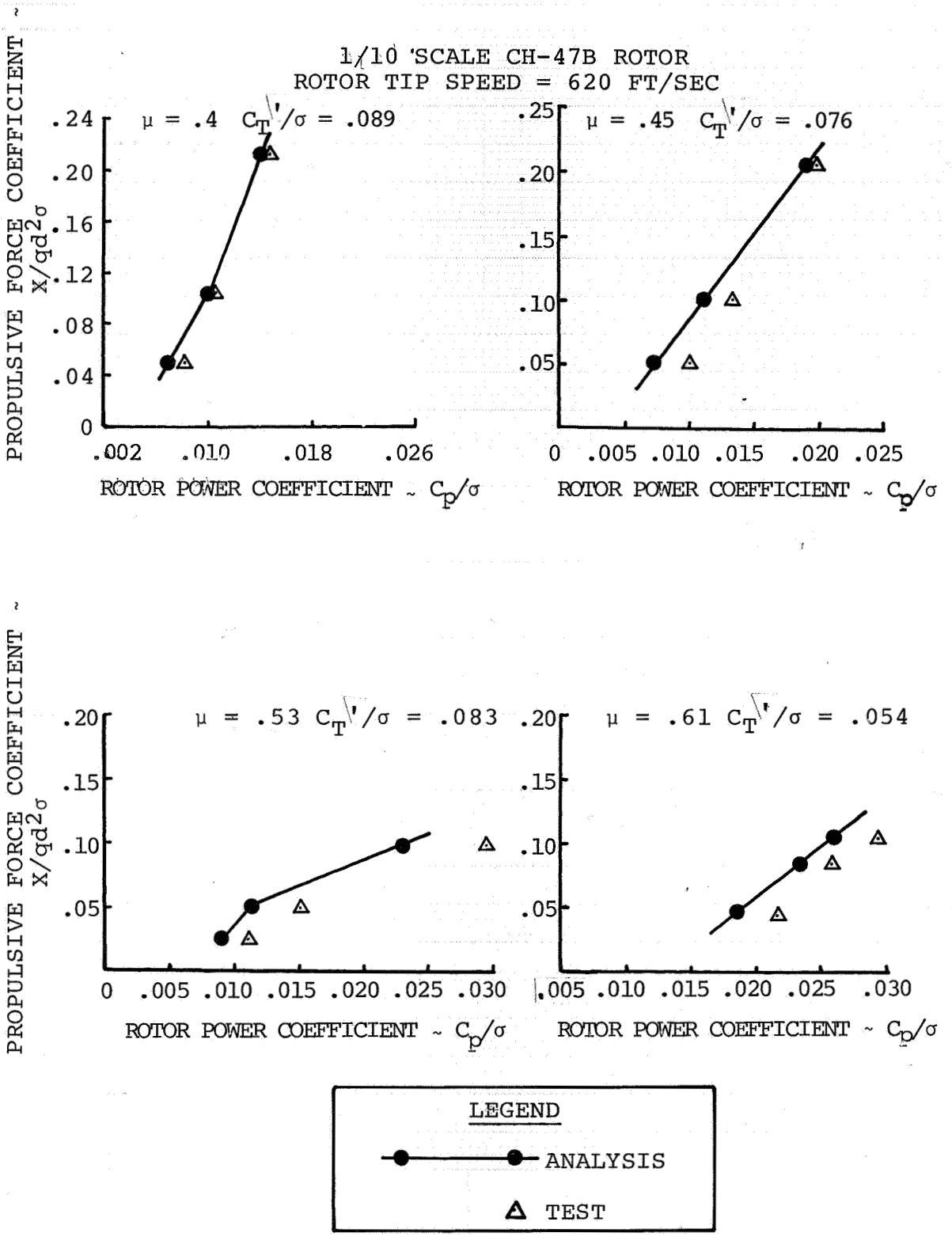

Figure 3.1.10 EFFECT OF PROPULSIVE FORCE REQUIREMENTS ON PERFORMANCE CORRELATION.

improves with higher propulsive force coefficients.

Before discussing the final performance correlation effort, an additional note about the C-60 Aeroelastic Rotor Analysis program is in order. There are several trim options available in C-60 for articulated rotors, but only two are of significance here. One trim option finds the smallest collective which results in the required thrust and then adjusts the cyclic pitch to match the desired propulsive force and side force. The second option finds the collective value closest to the input collective pitch which achieves the required thrust while matching the input values of cyclic pitch. In the latter case the propulsive force and side force which result are part of the rotor response and cannot be controlled directly.

For the purposes of this contract it was decided that the most direct approach was to match the thrust, propulsive force and side force and let the program compute its own cyclic trim schedule. At one intermediate advance ratio the second trim option, which matches the cyclic pitch input and finds the collective nearest the input value which results in the desired thrust, will be presented here. Since the μ = .45 condition resulted in the largest difference between analysis and test, this advance ratio was selected for this study. The resulting comparison of analytical and test performance data is shown in Figure 3.1.11. The correlation gives excellent agreement, but there is one problem. While the power required and

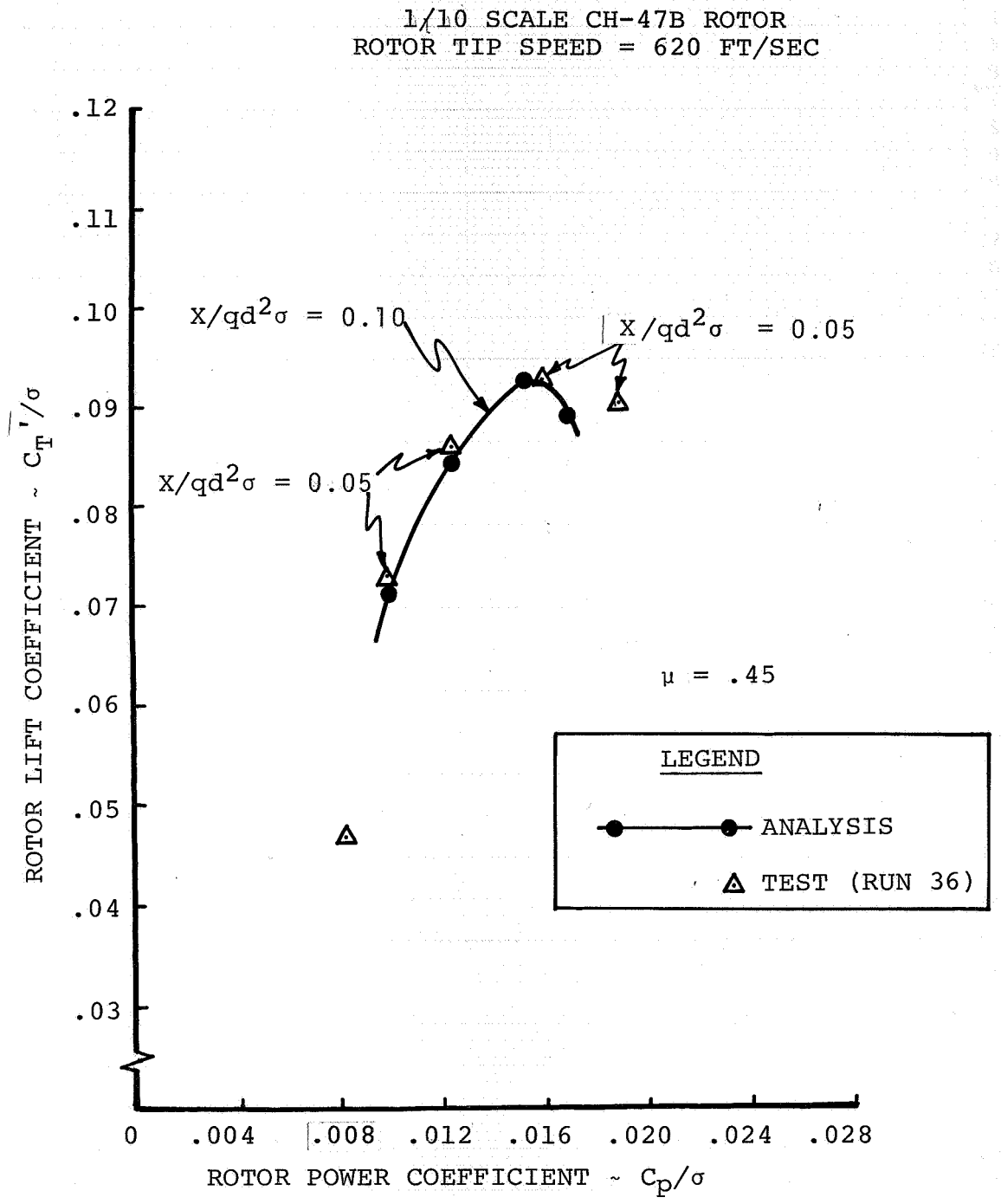

Figure 3.1.11 EFFECT OF ANALYTICAL TRIM SCHEDULE ON PERFORMANCE CORRELATION

cyclic pitch now match the test results, the propulsive force which the analysis predicts is from 70% to 250% higher than the nominal test propulsive force. A possible explanation is that the propulsive force measured in the test is low due to an error in the hub tares. This situation, while possible, is unlikely due to the excellent prediction of power required as a function of propulsive force seen in Figure 3.1.10 as well as to the loads azimuthal waveforms as will be seen at a later time.

The overall conclusion is that the analysis is effective in predicting the rotor lift limits at both low and high speeds but is optimistic in the rotor power prediction beyond an advance ratio of 0.40 for variations in both lift and propulsive force. At the intermediate speed range (165 knots) the region of the rotor that defines the maximum lift characteristics appears to be changing and the analysis shows the greatest variation from test data at this point.

These results indicate that the section drag characteristics are possibly too low at low and high Mach numbers for small angles of attack, but are too high in the reverse flow region where Mach numbers are low but angles of attack are much higher. This would account for the optimistic prediction of power required at advance ratios beyond 0.40 or the overprediction of the rotor propulsive force. Between the advance ratios of 0.40 and 0.53 there is either an inadequate definition of the local flow environment on the rotor or an optimistic maximum section lift characteristic in the middle

range of Mach numbers or in the reverse flow region.

3.2 Rotor Control Position Parameters

Three basic rotor control position parameters were investigated as part of the correlation of the C-60 analysis with test values. These parameters are: the blade collective pitch angle, the rotor disc tip path plane angle resulting from flapping, and the control axis angle. The correlation was performed for increasing thrust at constant advance ratio and propulsive force, and for increasing propulsive force at constant thrust and advance ratio.

The correlation of test and analysis for lift coefficient versus collective angle at a constant $\overline{x}$ = .05 is shown in Figures 3.2.1 and 3.2.2 for five advance ratios. The collective angle is defined as the collective pitch at the blade root projected to the 75% radial location by the built-in geometric twist. The predicted collectives at μ = .3 and μ = .4 appear to be higher than the test values by about 2 to 3 degrees. However, several of the test points at μ = .4 were repeated in the second half of the wind tunnel test, and these points are indicated by squares in Figure 3.2.1. The shift in collective pitch at a given thrust indicates the zero collective angle was repositioned after the original μ = .4 run. This appears to be confirmed by the excellent correlation of theory with test at μ = .45 and μ = .53, as shown in Figure 3.2.2.

At μ = .61 (Figure 3.2.2) the analysis shows a highly unusual trend of lift versus collective. The test data shows a similar, but less

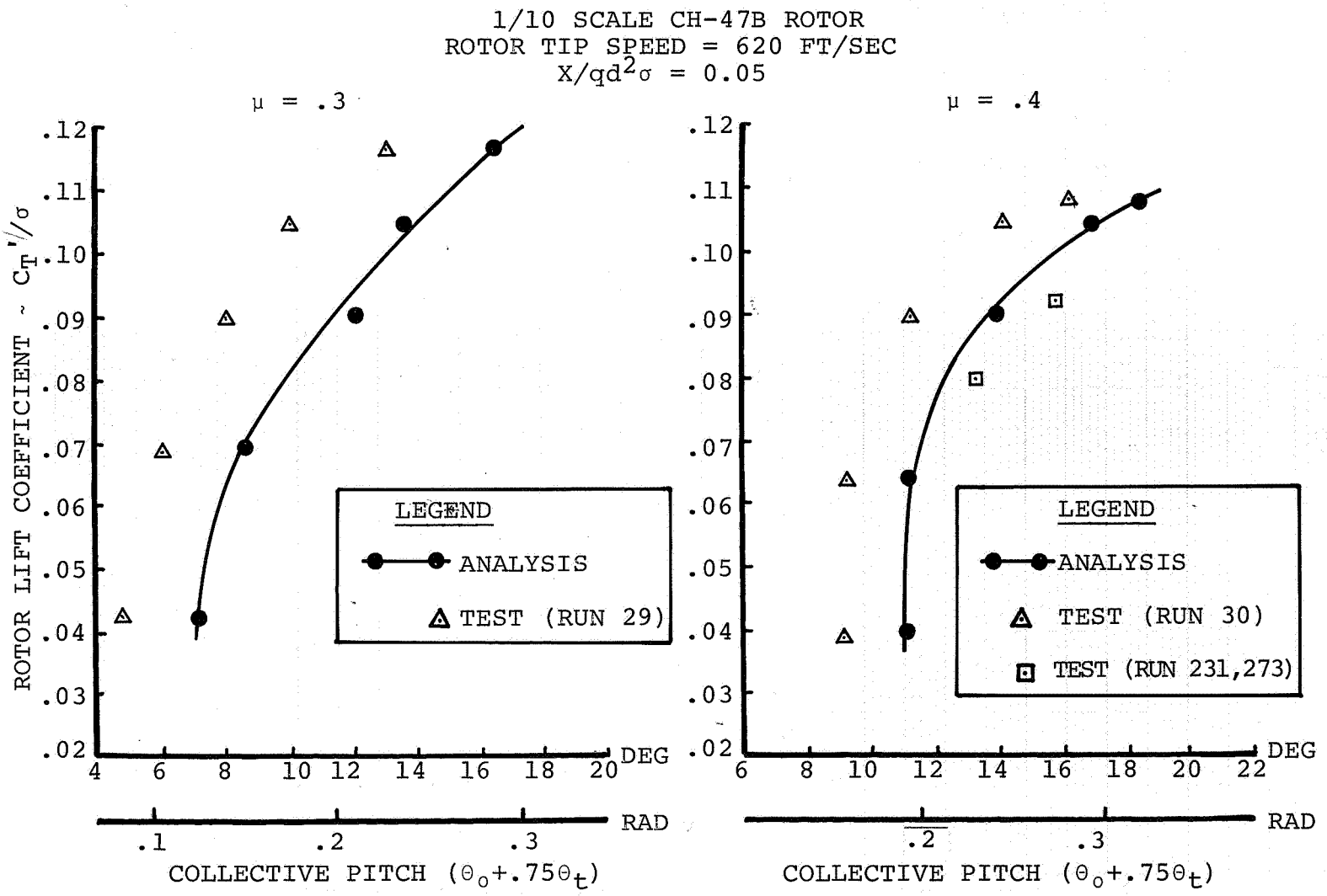

Figure 3.2.1 VARIATION OF LIFT WITH INCREASING COLLECTIVE PITCH
(μ = .3 and .4)

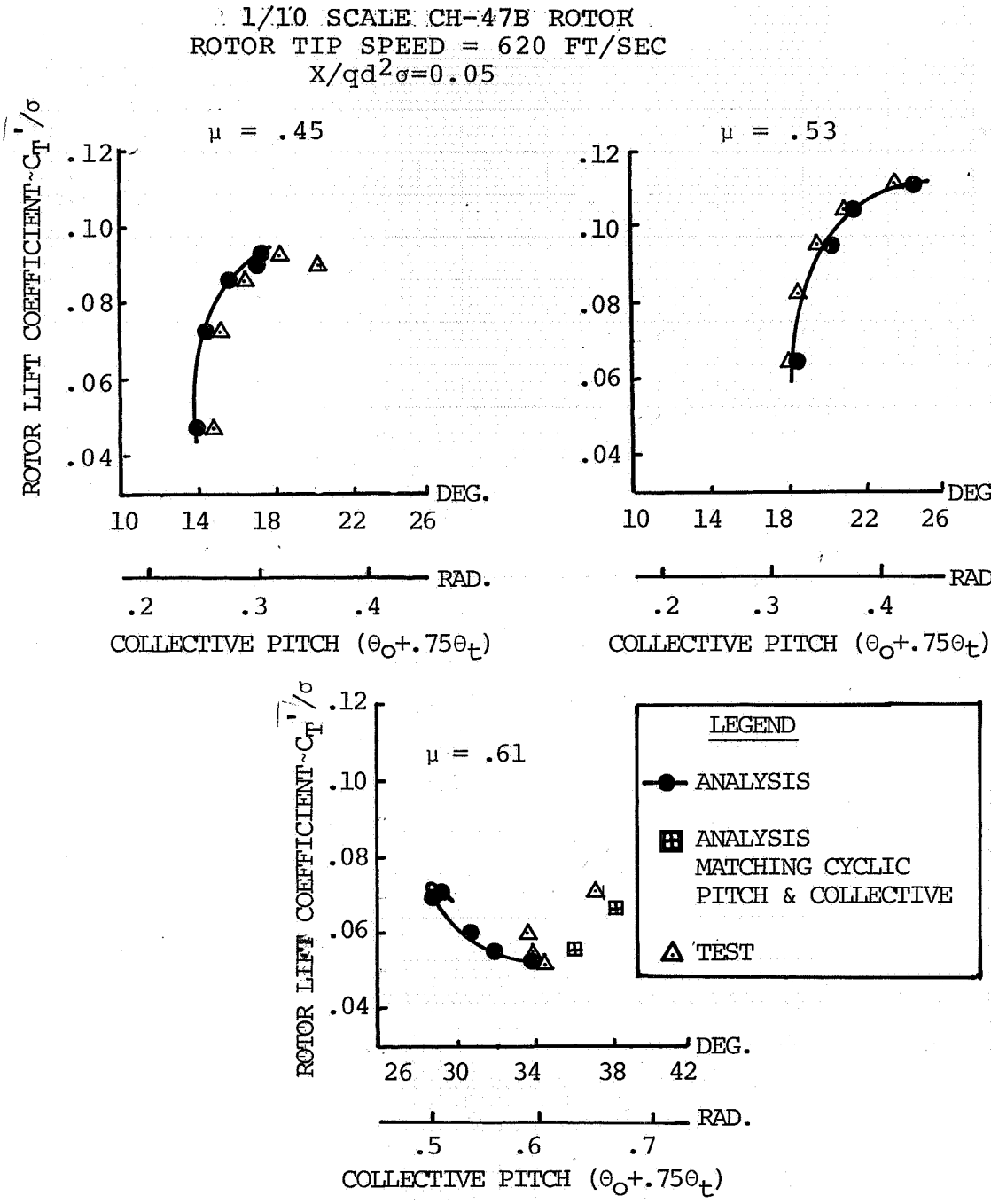

Figure 3.2.2 VARIATION OF LIFT WITH INCREASING COLLECTIVE PITCH (μ = .45, .53 and .61)

severe, trend of decreasing collective at higher lift up to a lift coefficient of $C_T'/\sigma = .06$. Beyond this point the test data reverses its trend while the analysis continues this trend up to a lift coefficient of $C_T'/\sigma = .07$.

Recall that the option used for the analysis searches for the smallest collective which produces the required thrust and propulsive force. Two points at $\mu = .61$ were recomputed matching cyclic and the input collective pitch but neglecting the side force and propulsive force trim. These points are shown as squares in Figure 3.2.2 and once again the analysis over-predicts propulsive force.

The variation of collective angle with propulsive force for a specified thrust is shown for four advance ratios in Figure 3.2.3. The correlation of test and analysis for the collective angle variation with propulsive force is good.

Also considered was the tip path plane angle resulting from cyclic flapping. A schematic of the relationship between free stream velocity, shaft tilt and cyclic flapping is shown in Figure 3.2.4. For positive shaft tilt aft and positive cosine flapping defined as flap up at an azimuth of 0^o (blade directly aft), the positive tip path plane angle is defined by the shaft tilt, i_s, minus the cosine cyclic flapping, β_{1C}. The comparisons of test and analysis for lift coefficient versus tip path plane angle at a constant $\overline{x} = .05$ are given in Figure 3.2.5 for advance ratios from $\mu = .3$ to

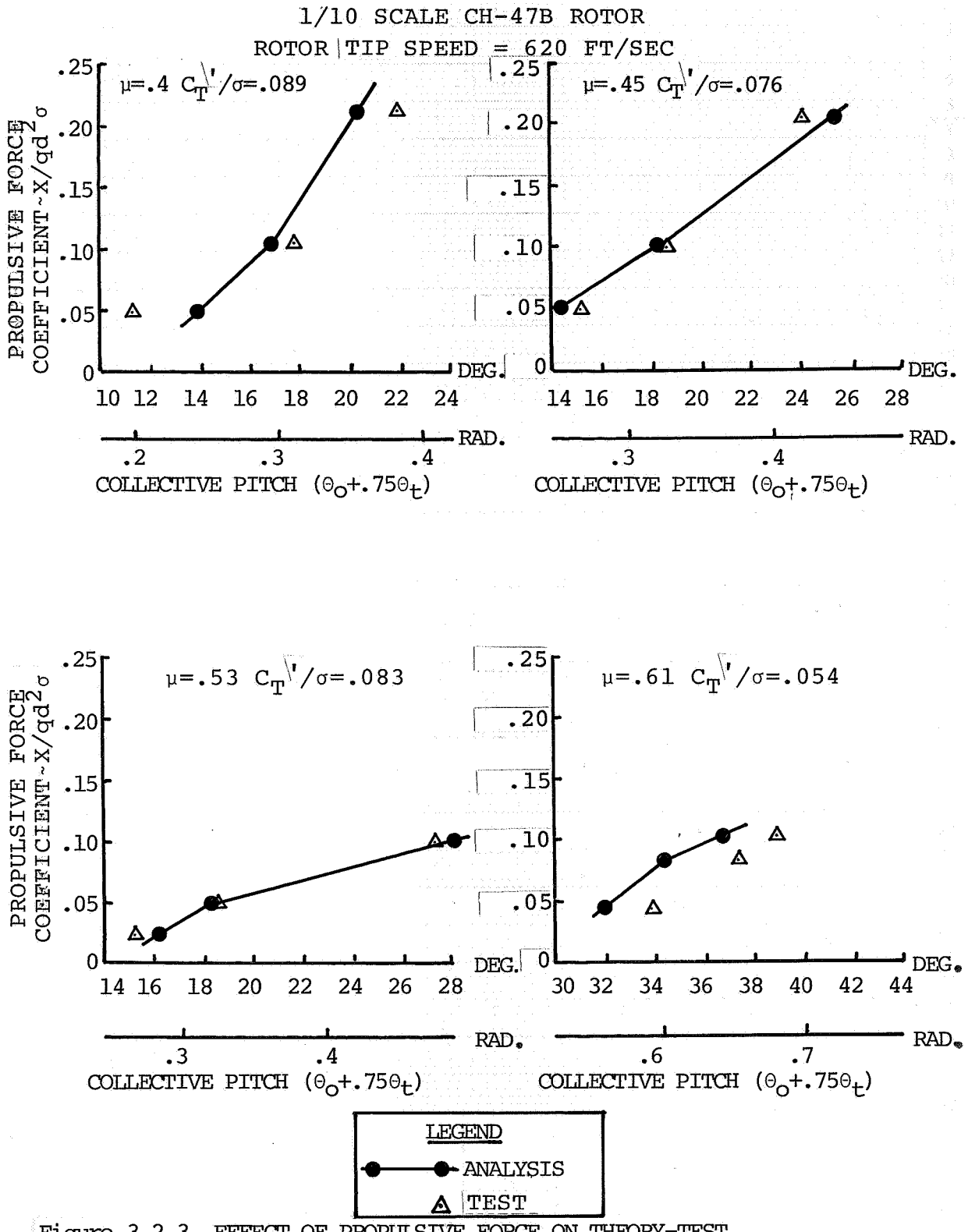

Figure 3.2.3 EFFECT OF PROPULSIVE FORCE ON THEORY-TEST CORRELATION OF COLLECTIVE PITCH ANGLE

SHAFT TILT POSITIVE AFT

COSINE FLAPPING POSITIVE UP AT 0^{o} AZIMUTH

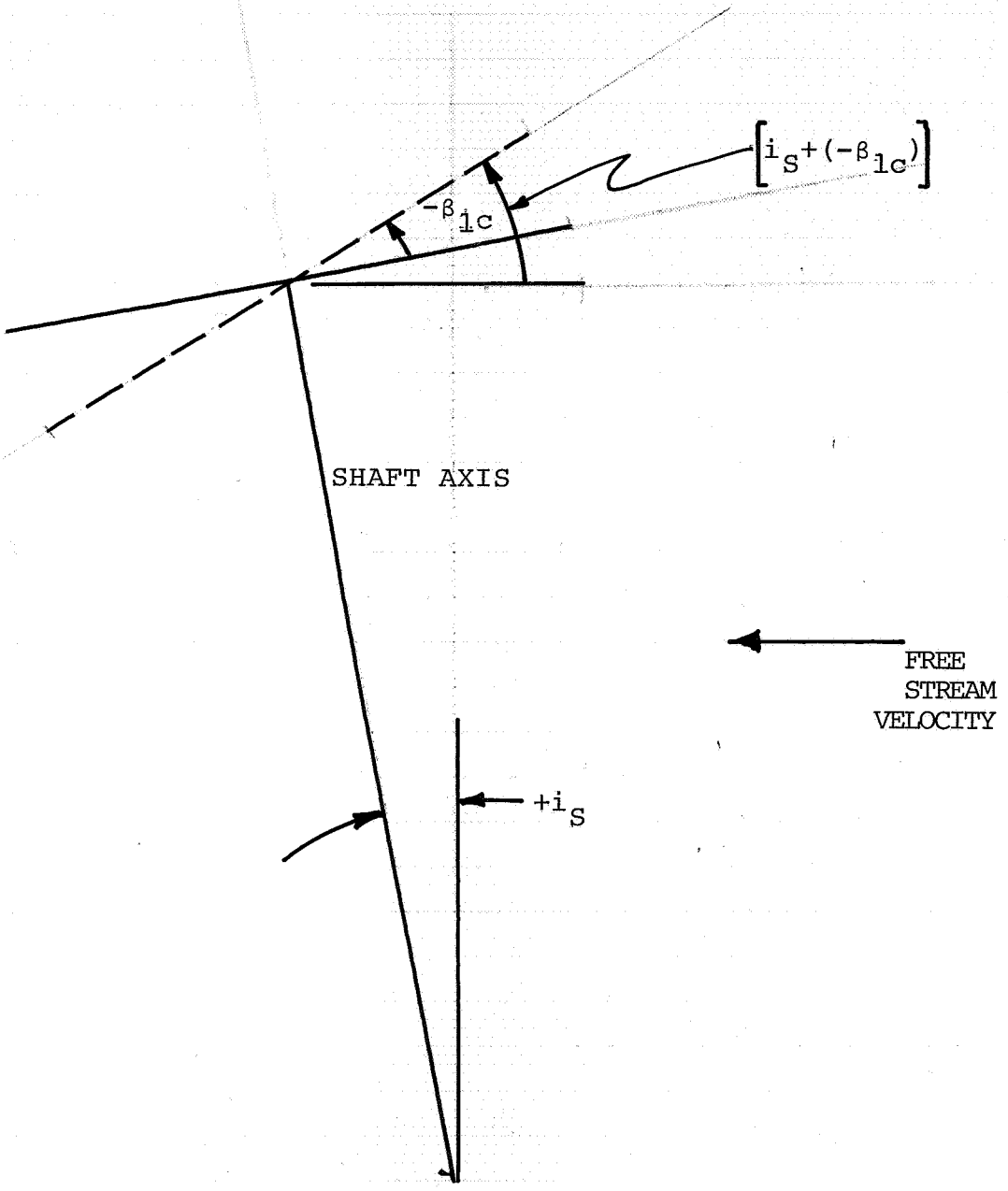

Figure 3.2.4 TIP PATH PLANE DEFINED BY CYCLIC FLAPPING

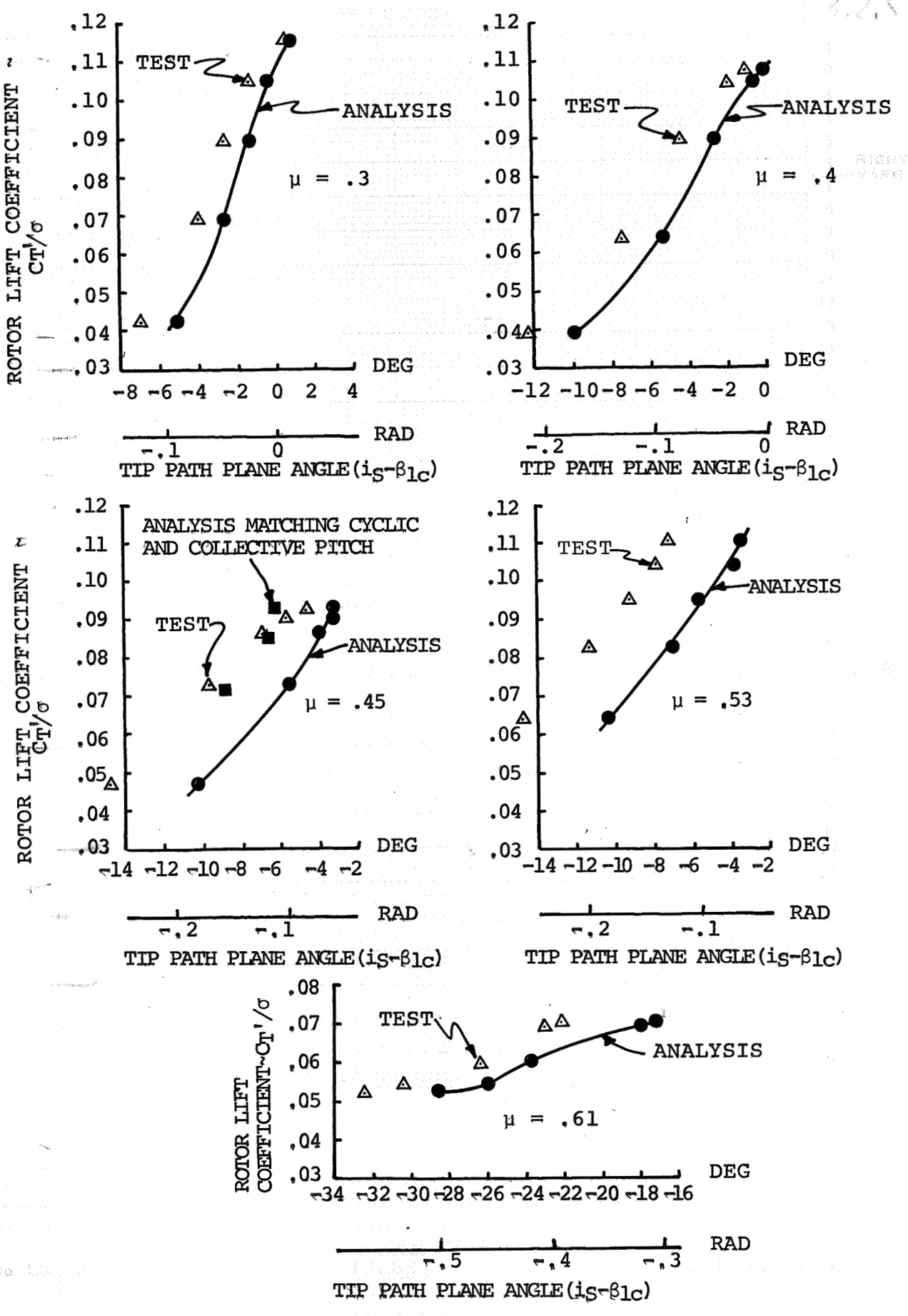

Figure 3.2.5 LIFT VARIATION WITH TIP PATH PLANE ANGLE RESULTING FROM CYCLIC FLAPPING

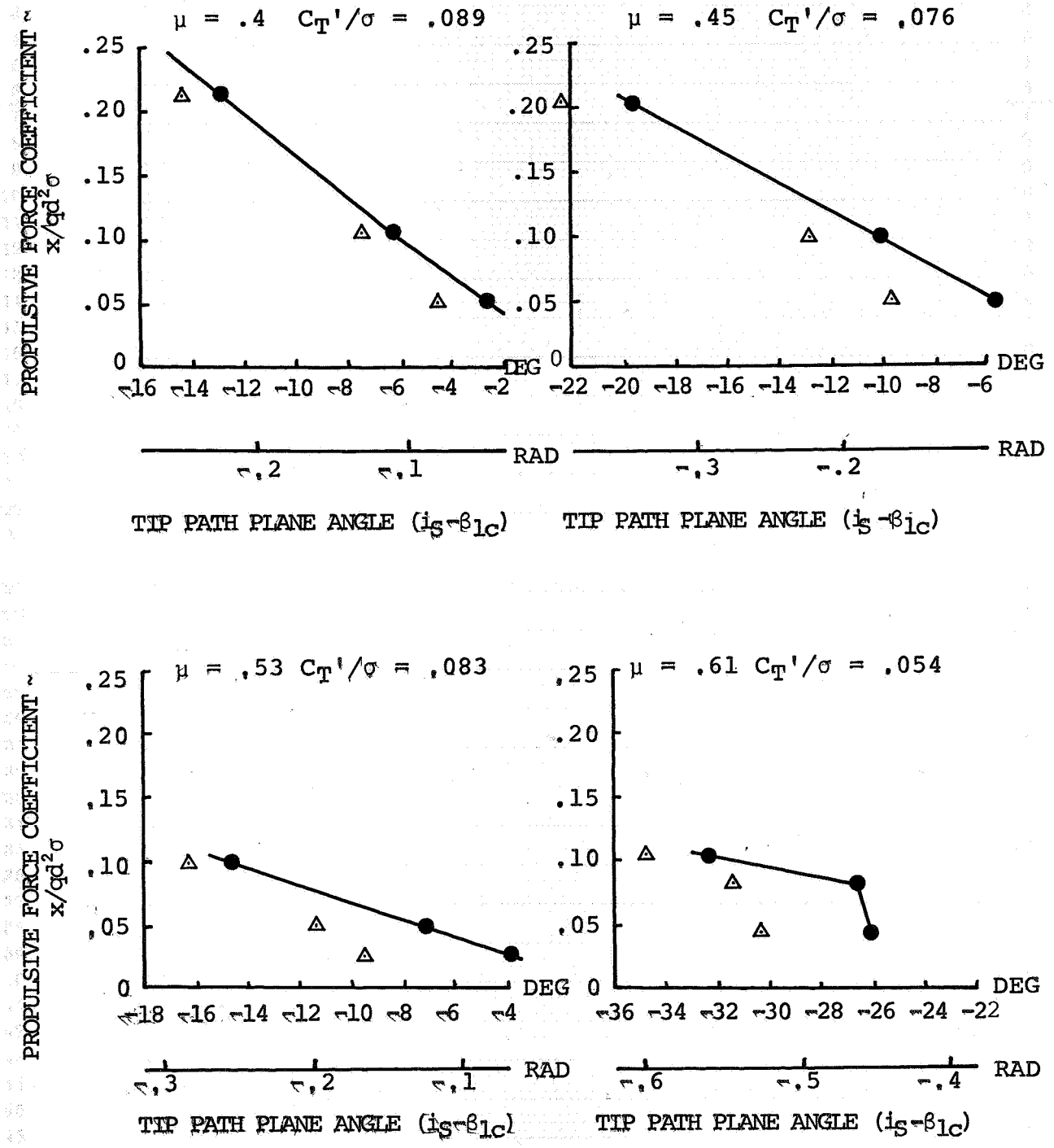

Figure 3.2.6 EFFECT OF PROPULSIVE FORCE ON THEORY-TEST CORRELATION OF TIP PATH PLANE ANGLE

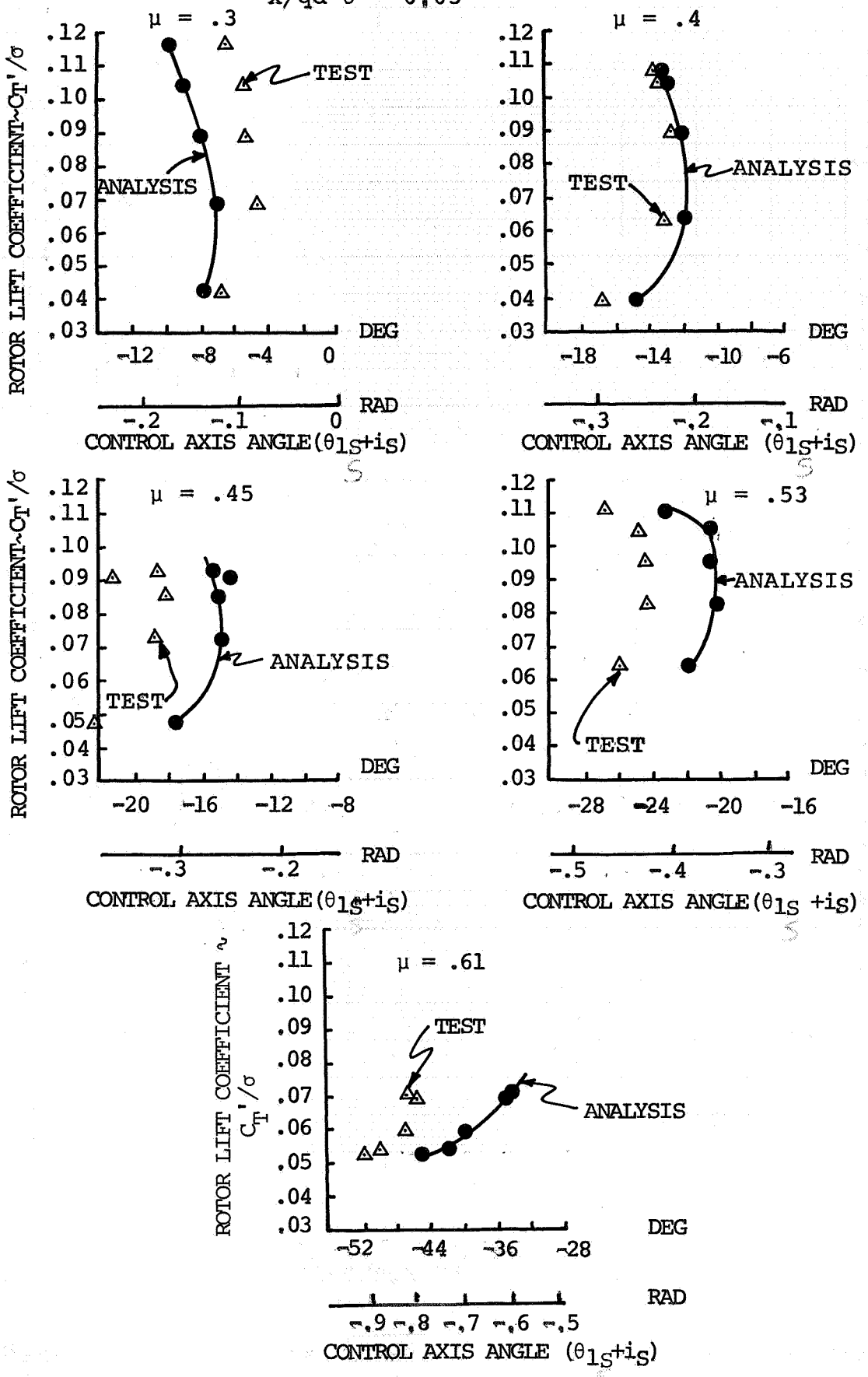

Figure 3.2.7 VARIATION OF LIFT WITH CONTROL AXIS ANGLE

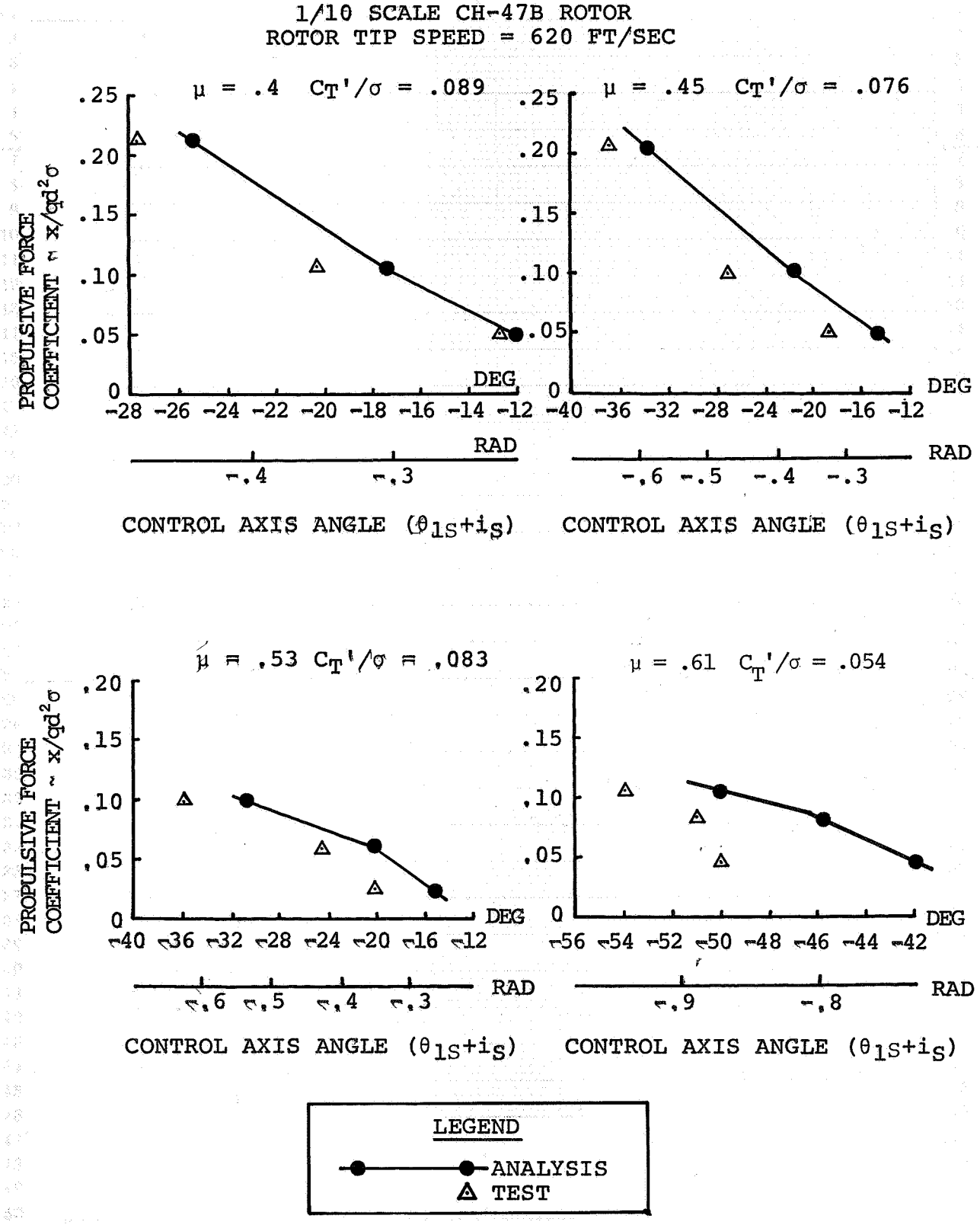

Figure 3.2.8 EFFECT OF PROPULSIVE FORCE ON CONTROL AXIS ANGLE

μ = .61. At every advance ratio the analysis is seen to follow the trend established during the test and the magnitude of the tip path plane predicted by C-60 is more positive than the value established in test. It can be concluded that the analysis generates a smaller value of drag in the disc plane (H-force) than the test would indicate. This is consistent with the performance correlation results established earlier, that the analysis shows lower power requirements than the test data.

At μ = .45 the analytical points generated by matching the cyclic and collective pitch angles are shown with the square symbols along with the test data. Again the analytical trim setting agrees with the test values but the propulsive force is higher. This is consistent with the conclusion that for a given tip path plane angle the analysis generates a smaller value of in-plane force.

The trend of tip path plane angle with increasing propulsive force at a specified thrust level is presented in Figure 3.2.6 for advance ratios from μ = .4 to μ = .61. The basic conclusion is that the correlation does not change with propulsive force.

The control axis angle of attack is defined by the sine value of the total blade pitch angle. In this case positive cyclic pitch input (θ_{1S}) at an azimuth of 90^{o} produces flap up at 180^{o} azimuth. The control axis angle is defined by $\theta_{1S} + i_{s}$. The analytical and measured variation of control axis angle with increasing lift is plotted in Figure 3.2.7 for $\overline{x}$ = .05 and advance ratios of μ = .3

through μ = 61. It can be seen that the analysis does predict the general trend of control axis angle due to cyclic pitch versus lift coefficient as measured in the wind tunnel for all values of advance ratio investigated.

The analysis starts out at low speed to require slightly higher negative values of control axis angle of attack but as the forward speed is increased the analysis rapidly shows a requirement for less forward tilt of the disc plane than required by the test data. This is consistent with the conclusion just established that for a given propulsive force the analysis requires less forward tilt of the disc plane, while still showing the proper trends with increasing lift coefficient.

Figure 3.2.8 shows the relationship between control axis angle due to cyclic pitch and the propulsive force for a specified value of thrust and advance ratio. From μ = .4 to μ = .53 the degree of correlation does not change with propulsive force. At μ = .61 the test data and analytical lines are no longer parallel.

3.3 Loads Correlation

The blade loads correlation between the C-60 analysis and the test data was performed for the midspan flap bending moment and for both the inboard and midspan torsion loads. The inboard flap moments were not used for correlation due to the fact that for an articulated rotor the root loads are so low that no meaningful waveform analysis would be possible.

The comparisons of the measured and analytical flap bending moments versus azimuth position for advance ratios from 0.30 to 0.53 are given in Figures 3.3.1 and 3.3.2. For each advance ratio the midspan flap bending waveform is shown at a low thrust level and at the lift limit for that particular advance ratio at a propulsive force coefficient of .05. The analysis predicts the phase and magnitude of the midspan flap bending moment with reasonable accuracy for all thrust levels and advance ratios considered. Similar results are shown in Figure 3.3.3 for μ = .53 for two other propulsive force coefficients, indicating the same degree of correlation of theory and test as at the other propulsive force coefficients.

The torsion loads correlation was performed using both the inboard and midspan blade torsion loads waveforms. Figures 3.3.4 through 3.3.8 present the comparison of inboard torsion waveforms for both test and analysis at five different advance ratios. Each figure contains the correlation of test and analysis for a particular advance ratio at $\bar{x}$ = .05 as thrust is increased up to the lift limit. Figures 3.3.9 through 3.3.12 display the same data for the midspan torsion waveforms. No data was available for the midspan torsion waveforms at μ = .61 since that gauge had failed prior to that high speed run. Briefly, the correlation is good at low thrust levels, particularly on the advancing side of the disc, and the correlation degrades to some extent as the thrust is increased. The largest difference between theory and test is the failure of the theory to predict the nose down stall at 225^{o} azimuth at high thrusts. In general there is a phase shift of approximately 30 degrees between

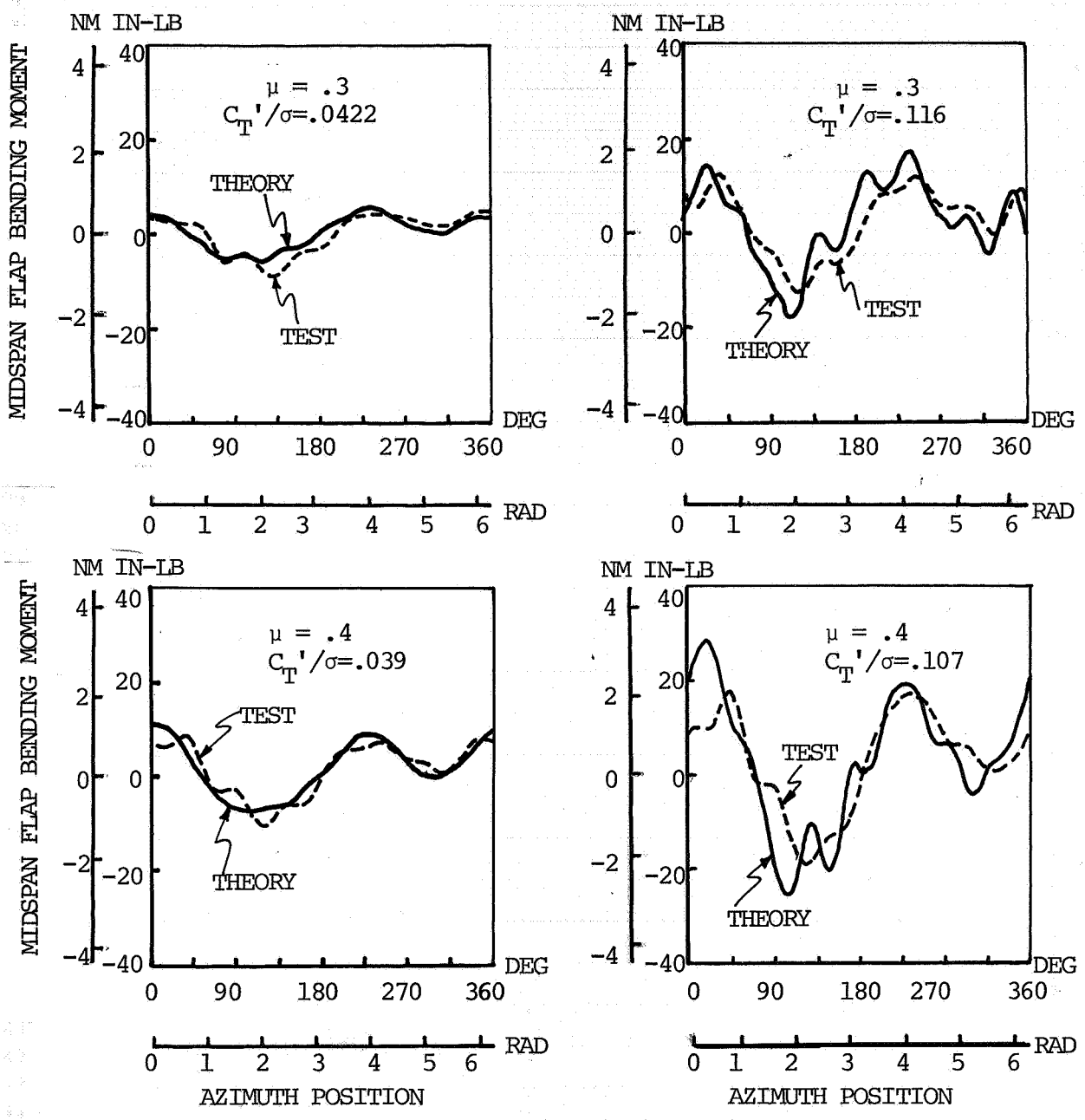

Figure 3.3.1 CORRELATION OF MIDSPAN FLAP BENDING WAVEFORMS AT 110 KNOTS AND 147 KNOTS

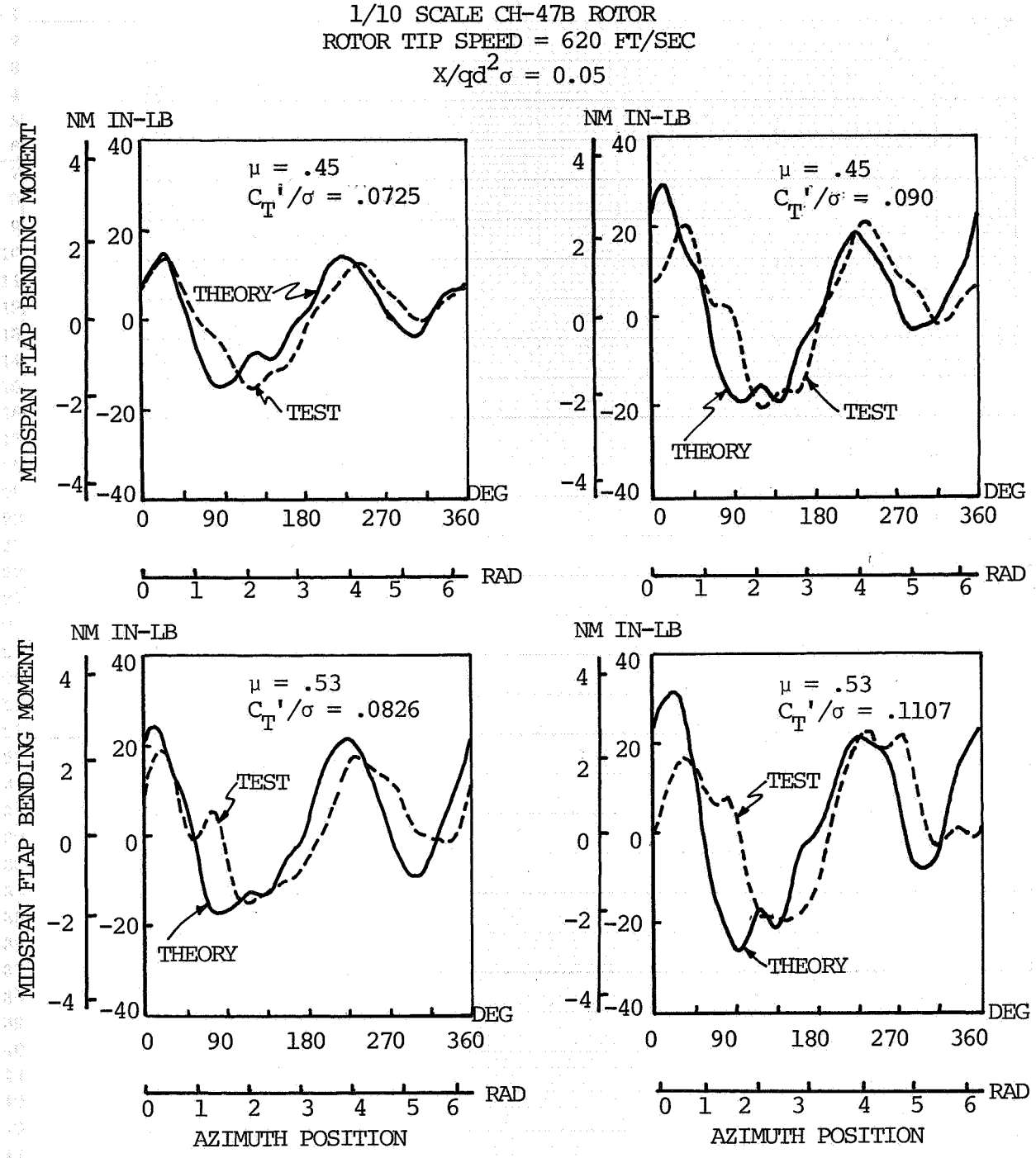

Figure 3.3.2 CORRELATION OF MIDSPAN FLAP BENDING WAVEFORMS AT 165 KNOTS AND 195 KNOTS

1/10 SCALE CH-47B ROTOR
ROTOR TIP SPEED = 620 FT/SEC
μ = 0.53

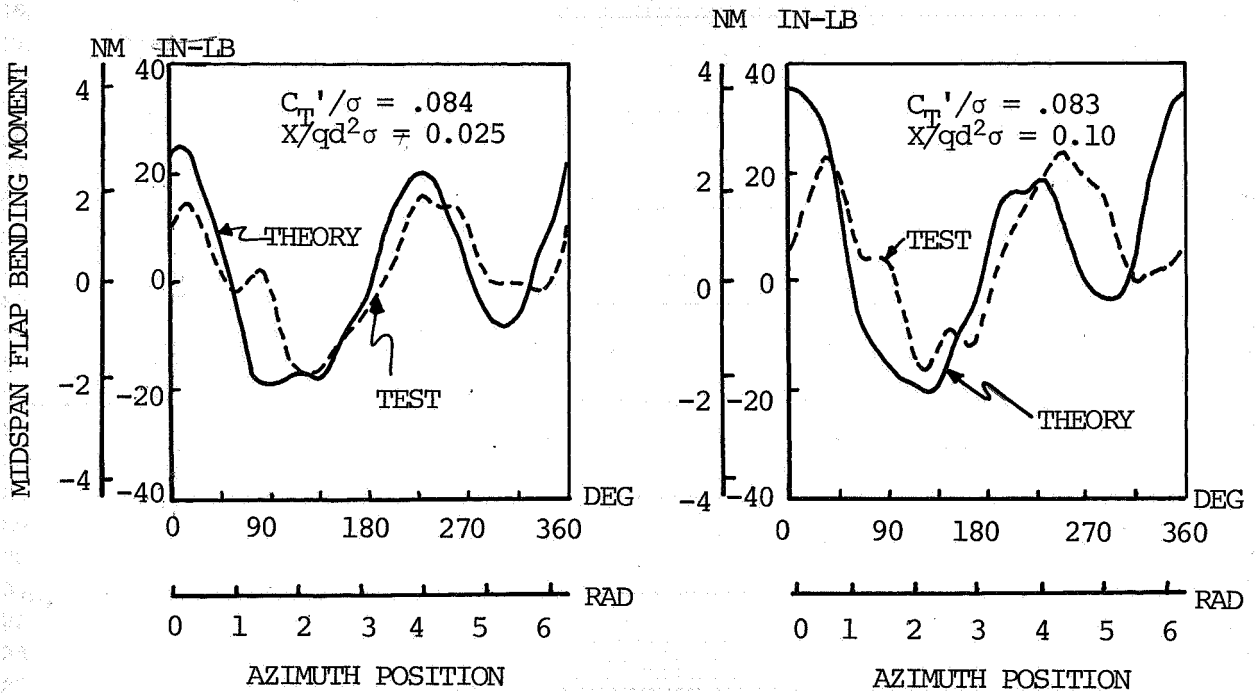

Figure 3.3.3 EFFECT OF PROPULSIVE FORCE ON MIDSPAN FLAP BENDING WAVEFORM CORRELATION

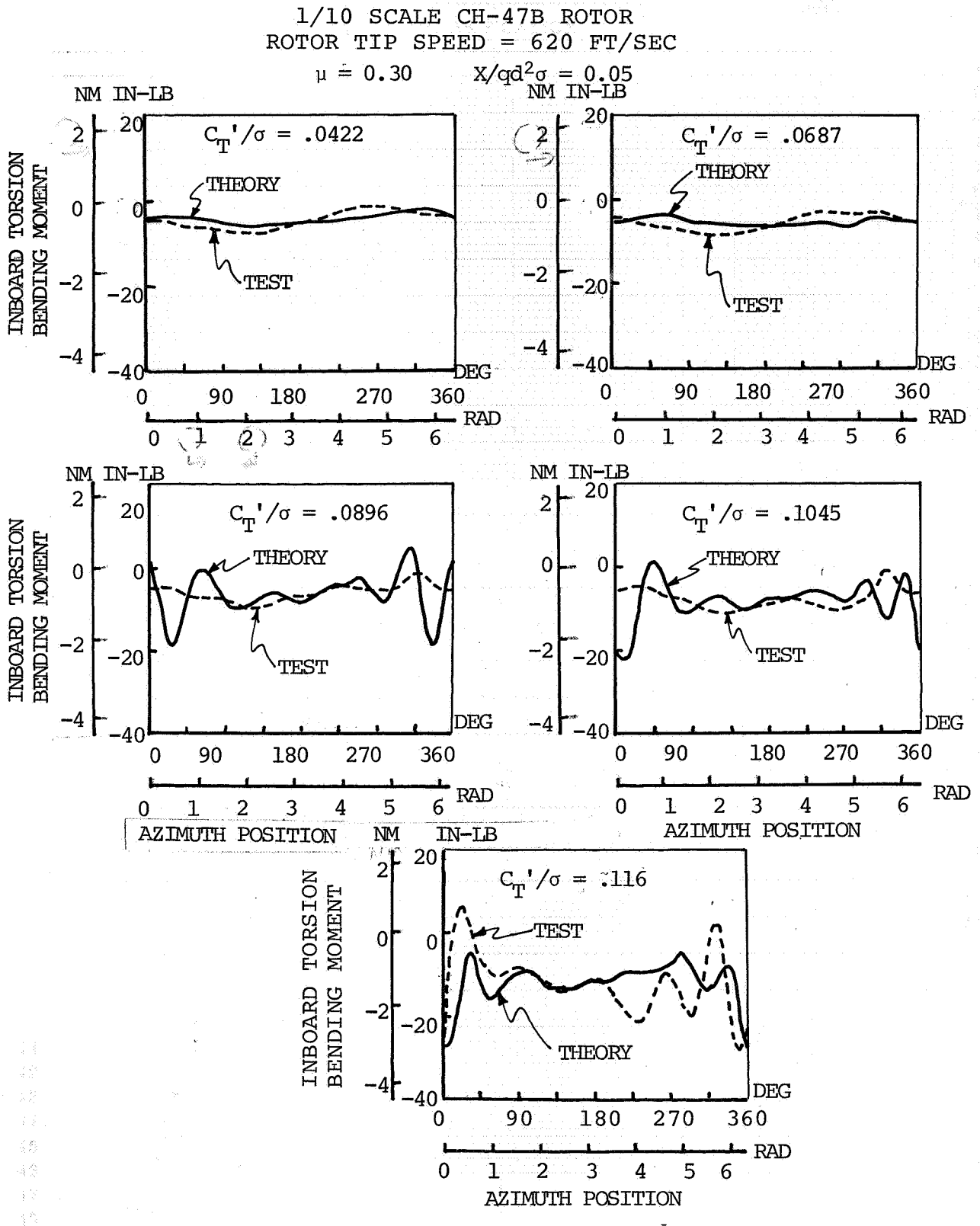

Figure 3.3.4 INBOARD TORSION WAVEFORM CORRELATION AT 110 KNOTS

1/10 SCALE CH-47B ROTOR
ROTOR TIP SPEED = 620 FT/SEC
$\mu = 0.40 \quad X/qd^2\sigma = 0.05$

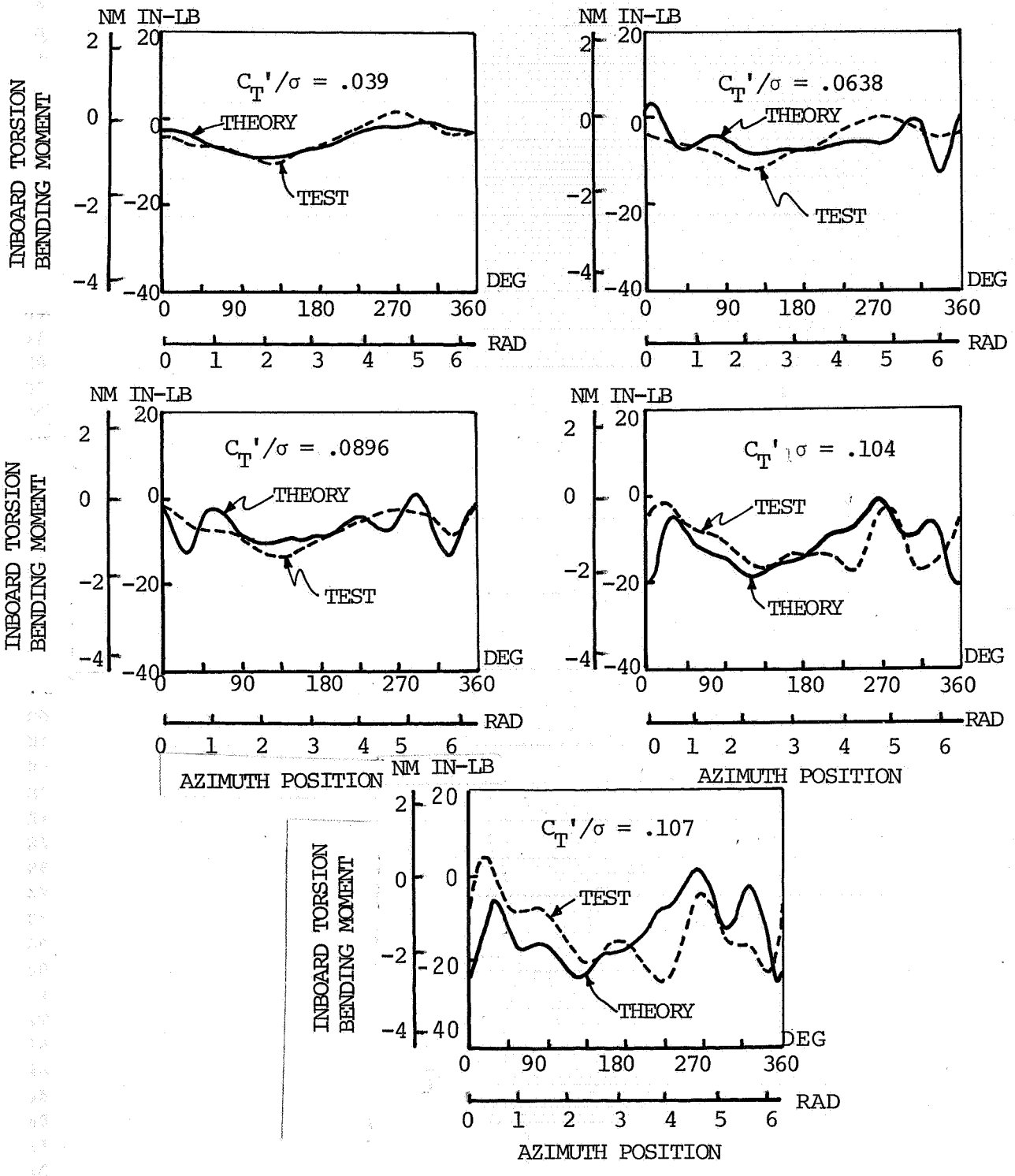

Figure 3.3.5 INBOARD TORSION WAVEFORM CORRELATION AT 147 KNOTS

1/10 SCALE CH-47B ROTOR
ROTOR TIP SPEED = 620 FT/SEC
μ = 0.45 $X/qd^2\sigma$ = 0.05

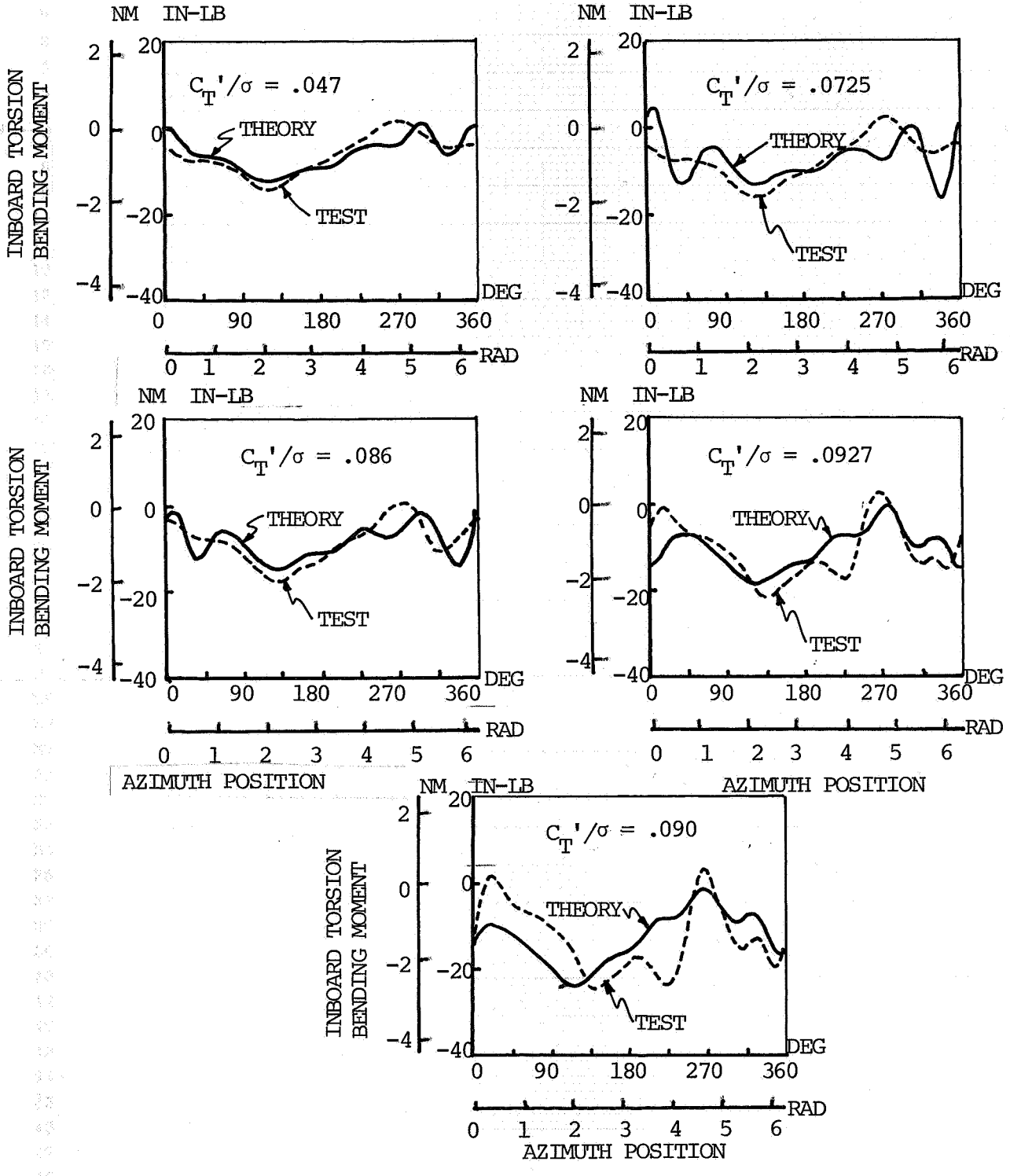

Figure 3.3.6 INBOARD TORSION WAVEFORM CORRELATION AT 165 KNOTS

1/10 SCALE CH-47B ROTOR
ROTOR TIP SPEED = 620 FT/SEC
μ = 0.53 $X/qd^2\sigma$ = 0.05

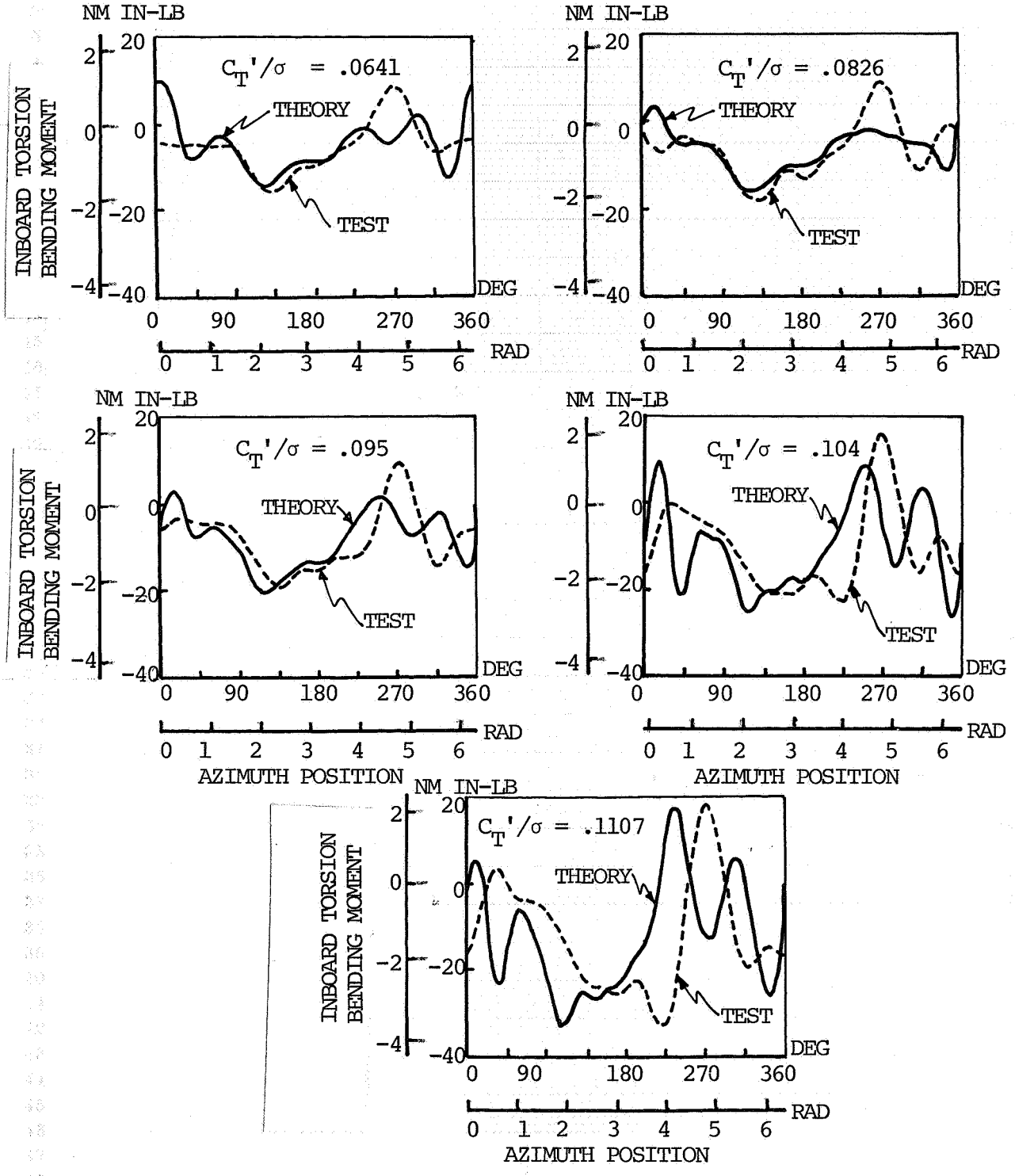

Figure 3.3.7 INBOARD TORSION WAVEFORM CORRELATION AT 195 KNOTS

1/10 SCALE CH-47B ROTOR
ROTOR TIP SPEED = 620 FT/SEC
$\mu = 0.61$ $X/qd^2\sigma = 0.05$

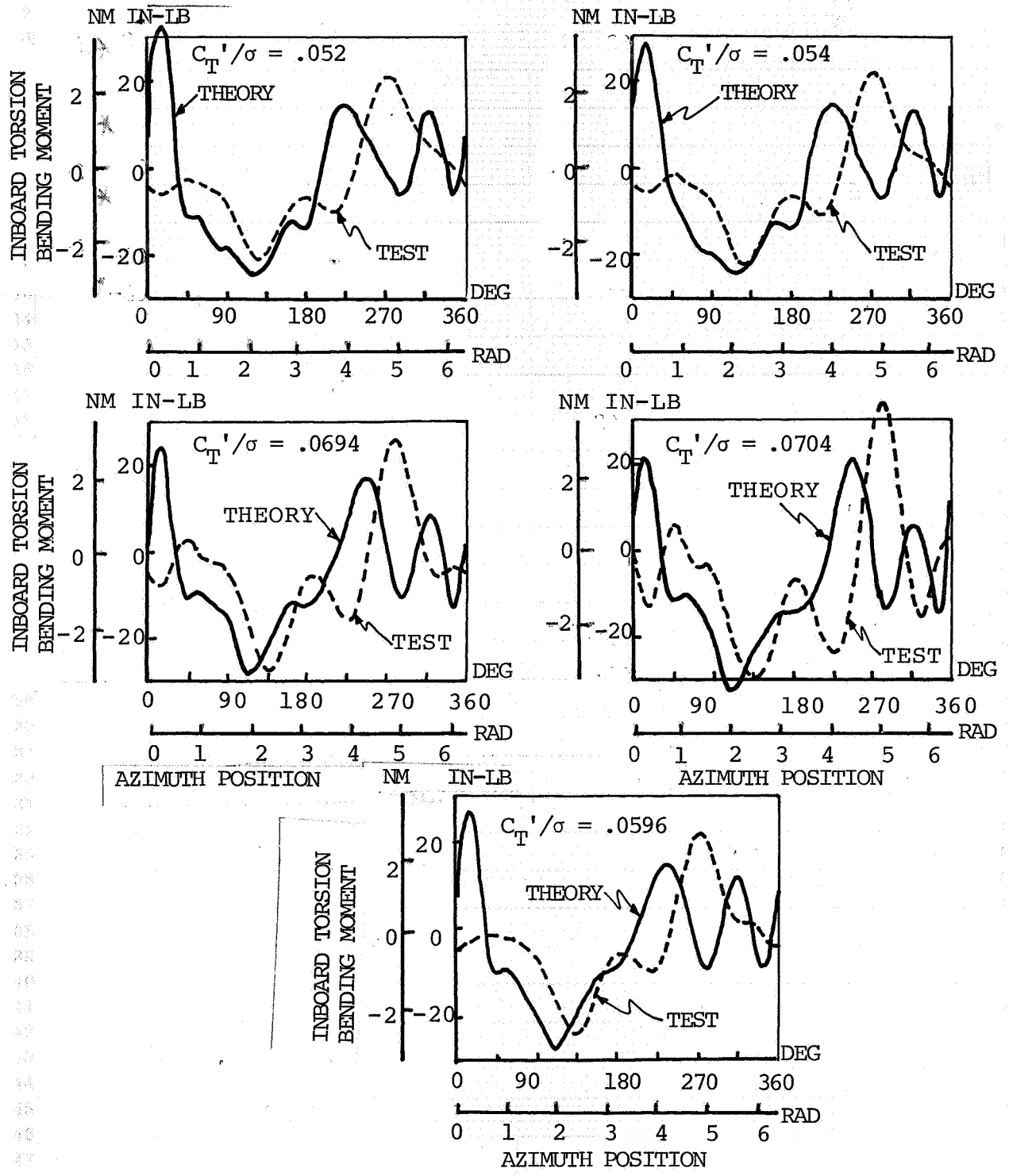

Figure 3.3.8 INBOARD TORSION WAVEFORM CORRELATION AT 224 KNOTS

1/10 SCALE CH-47B ROTOR

ROTOR TIP SPEED = 620 FT/SEC

$\mu = 0.30 \quad X/qd^2\sigma = 0.05$

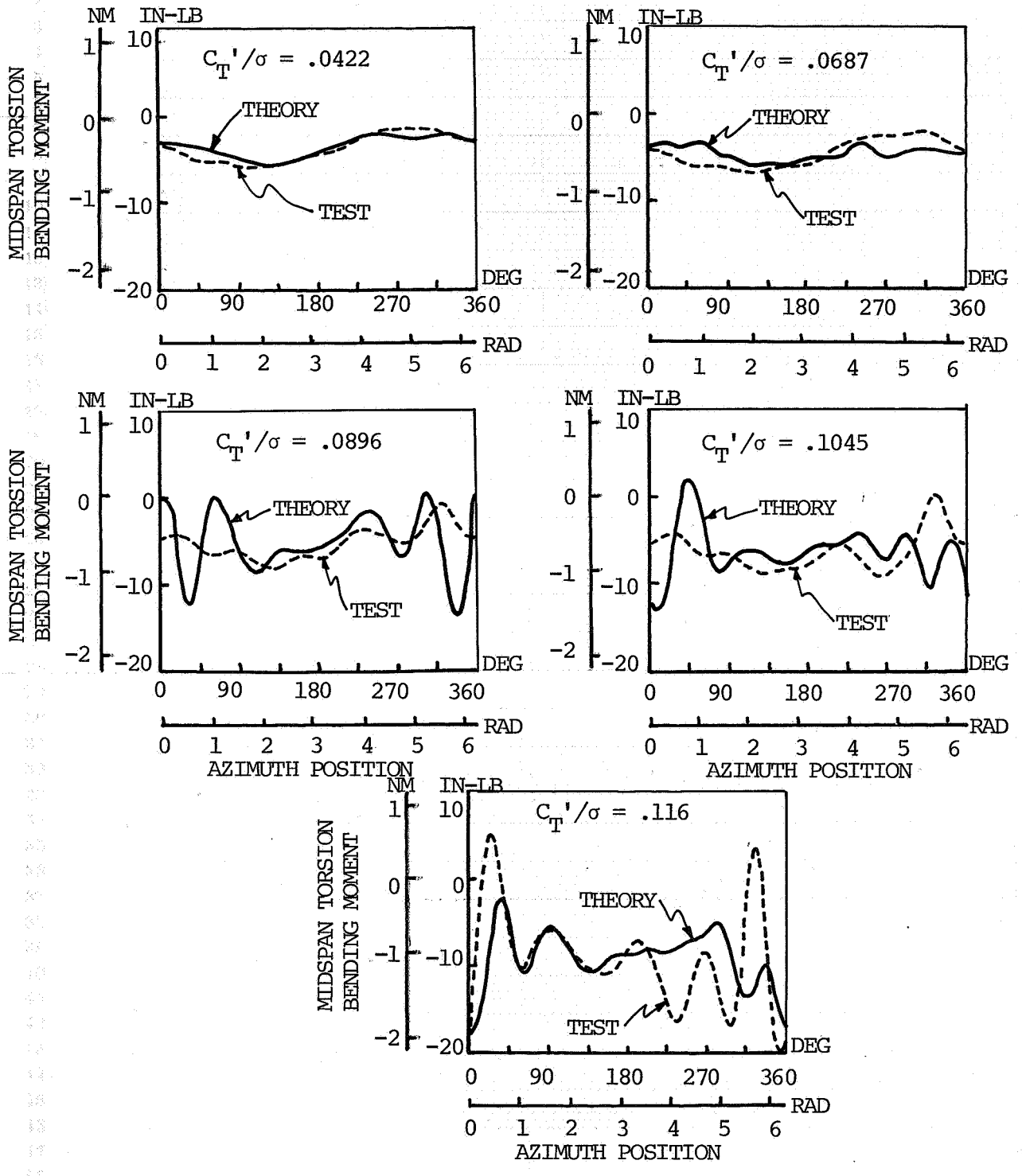

3.3.9 MIDSPAN TORSION WAVEFORM CORRELATION AT 110 KNOTS

1/10 SCALE CH-47B ROTOR
ROTOR TIP SPEED = 620 FT/SEC
$\mu = 0.40$ $X/qd^2\sigma = 0.05$

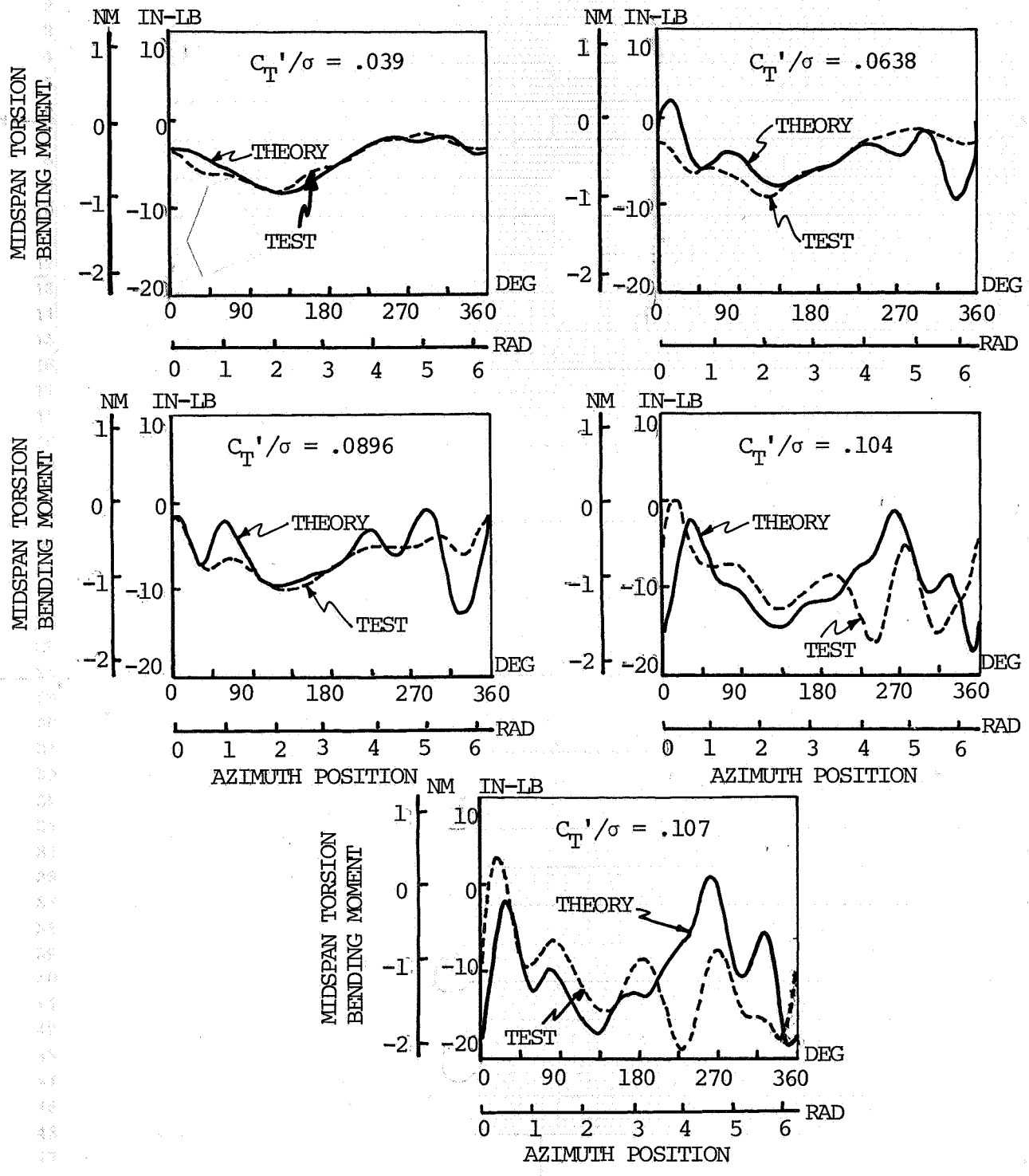

Figure 3.3.10 MIDSPAN TORSION WAVEFORM CORRELATION AT 147 KNOTS

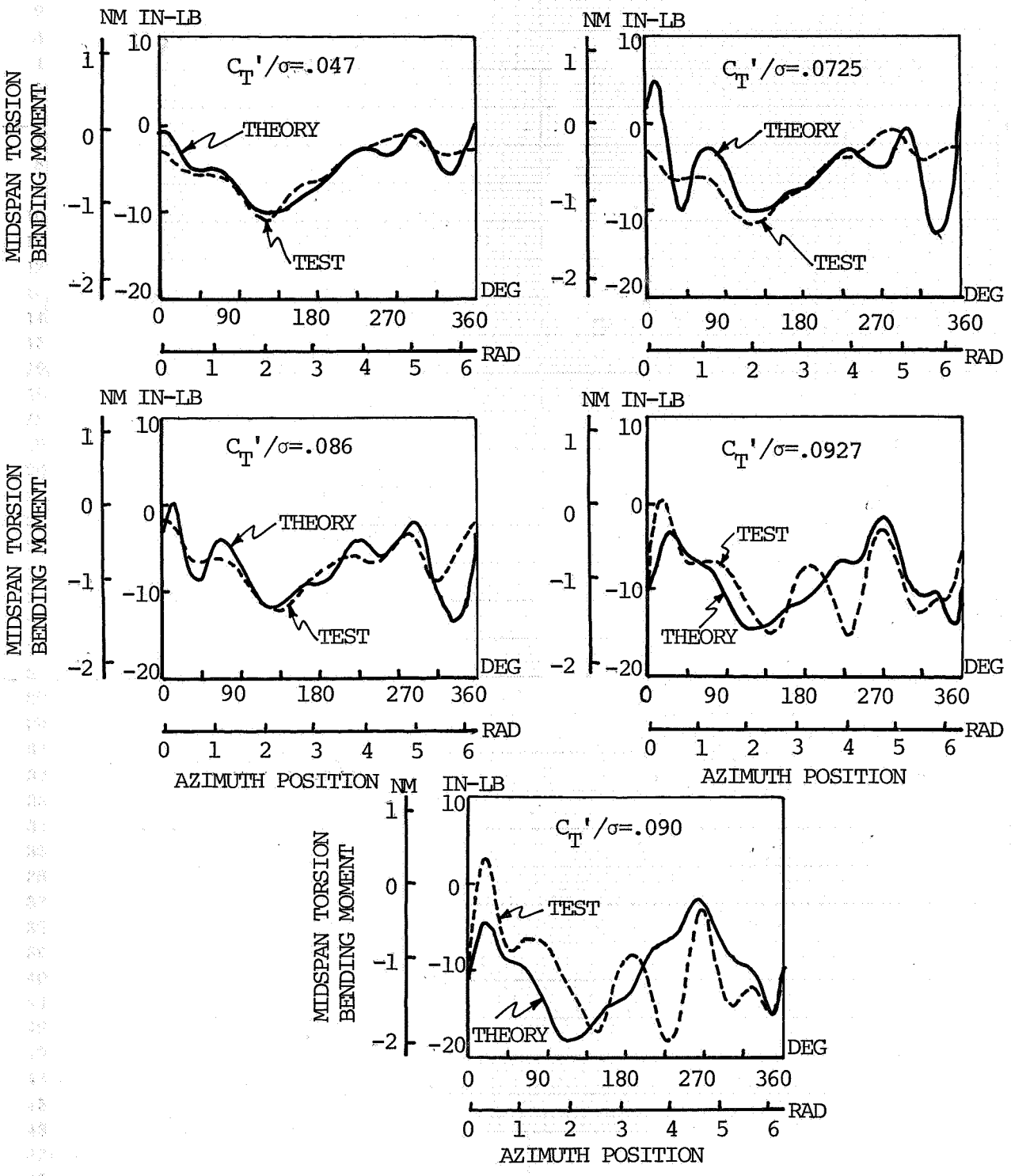

Figure 3.3.11 MIDSPAN TORSION WAVEFORM CORRELATION AT 165 KNOTS

1/10 SCALE CH-47B ROTOR
ROTOR TIP SPEED = 620 FT/SEC
μ = 0.53 $X/qd^2\sigma$ = 0.05

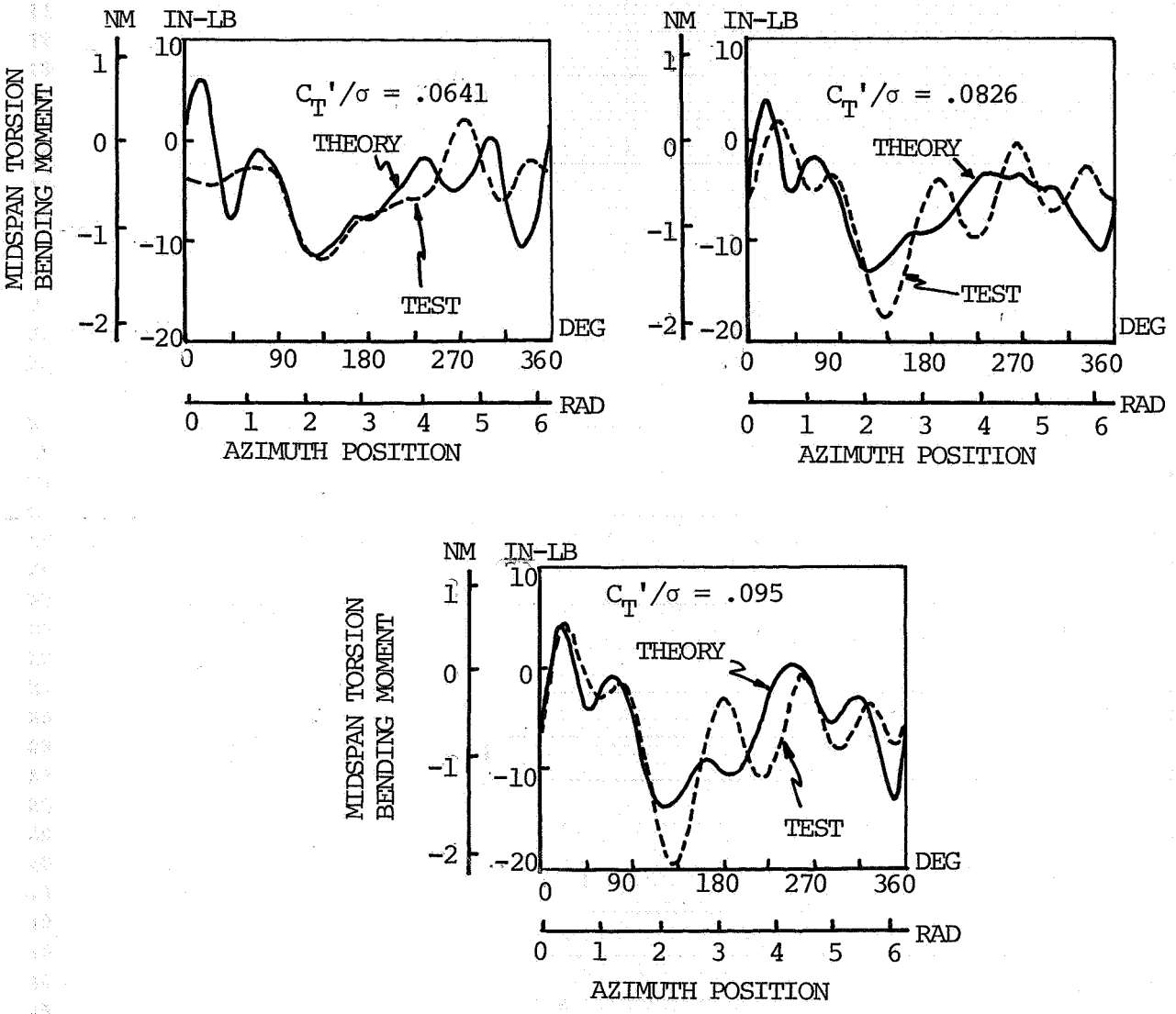

Figure 3.3.12 MIDSPAN TORSION WAVEFORM CORRELATION AT 195 KNOTS

theory and test.

The results of the correlation effort are essentially the same for both inboard and midspan torsion loads at each advance ratio. A typical example is at $\mu = .4$ for the inboard torsion load (Figure 3.3.5). At the lowest thrust level the test and analytical waveform are nearly identical. As the thrust is increased the analysis shows an earlier tendency to stall. Note that at $C_T'/\sigma = .0638$ and $C_T'/\sigma = .0896$ over the retreating blade region of the rotor disc the analysis is responding at approximately six per rev, which is close to the first torsional natural frequency. This is an indication of stall. At $C_T'/\sigma = .104$ the test data now shows the same characteristics, and the analysis and test are again in good agreement. Finally, as the lift limit is approached ($C_T'/\sigma = .1075$) the test waveform now shows more pronounced peaks which is a good indication that the test is now experiencing a greater amount of stall. To summarize, the analysis shows a tendency to stall at lower lift coefficients, but the slope of the stall curve is more gradual than the test data so that at higher thrusts the test blade is further into the stall.

In general the torsion loads correlation is fair. The peak-to-peak amplitudes agree and in most instances the phases do not vary more than 30^o. The major difference is at the lift limit where the analytical waveform does not show the conventional stall at an azimuth of 225^o that is shown in the test waveform. At the highest forward speeds ($\mu = .53$ and $\mu = .61$) the test does indicate some

negative stall (which is occurring in the reverse flow region) represented by the large positive (nose-up) moment at a rotor azimuth of 270^{o}. This appears in the analytical waveform at approximately 225^{o} and to a lesser extent at 315^{o} azimuth.

The correlation of theory with test data is of sufficient accuracy for the purposes of this contract, especially at the higher speeds, which makes it a useful tool in determining the rationale for the rotor lift limits.

Some typical results for two different propulsive force coefficients are shown in Figure 3.3.13 at an advance ratio of $\mu = .45$. The lift coefficient is essentially the same for both graphs. In each case the analysis is predicting stall while the test shows no indication of stall. This shows that for both propulsive force levels the analysis predicts stall inception at a lower lift coefficient than occurs in test.

It was mentioned in Section 3.1 that the investigation of performance correlation using the analytical trim procedure of matching thrust and cyclic pitch appeared to correlate better on power required but was high on propulsive force. A possible reason for that difference could be due to an error in the calibration of hub drag during the test. However, a look at the resulting torsion waveforms seems to discount this possibility. Figure 3.3.14 shows the correlation at $\mu = .45$ for two thrust levels for $\overline{x} = .05$ using the trim option to match cyclic pitch. Recall that the analytical propulsive force coefficient was close to $\overline{x} = .1$ as a consequence of the resultant flapping motion. The analytical waveforms now show a much greater response than the test as opposed to the previously good correlation

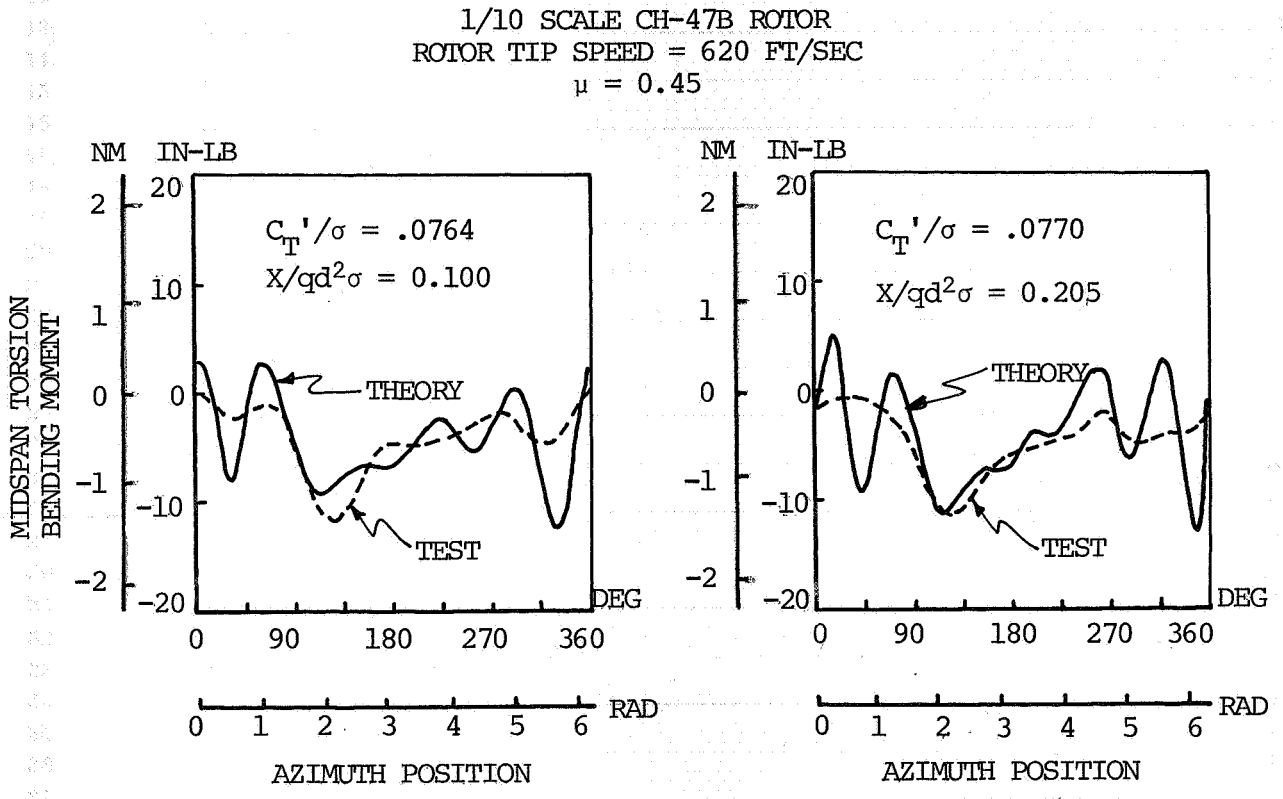

Figure 3.3.13 EFFECT OF PROPULSIVE FORCE ON MIDSPAN TORSION WAVEFORM CORRELATION

1/10 SCALE CH-47B ROTOR
ROTOR TIP SPEED = 620 FT/SEC
$\mu = 0.45$ $X/qd^2\sigma = 0.05$
ANALYSIS MATCHING TEST CYCLIC AND
COLLECTIVE PITCH ANGLES

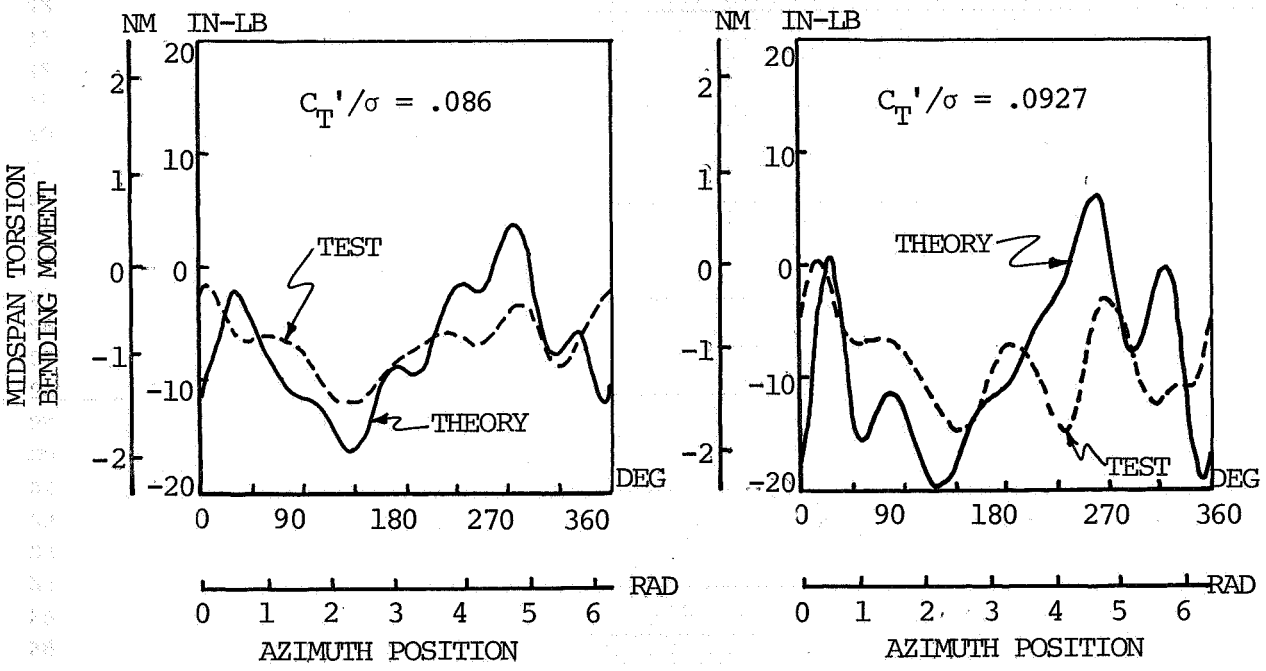

Figure 3.3.14 EFFECT OF TRIM ANALYSIS ON MIDSPAN TORSION WAVEFORM CORRELATION

seen in Figure 3.3.11. The conclusion is that the difference between test and analysis is not due to a hub tare calibration error in the wind tunnel test. The difference is due to a difference in the analytical drag characteristics of the rotor blade which quite possibly is in the airfoil dynamic drag representation and/or in the unsteady flow analysis.

4.0 RATIONALE FOR ROTOR LIMITS

Having established a reasonable correlation of the C-60 Aeroelastic Rotor Analysis Program with loads and performance data, the next task is to use the analysis to aid in the understanding of the limits of the conventional rotor by looking at the rotor behavior as the lift limit is approached. To aid in the investigation of the rotor limits, both the elastic properties of the rotor and the aerodynamic characteristics of the flow environment were varied in the analysis in order to determine their influence on the rotor lift charactertistics. The azimuthal and radial distributions of lift and angle of attack as well as the variation of blade flap deflection with azimuth were examined in this investigation.

In order to isolate the factors which provide the major contribution in establishing a lift limit, one typical flight condition near the lift limit was chosen for the parametric variation. The trim condition selected was:

$$\mu = .53$$

$$\bar{\lambda} = .05$$

$$C_T'/\sigma = .114$$

The azimuthal distribution of thrust per blade determined analytically is presented in Figure 4.1. Note that the thrust is generated in the fore and and aft regions of the rotor disc. The regions of the rotor disc around the advancing and retreating blade

1/10 SCALE CH-47B ROTOR
ROTOR TIP SPEED = 620 FT/SEC

$\mu = 0.53$ $C_T'/\sigma = .114$ $X/qd^2\sigma = 0.05$

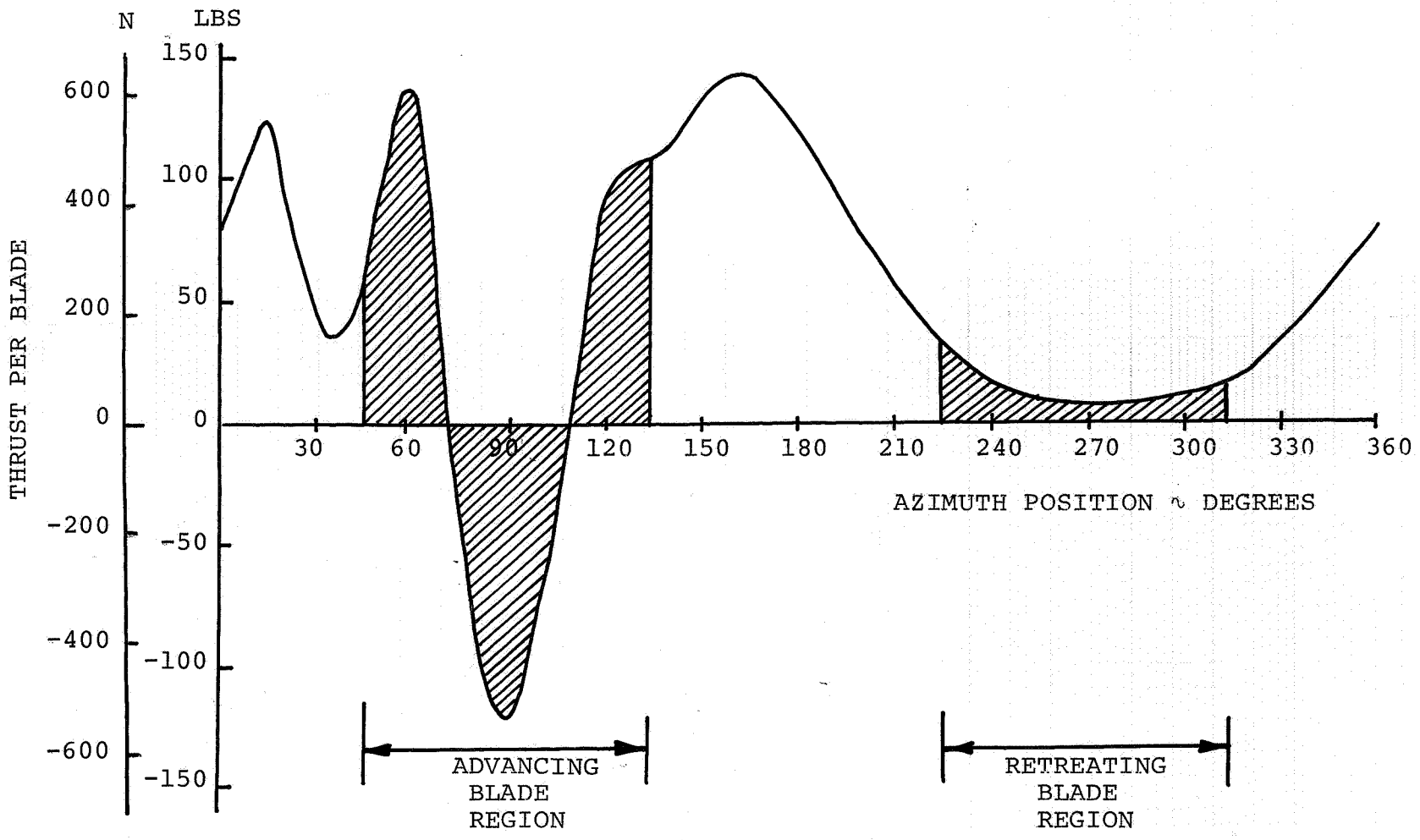

Figure 4.1 AZIMUTHAL DISTRIBUTION OF PREDICTED THRUST PER BLADE

have been shaded in the figure for convenience. On the advancing side, there are areas of large positive and negative levels of thrust, but the integrated thrust does sum to a small positive value. This is essential to maintain roll equilibrium of the rotor system.

There are two regions of significance which should be noted in the figure. At $\psi = 30^{o}$, there is a rapid drop in thrust that could be stall related. The blade does recover at $\psi = 60^{o}$, where the thrust is a maximum. There is a second region of high thrust between 120^{o} and 210^{o} rotor azimuth which is considerably larger. This time the thrust continues to rise until it becomes a maximum at $\psi = 180^{o}$, but there is a slight discontinuity in the lift trend at $\psi = 135^{o}$. It appears that these two regions may be the key to the understanding of the rotor lift limits, and they were the subject of extensive investigation.

Figure 4.2 is a plot of the spanwise distribution of lift at several azimuth locations for the subject flight condition. The azimuth locations selected are concentrated around the regions where there is a rapid loss of thrust, between $\psi = 0^{o}$ and $\psi = 90^{o}$. Note that the lift, both positive and negative, is predominantly generated on the outboard 40% of the rotor blade. The one notable exception is at $\psi = 30^{o}$, where the lift peaks at midspan and then falls off to zero. This indicates that the drop in thrust at $\psi = 30^{o}$ seen in Figure 4.1 is a result of the blade not developing lift on the outboard portion of the blade at this azimuth.

1/10 SCALE CH-47B ROTOR
ROTOR TIP SPEED = 620 FT/SEC

$\mu = 0.53 \quad C_T'/\sigma = .114 \quad X/qd^2\sigma = 0.05$

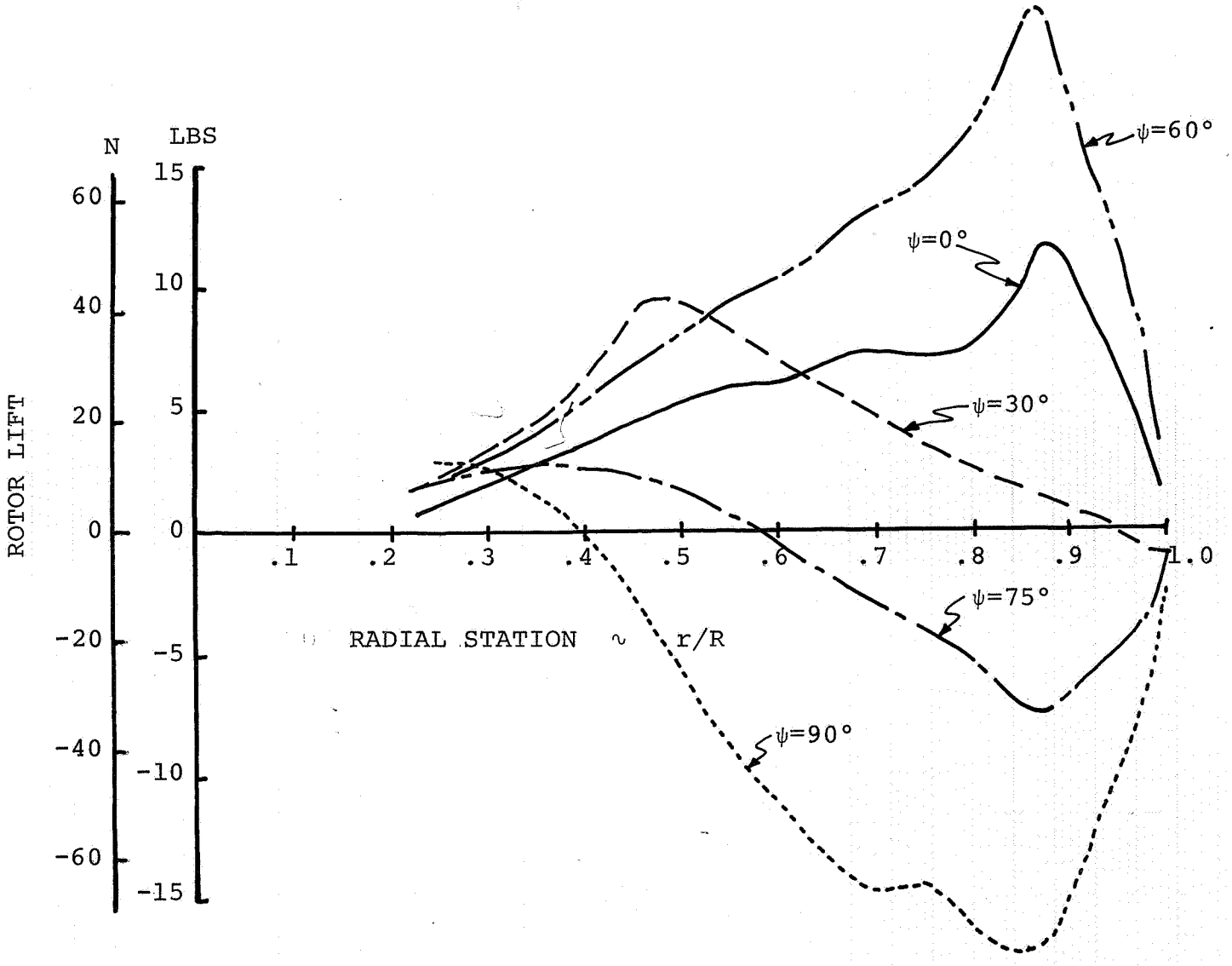

Figure 4.2 SPANWISE VARIATION OF LIFT AT SELECTED AZIMUTH LOCATIONS

As mentioned earlier, a parametric study was performed to determine which factor contributed the most in defining the lift limit. The first parameter studied was the elastic effects of blade motion. The blade was made rigid in the analysis both flapwise and torsionally, i.e. $GJ = EI_\beta = \infty$. The blade can only flap or twist as a rigid body in this case, so the influence of any elastic phenomena are eliminated. A comparison of the azimuthal variation of thrust for the rigid and elastic blade cases is shown in Figure 4.3 at the same condition, $\mu = .53$ and $C_T'/\sigma = .114$. The major difference between the two cases is that the rigid blade no longer experiences a loss of lift at $\psi = 30^o$ or $\psi = 135^o$. Figure 4.4 presents the radial lift distribution at $\psi = 30^o$ and indicates that the thrust is now able to develop on the outboard portion of the blade. The drop in total thrust at this azimuth appears to be a result of the elastic blade response. To further understand this point, the azimuthal variation of pitch and flap motion was investigated.

In order to match both the thrust and propulsive force requirements, the rotor tip path plane must assume a specific angle of attack with respect to the free stream velocity. The rotor with rigid blades requires more cyclic pitch for a given shaft angle of attack to bring the disc plane over far enough to produce the propulsive force equal to that of the elastic blade. This is because there is no elastic torsional wind-up of the blade inducing an effective cyclic pitch in the rigid blade. The greater nose down cyclic pitch requirements reduce the lift along the advancing blade and

1/10 SCALE CH-47B ROTOR
ROTOR TIP SPEED = 620 FT/SEC

$\mu = 0.53$ $C_T'/\sigma = .114$ $X/qd^2\sigma = 0.05$

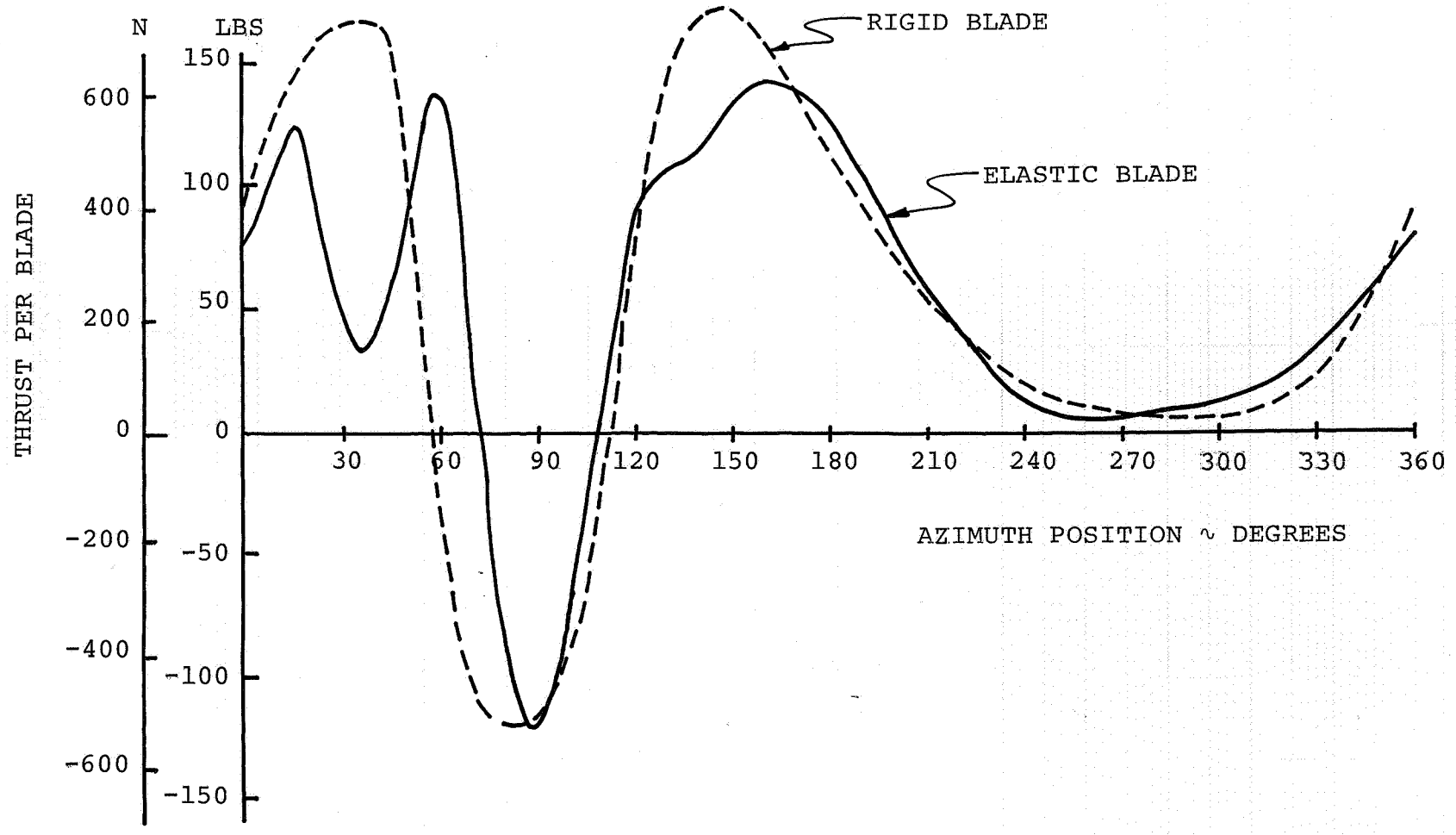

Figure 4.3 COMPARISON OF THRUST WAVEFORMS FOR RIGID AND ELASTIC BLADES

1/10 SCALE CH-47B ROTOR
ROTOR TIP SPEED = 620 FT/SEC

$\mu = 0.53 \quad C_T'/\sigma = .114 \quad X/qd^2\sigma = 0.05$

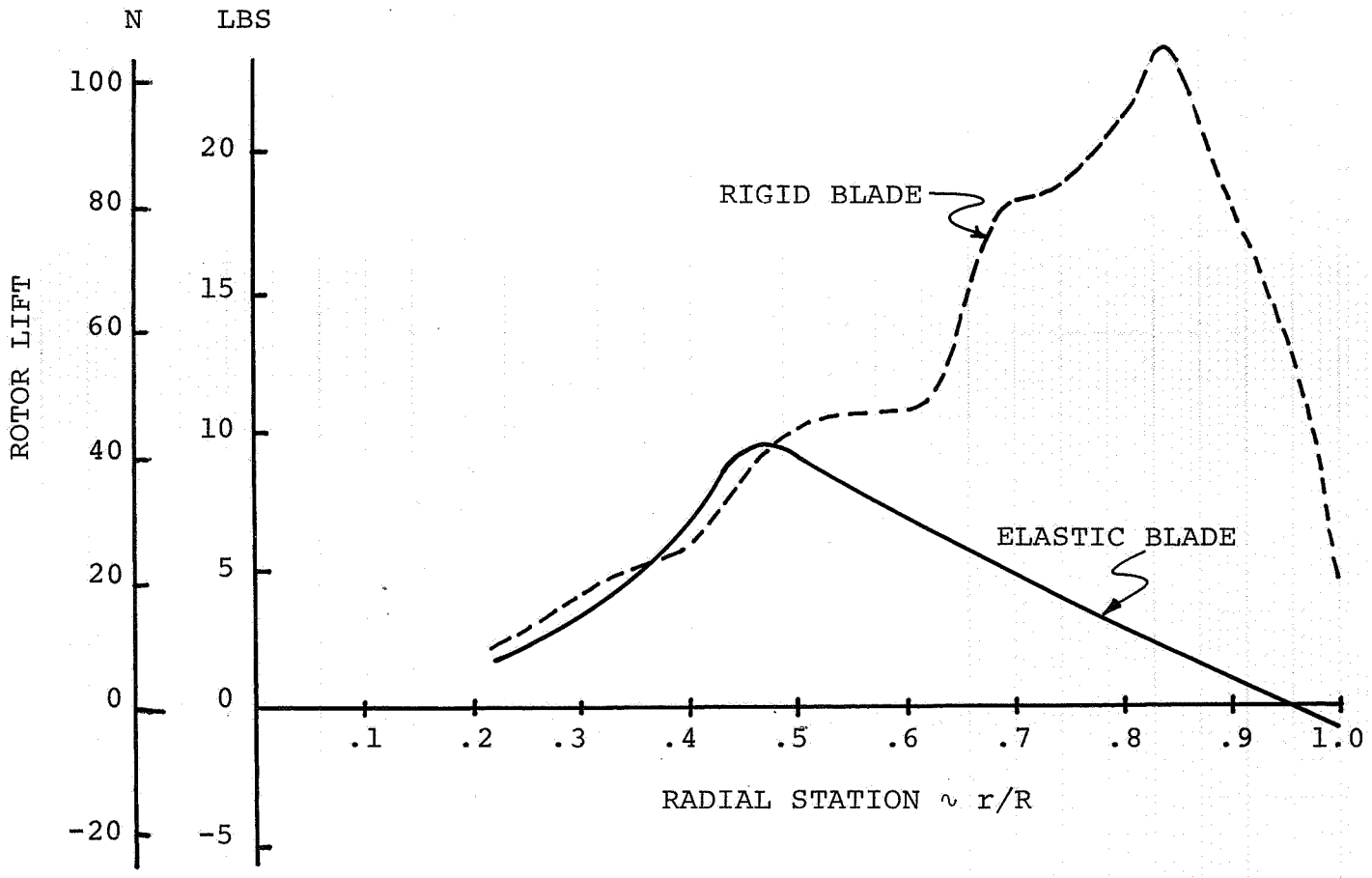

Figure 4.4 SPANWISE VARIATION OF LIFT FOR RIGID AND ELASTIC BLADE AT $\psi = 30^0$

necessitates a larger collective pitch to produce a larger section angle of attack on the fore and aft portion of the rotor disc to maintain the same thrust as for the elastic blade. The negative (nosedown) blade pitch rate results, at all azimuths where the blade is pitching down, in an inertially induced decrease in blade twist for the elastic blade which offsets the increased collective of the rigid blade. Since blades are normally built with the CG ahead of the pitch axis, blade pitching down tends to untwist the blade. Negative pitch rate also reduces the maximum section lift coefficient or angle of attack at which stall occurs. Both of these items increase the potential for stall to occur on the aft side of the rotor disc.

The basic difference between the elastic blade and the rigid blade is downward bending of the outboard portion of the elastic blade due to the high lift causing coning and the downward bending due to centrifugal force. As the lift approaches the stall limit the high drag acts on the downward deflected elastic blade to produce a nosedown twist, which reduces the lift. Since the blade then becomes unstalled the drag reduces and the blade twists back to its normal position. The lift then can return to its former level. As the blade moves around the azimuth towards $\psi = 90^{o}$, the longitudinal cyclic is rapidly reducing blade pitch and the inplane velocity acting on the blade is rapidly increasing further reducing the section angle of attack of the blade. The net result is a substantial negative angle of attack on the outboard portion of the blade producing the negative lift shown in Figure 4.2.

As the blade rotates past $\psi = 120^{o}$ towards 150^{o} the blade pitch is increasing because of the cyclic pitch. This produces a positive

pitch rate which results in a stall delay. As the pitch is increased so is the lift as it approaches a maximum. The centrifugal force plus blade coning again produces a downward deflection of the blade, and the high drag twists the blade down decreasing the lift. With the stall delay the reduction in lift between $\psi = 120^{o}$ and 150^{o} is not as large as between $\psi = 15^{o}$ and 60^{o}.

The variation of the input blade pitch around the azimuth is presented in Figure 4.5. The mean value is the collective and the variation above and below is the cyclic pitch. Since the minimum pitch occurs at $\psi = 90^{o}$ and the maximum is at $\psi = 270^{o}$ the figure indicates only longitudinal cyclic is required. The flapwise deflection of the tip of the elastic blade relative to the infinitely rigid blade deflected shape is shown in Figure 4.6. Around an azimuth location from $\psi = 30^{o}$ to $\psi = 60^{o}$ the deflection is down, and as observed in Figure 4.5 the blade root pitch is greater for the elastic blade. These two facts support the above rationale for the azimuthal variation of lift presented in Figures 4.1 and 4.2. At this point, it should be emphasized that in making the blade rigid in the analysis, the same high lift and high drag was encountered as with the elastic blade. In fact, at the high C_T'/σ conditions there is a severe power penalty observed for both blades.

The next phase of the investigation was to determine what aspect of the aerodynamics of the rotor system had the greatest influence in limiting the maximum attainable lift of the rotor. First of all, the non-linear compressible aerodynamics terms were removed from the analysis so that only linear aerodynamics remained for the lift

1/10 SCALE CH-47B ROTOR
ROTOR TIP SPEED = 620 FT/SEC

$\mu = 0.53 \quad C_T'/\sigma = .114 \quad X/qd^2\sigma = 0.05$

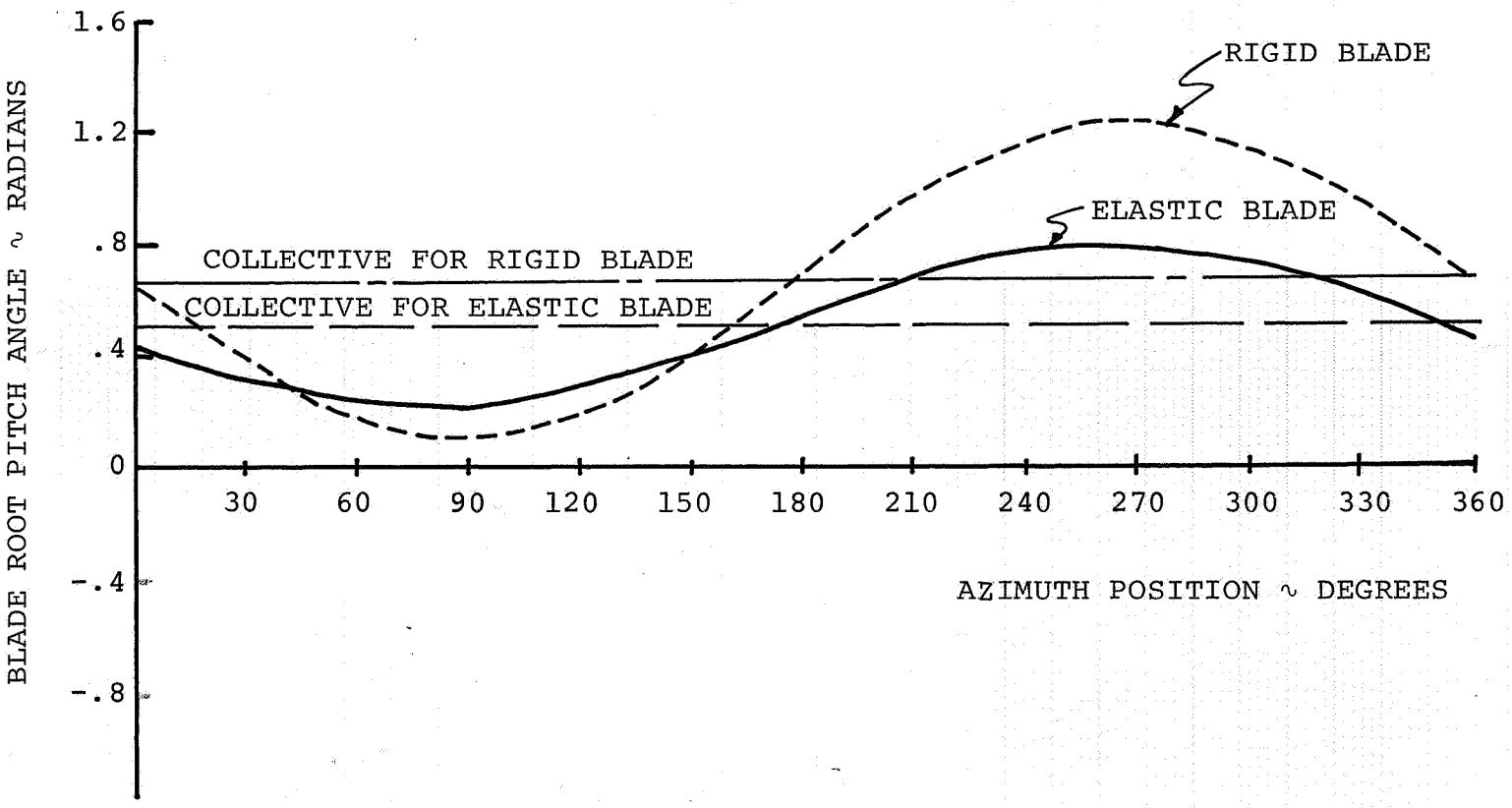

Figure 4.5 AZIMUTHAL DISTRIBUTION OF BLADE ROOT PITCH FOR RIGID AND ELASTIC BLADES

1/10 SCALE CH-47B ROTOR
ROTOR TIP SPEED = 620 FT/SEC

$\mu = 0.53$ $C_T'/\sigma = .114$ $X/qd^2\sigma = 0.05$

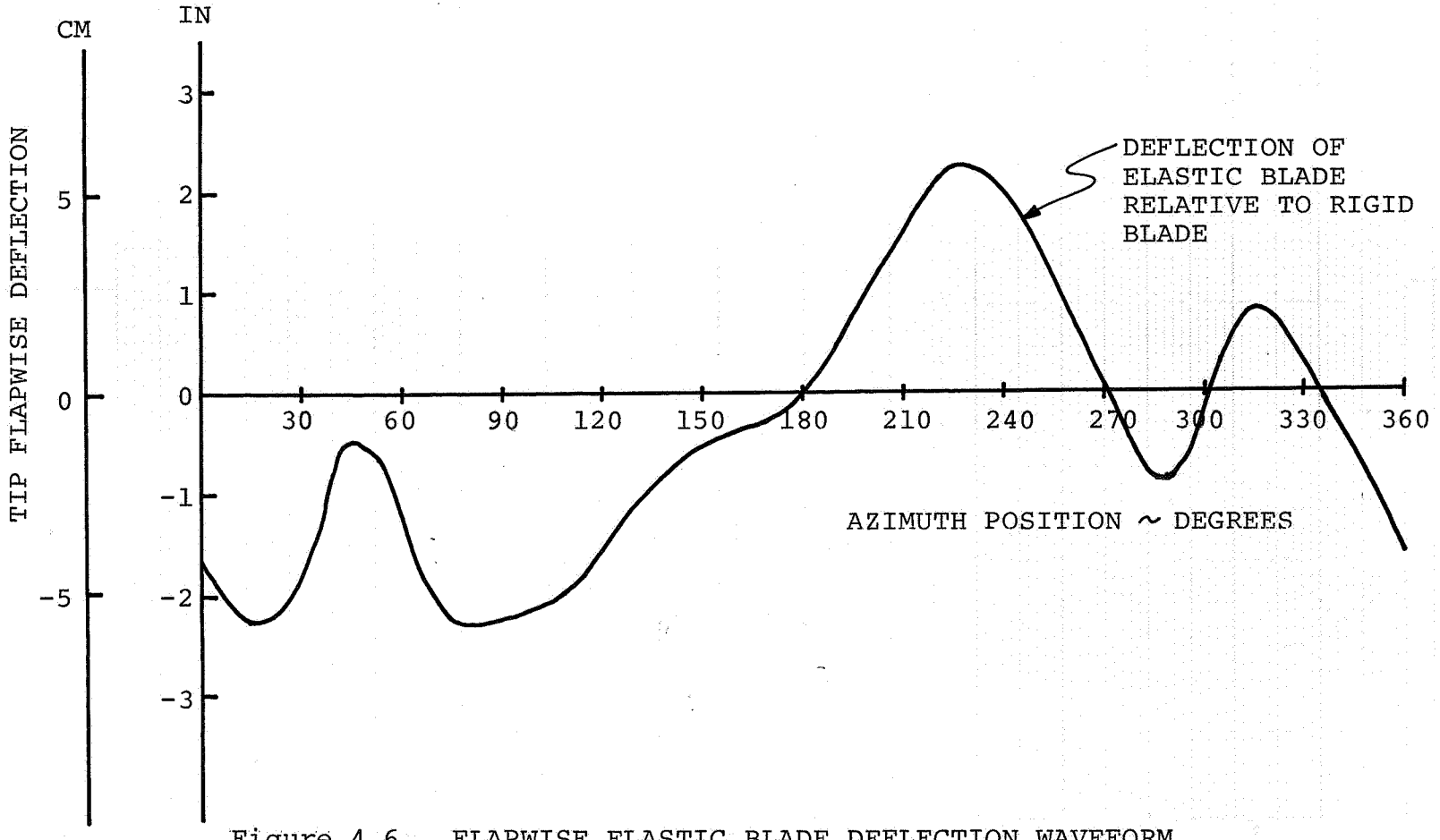

Figure 4.6 FLAPWISE ELASTIC BLADE DEFLECTION WAVEFORM

and drag coefficients. These coefficients were computed as follows:

$$C_{\ell} = 5.73\alpha$$

$$C_{d} = .012 + .540\alpha$$

where α is the section angle of attack. The values of the pitching moment coefficient, C_m, were obtained from the compressible aerodynamics airfoil tables as before.

The resulting thrust distribution using linear aerodynamics is given in Figure 4.7 at the $\mu = .53$, $C'_T/\sigma = .114$ condition. Also shown for comparison is the elastic blade non-linear, compressible aerodynamics case. It can be seen that the azimuthal variation of total thrust is significantly altered when the analysis is run with linear aerodynamics only. The region of negative thrust around $\psi = 75^o$ to $\psi = 90^o$ has been virtually eliminated because the retreating blade can now provide a high level of lift, and the thrust is now more uniformly distributed around the azimuth. The root pitch angle distribution around the azimuth for this case is given in Figure 4.8. The results are not noticeably different from the basic elastic blade case with non-linear, compressible aerodynamics. This is evidence that the mechanism which restricts the maximum attainable lift is related to aerodynamic stall effects.

With the knowledge that it is some aspect of the non-linearities and effects of the maximum section lift coefficient in the aerodynamics of the rotor as well as blade flexibility that leads to a lift limit, the next step was to vary certain parameters individually

1/10 SCALE CH-47B ROTOR
ROTOR TIP SPEED = 620 FT/SEC

$\mu = 0.53$ $C_T'/\sigma = .114$ $X/qd^2\sigma = 0.05$

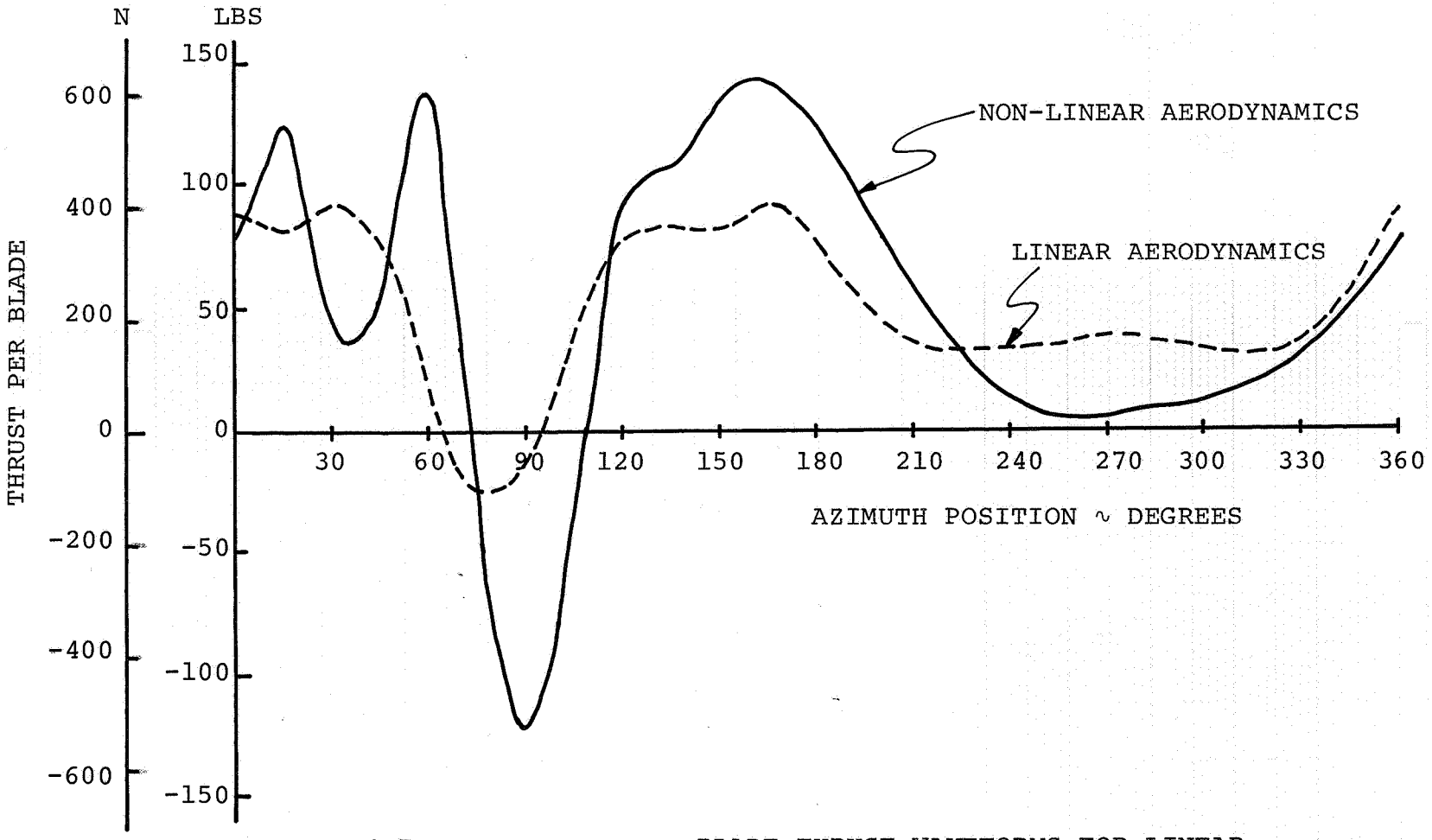

Figure 4.7 COMPARISON OF BLADE THRUST WAVEFORMS FOR LINEAR AND NON-LINEAR AERODYNAMIC ANALYSIS

1/10 SCALE CH-47B ROTOR
ROTOR TIP SPEED = 620 FT/SEC

$\mu = 0.53$ $C_T'/\sigma = .114$ $X/qd^2\sigma = 0.05$

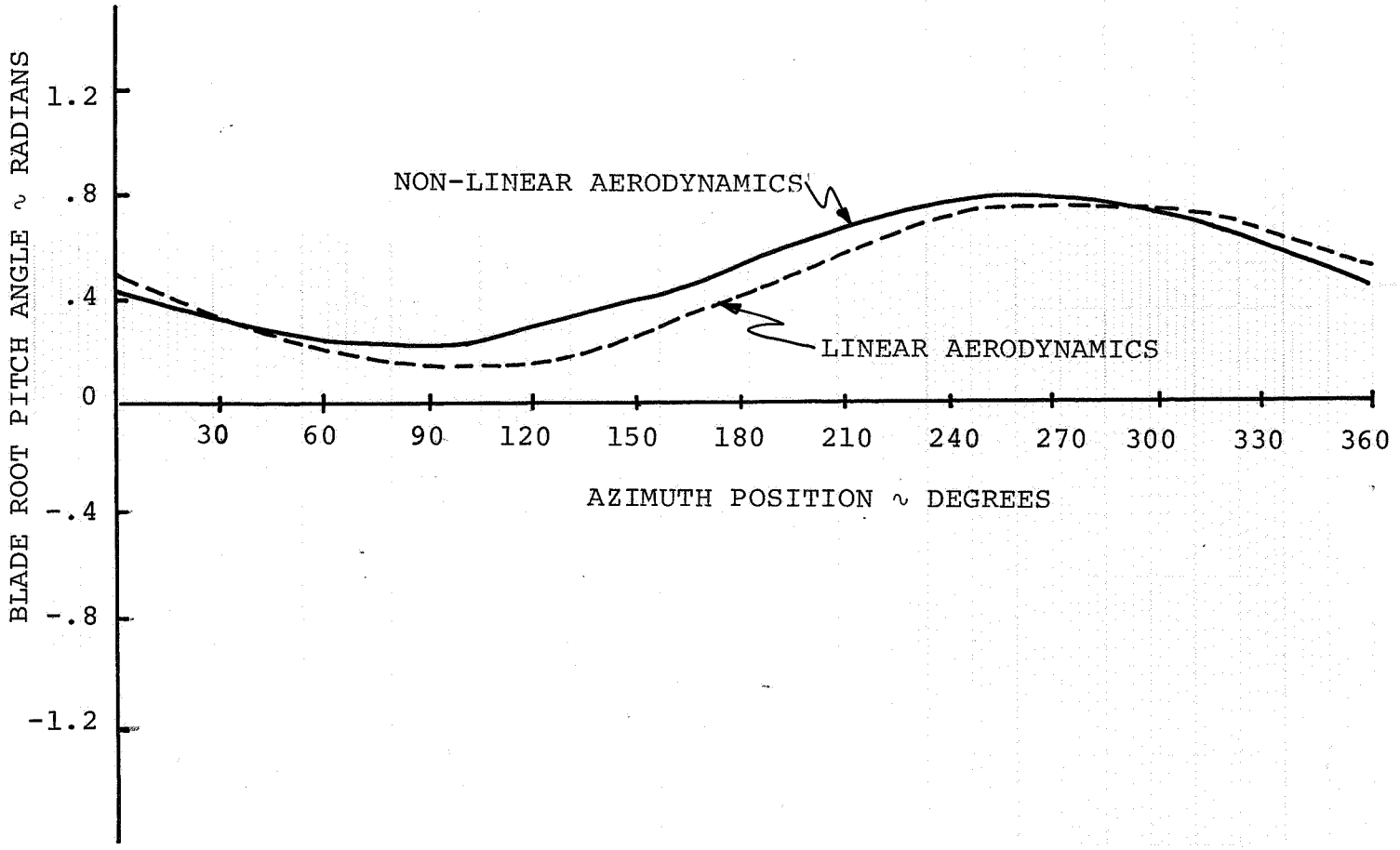

Figure 4.8 AZIMUTHAL DISTRIBUTION OF ROOT BLADE PITCH ANGLE FOR LINEAR AND NON-LINEAR AERODYNAMIC ANALYSIS

to determine which of the aerodynamic effects define the lift limit. The first item to be investigated was compressibility or high Mach number effects. In the analysis, the speed of sound was artificially doubled so that all Mach numbers computed would be half their actual value. The advancing blade tip Mach number thus never exceeded $M_{1(90)} = .5$. This eliminated any compressibility due to Mach number effects. The resulting thrust variation with azimuth is shown in Figure 4.9. Also shown for comparison is the variation of total thrust for the elastic blade with full non-linear, compressible aerodynamics. It is quite evident that there is only a small effect of compressibility or other Mach number related effects on the lift capability of the rotor.

Next the impact of stall delay on the thrust distribution was considered. The stall delay functions in the analysis were input as zero, removing the stall delay effects from the results. The azimuthal variation of total thrust for this case is given in Figure 4.10 along with the corresponding case with stall delay included. The stall delay effect appears as a 15^{o} to 20^{o} shift in azimuth of the waveform but does not change the magnitude and will not significantly alter the lift limit.

With the stall delay and compressibility effects eliminated as a source of the lift limits, the drag rise at large angles was investigated as a possible mechanism. The non-linear, compressible aerodynamics airfoil tables were used to obtain C_L and C_M. The drag coefficient was input as a constant of $C_D = .012$, which is the value

1/10 SCALE CH-47B ROTOR
ROTOR TIP SPEED = 620 FT/SEC

$\mu = 0.53$ $C_T'/\sigma = .114$ $X/qd^2\sigma = 0.05$

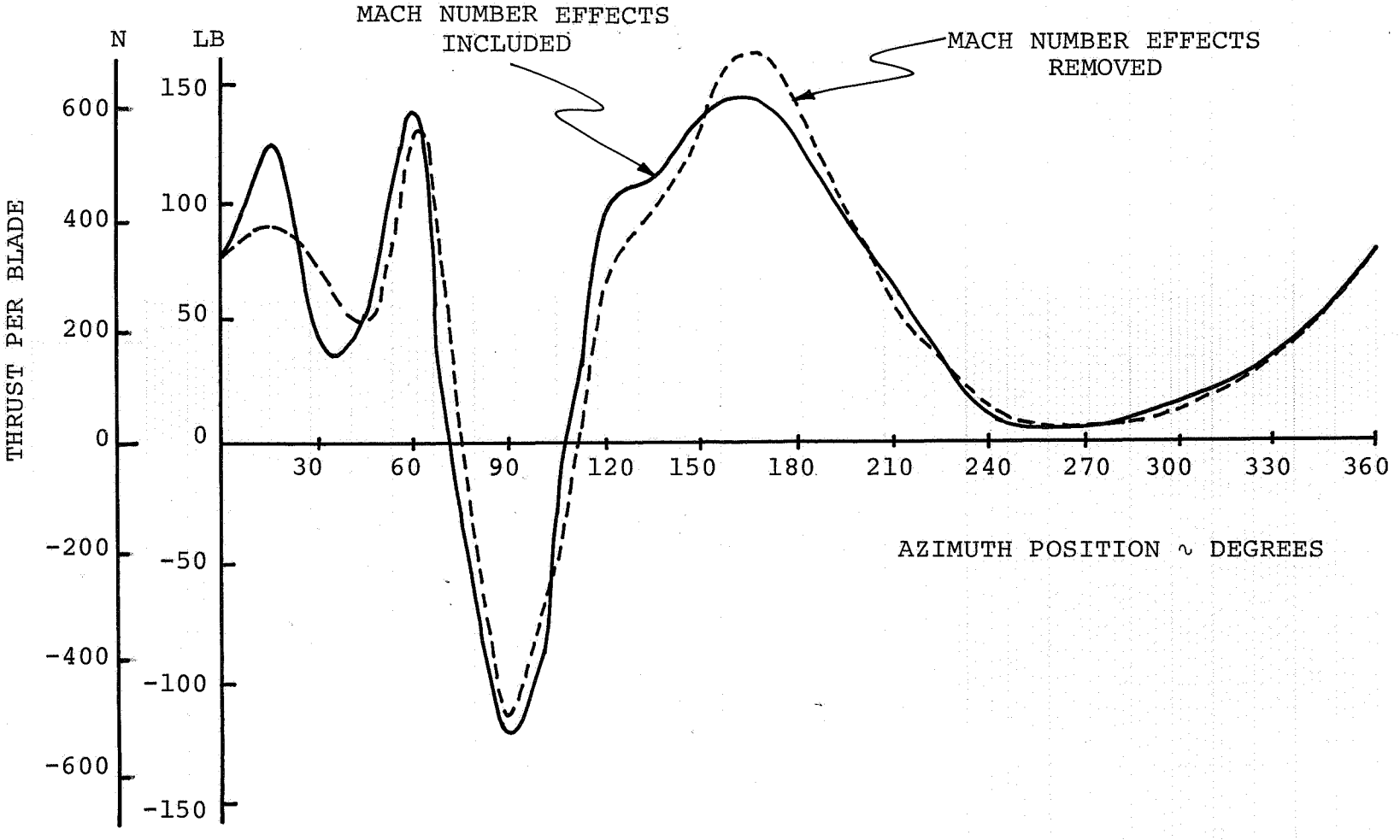

Figure 4.9 EFFECT OF MACH NUMBER ON BLADE THRUST WAVEFORM

1/10 SCALE CH-47B ROTOR
ROTOR TIP SPEED = 620 FT/SEC

$\mu = 0.53 \quad C_T'/\sigma = .114 \quad X/qd^2\sigma = 0.05$

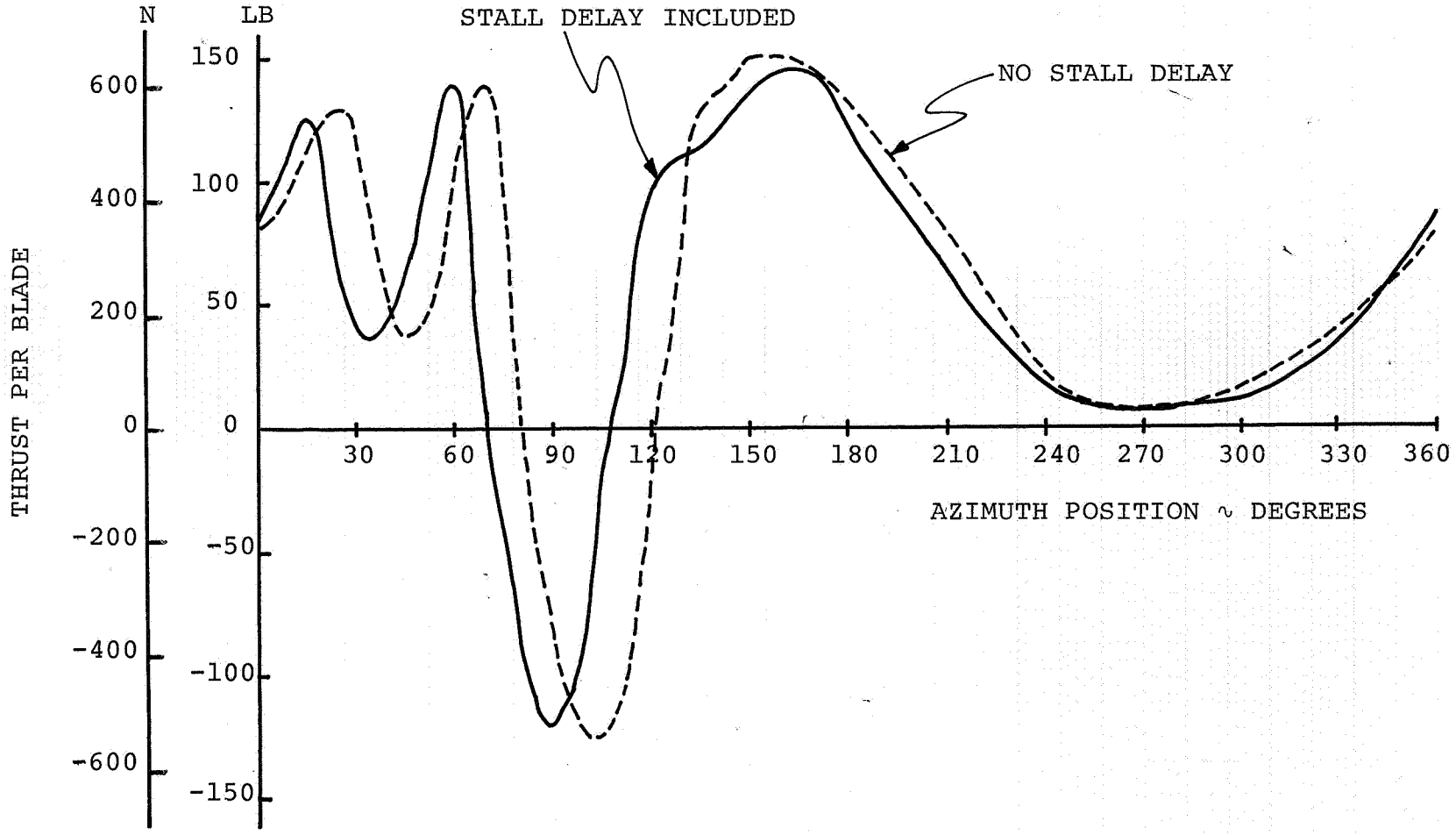

Figure 4.10 EFFECT OF STALL DELAY ON THRUST WAVEFORM

of C_D at M = .5 for small angles. As seen in Figure 4.11, there is essentially no difference in thrust versus azimuth between the two cases of an elastic blade with and without induced drag. However, the analytical case with no drag rise at high angles of attack has a power requirement considerably less than the elastic blade with induced drag. The difference in power coefficients is C_P/σ = .0098 for no drag rise versus C_P/σ = .0243 for the case with induced drag. Due to the lower power requirement, a higher value of lift can be obtained before the sharp rise in power required is encountered. This comparison is seen in Figure 4.12, showing that the lift limit is indeed influenced by the increase in drag due to induced drag effects at high Mach number.

To ascertain why the region of negative thrust develops at $\psi = 90^o$ we look at the requirement for roll moment equilibrium. As mentioned earlier and seen in Figure 4.1, the thrust is primarily developed fore and aft on the rotor. Due to the very low dynamic pressure on the retreating blade there is only a small amount of thrust generated around this region. The demand for higher and higher thrust levels results in some thrust being developed in the advancing blade region. To maintain roll equilibrium, therefore, some negative thrust must be developed.

The contribution of thrust at each azimuth location to the total roll moment is presented in Figure 4.13. For the elastic blade case with nonlinear compressible aerodynamics used in the lift

calculations, note how the small amount of thrust on the retreating blade contributes only a small amount to the roll moment. On the advancing blade side of the disc plane, there is a large contribution to the moment between $\psi = 120^{o}$ and $\psi = 150^{o}$. To balance the roll moment, the region of negative moment between $\psi = 75^{o}$ and $\psi = 120^{o}$ is required.

Note what happens when linear, incompressible aerodynamics are used in the calculation of lift. Now there is the capability to develop much larger levels of thrust on the retreating blade (see Figure 4.7). For this reason there is a greater contribution to the roll moment on the retreating side, which allows for a greater positive moment on the advancing side. As can be seen in Figure 4.13, this noticeably reduces the need for a negative moment (hence negative thrust) region on the advancing blade portion of the rotor disc.

With the explanation of the source of the negative thrust region, the resulting high negative angles of attack and the increased drag due to compressibility; it is now possible to explain some of the trends of lift versus power required and lift limit versus advance ratio brought up in section 3 of this report.

The primary issue is the shape of the lift limit curve versus advance ratio (Figure 3.1.9). To understand this trend, it is useful to look at the total thrust versus azimuth location at the lift limit for each advance ratio as shown in Figure 4.14. Each

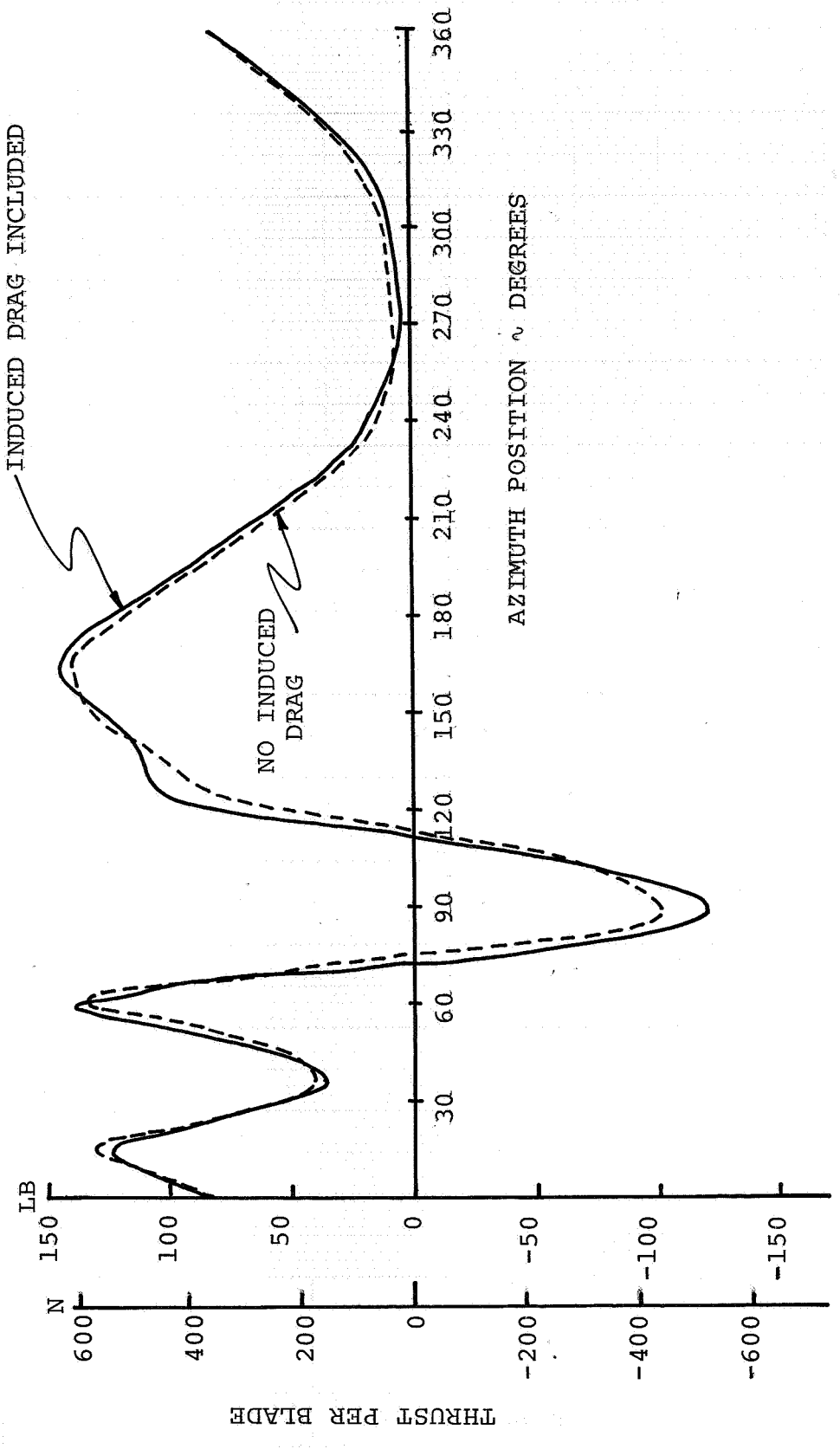

Figure 4.11 EFFECT OF INDUCED DRAG ON THRUST WAVEFORM

1/10 SCALE CH-47B ROTOR
ROTOR TIP SPEED = 620 FT/SEC

$\mu = 0.53$ $X/qd^2\sigma = 0.05$

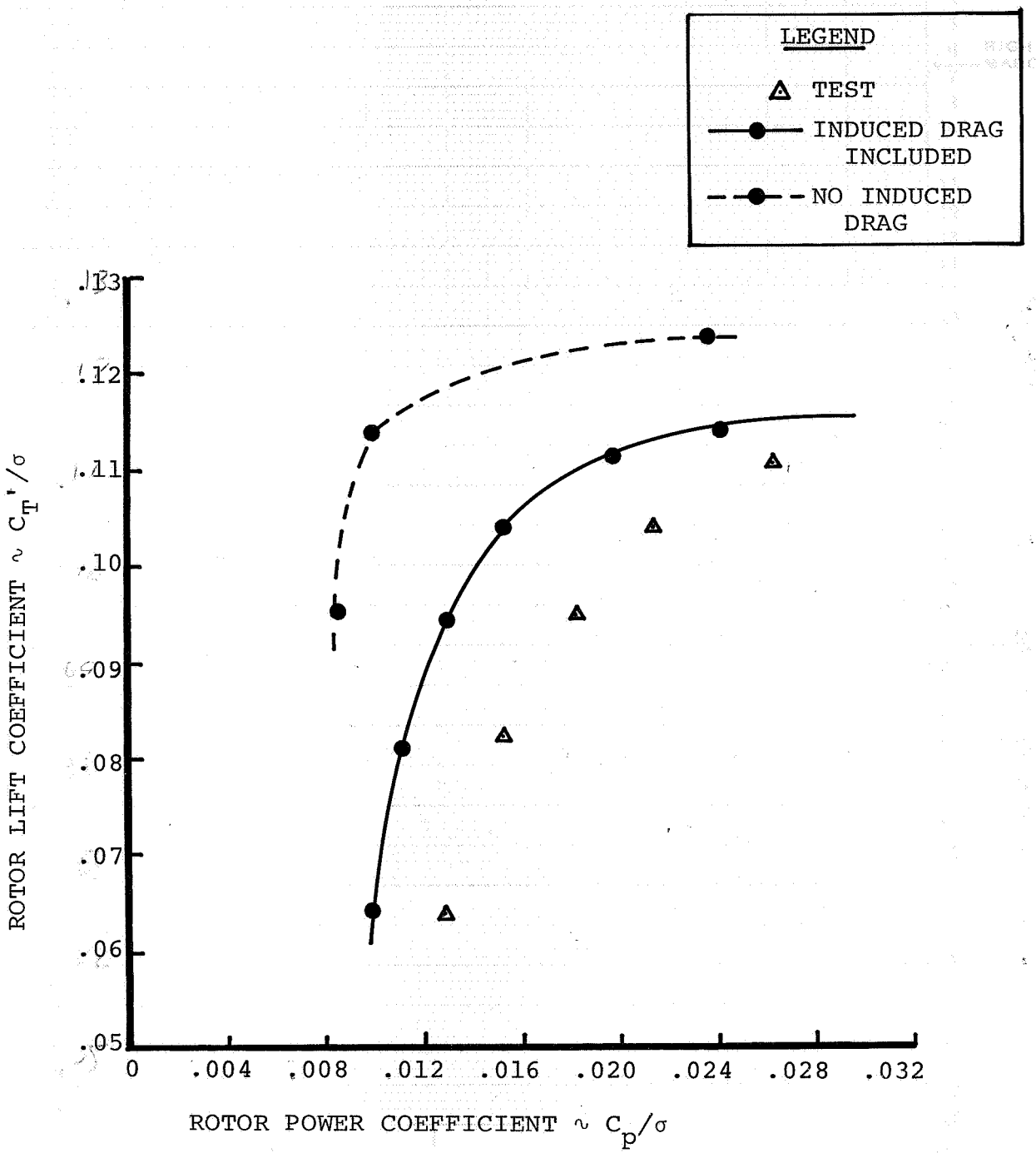

Figure 4.12 EFFECT OF INDUCED DRAG ON ANALYTICAL LIFT LIMIT

1/10 SCALE CH-47B ROTOR
ROTOR TIP SPEED = 620 FT/SEC

$\mu = .053 \quad C_T'/\sigma = .114 \quad X/qd^2\sigma = 0.05$

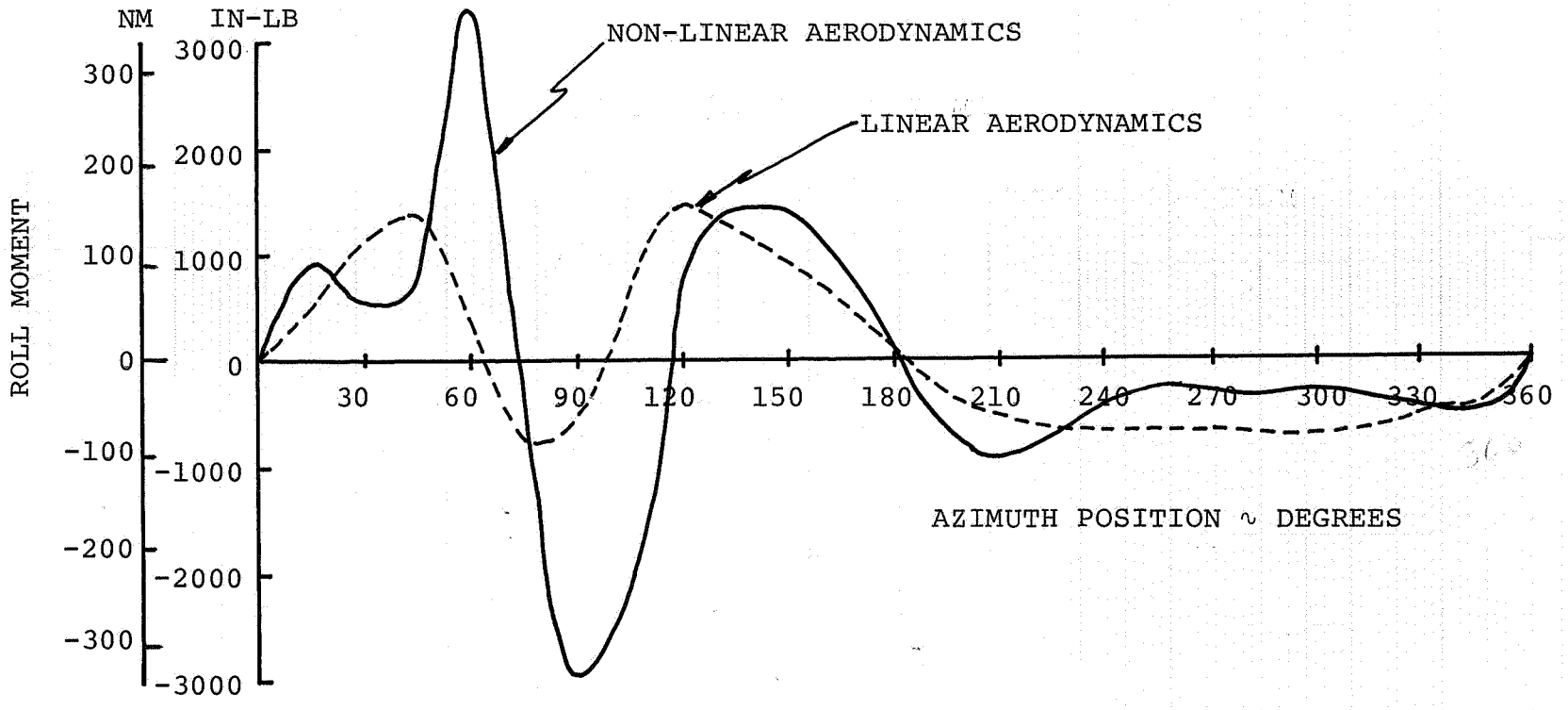

Figure 4.13 CONTRIBUTION OF EACH AZIMUTH TO ROLL MOMENT

1/10 SCALE CH-47B ROTOR
ROTOR TIP SPEED = 620 FT/SEC

$X/qd^2\sigma = 0.05$

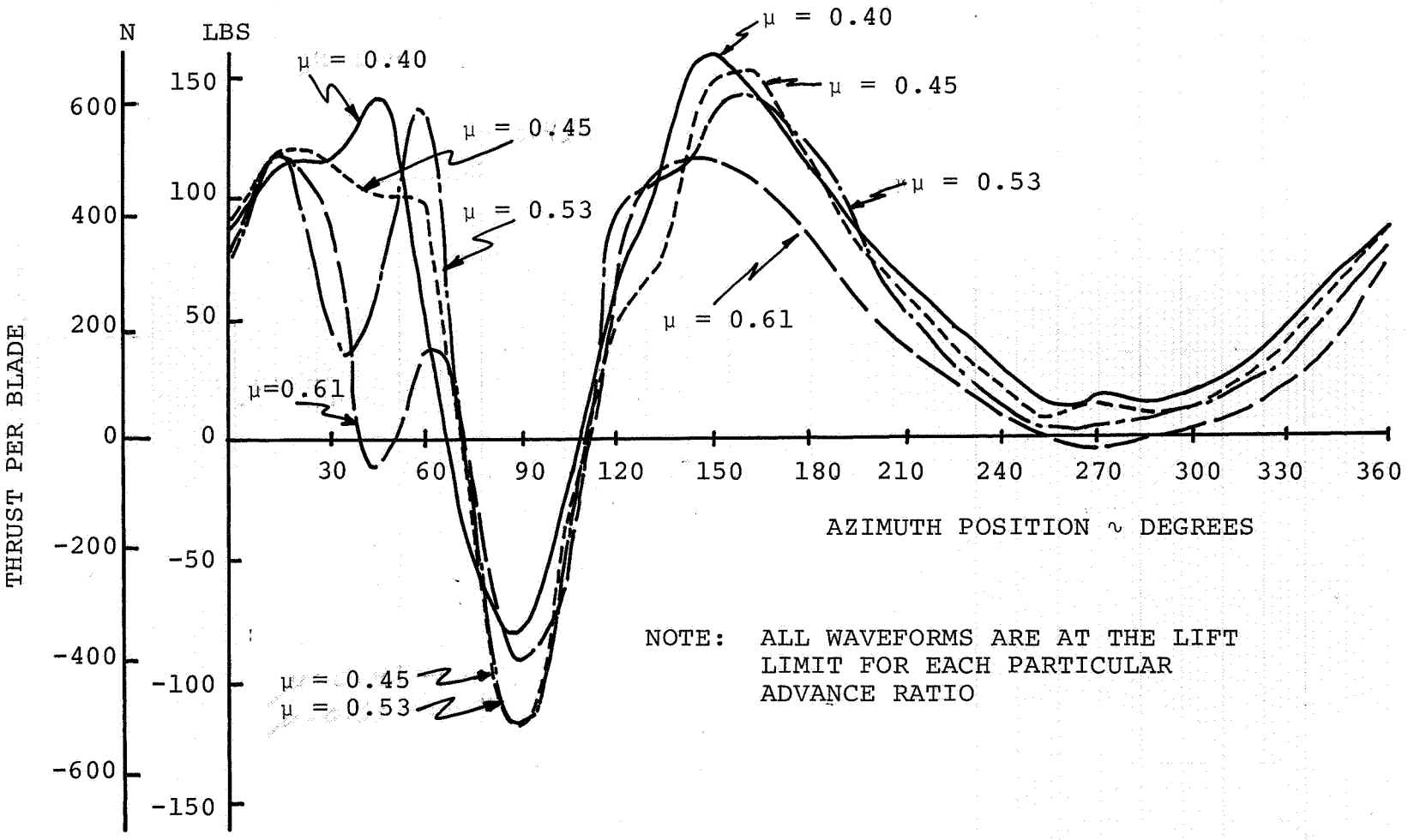

Figure 4.14 EFFECT OF FORWARD SPEED ON AZIMUTHAL VARIATION OF THRUST PER BLADE AT THE LIFT LIMIT

curve has the characteristic negative lift region around $\psi = 90^{o}$ which has been shown to be symptomatic of the need to maintain roll moment equilibrium, and the resulting negative angles of attack leads to a drag rise which limits the rotor performance. There is a distinct change in the shape of the curves around $\psi = 15^{o}$ to $\psi = 60^{o}$ in going from $\mu = .45$ to $\mu = .53$. There is a distinct stalled region at $\psi = 30^{o}$ for the higher advance ratios which is not present at advance ratios of $\mu = .45$ and below.

This region of stall was shown earlier to be related to elastic blade effects because when the blade was made rigid flapwise and torsionally in the analysis this stalled region disappeared (Figure 4.3). The hypothesis was proposed when first discussing Figure 4.3 that the stalled region at $\psi = 30^{o}$ was related to high drag and blade flap deflection combining to decrease the twist. Similar reasoning is apparently applicable in this situation as well. At $\mu = .4$ and $\mu = .45$, the mechanism which produces the elastic response is present and is indicated by the plateau in thrust at $\psi = 30^{o}$. There is a severe stall effect on the aft portion of the rotor disc at $\psi = 45^{o}$ for $\mu = .61$ and there is a slight degradation in lift on the forward part of the rotor disc at $\psi = 165^{o}$.

Figures 4.15 and 4.16 show the azimuthal variation of thrust per blade with increasing levels of thrust for $\mu = .4$ and $\mu = .53$ respectively. Note that while the $\psi = 90^{o}$ negative lift region does not develop until the lift limit is approached, the stalled

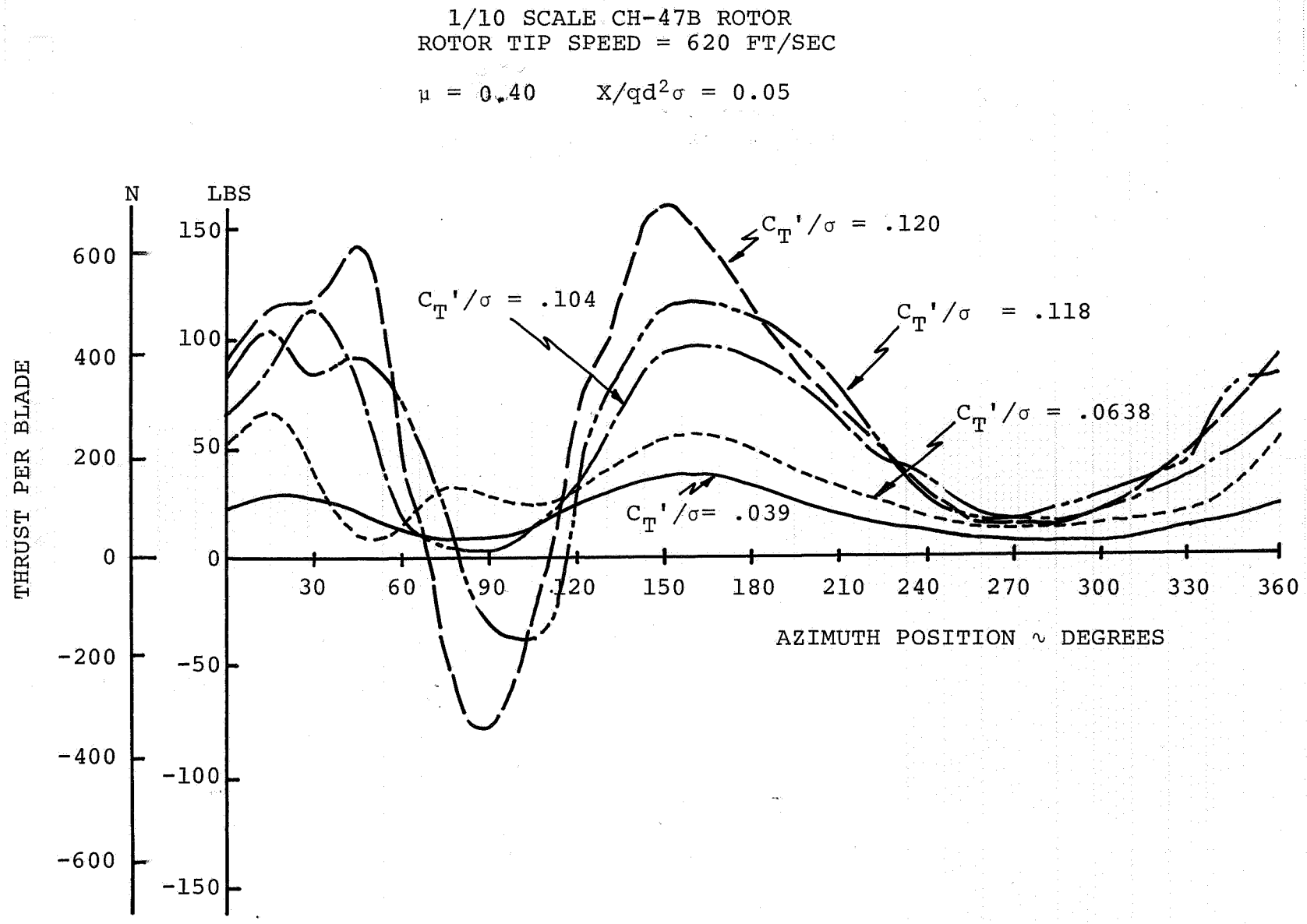

Figure 4.15 EFFECT OF ROTOR LIFT COEFFICIENT ON AZIMUTHAL VARIATION OF THRUST PER BLADE AT 147 KNOTS

1/10 SCALE CH-47B ROTOR
ROTOR TIP SPEED = 620 FT/SEC

$\mu = 0.53 \quad X/qd^2\sigma = 0.05$

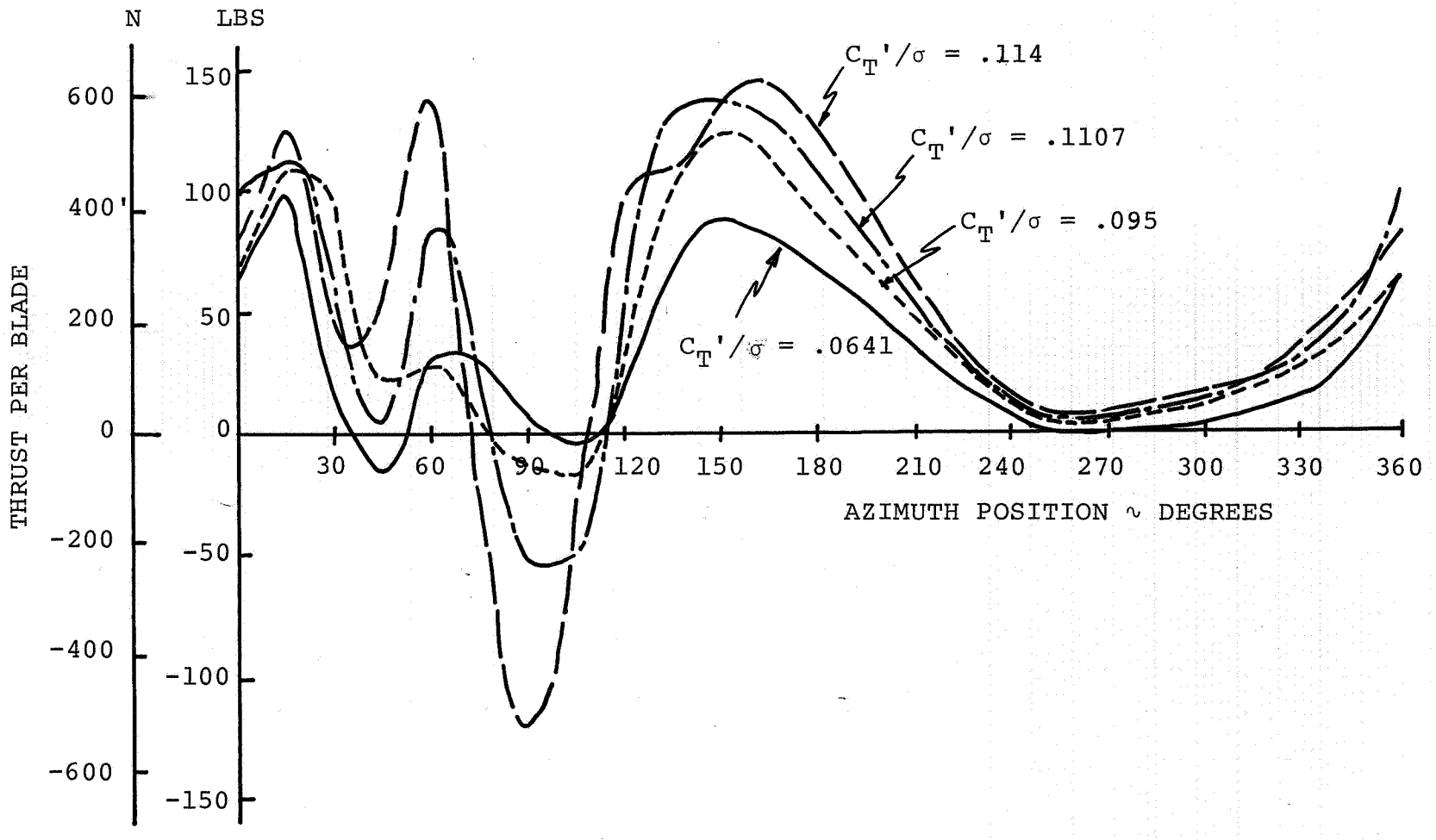

Figure 4.16 EFFECT OF ROTOR LIFT COEFFICIENT ON AZIMUTHAL VARIATION OF THRUST PER BLADE AT 165 KNOTS

region at $\psi = 30^{o}$ to $\psi = 45^{o}$ occurs throughout the thrust range for $\mu = .53$. The explanation for this may be due to the 76% increase in propulsive force required for a constant $X/qd^{2}\sigma$ requiring a larger shaft angle and cyclic angle to generate the needed tip path plane angle.

Consider Figure 4.17 which is a duplication of a portion of Figure 3.1.11. Recall that the analytical points were generated matching thrust and cyclic pitch. While the propulsive force is higher than that obtained in test, the propulsive force for each analytical point is the same. Of particular interest are the points labeled "A" and "B" in the figure. Point "B" is obtained by allowing the rotor to flap more in the forward part of the disc plane, increasing the angle of attack in that region and producing more thrust, and by reducing the angle of attack on the aft portion of the rotor disc producing less thrust in this region. The increase in thrust is greater than the loss in thrust, resulting in a net increase in rotor lift. This indicates the amount of stall experienced by the rotor is lower and hence the power required for point "B" can be the same as point "A" even though the lift is higher. Figure 4.18 is a plot of the azimuthal variation of total thrust for these two analytical cases. Note that case "B" does have a drop in thrust at $\psi = 45^{o}$ followed by a recovery from stall, while case "A" shows only the development of a small negative lift region around $\psi = 75^{o}$ to $\psi = 105^{o}$. Therefore it does appear that the stall region can be a function of trim, affecting the trend of thrust versus power required.

1/10 SCALE CH-47B ROTOR
ROTOR TIP SPEED = 620 FT/SEC

$\mu = 0.45$ $X/qd^2\sigma = 0.05$

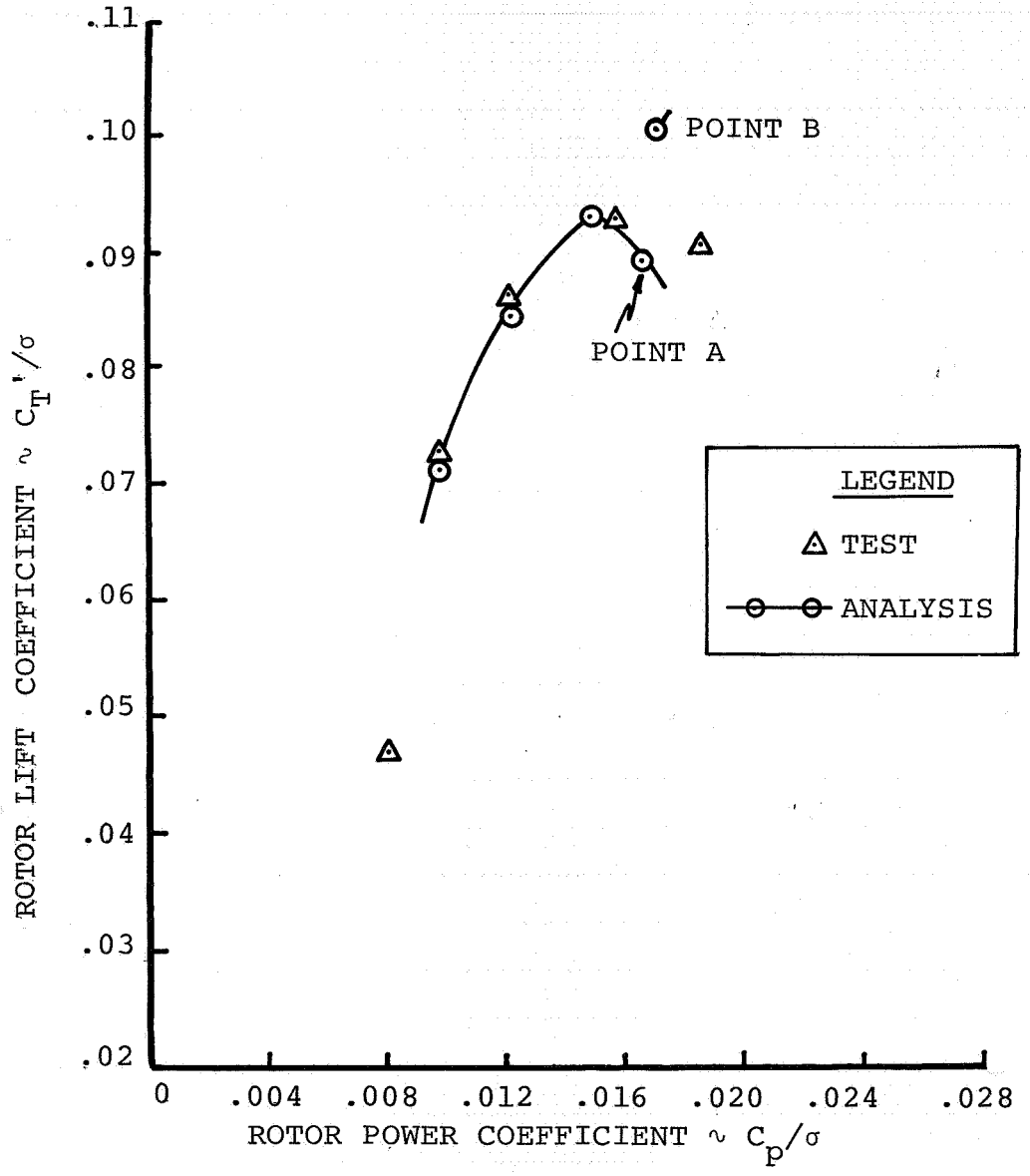

Figure 4.17 EFFECT OF ANALYTICAL TRIM ON PERFORMANCE PREDICTIONS

1/10 SCALE CH-47B ROTOR
ROTOR TIP SPEED = 620 FT/SEC

$\mu = 0.45$ $X/qd^2\sigma = 0.05$

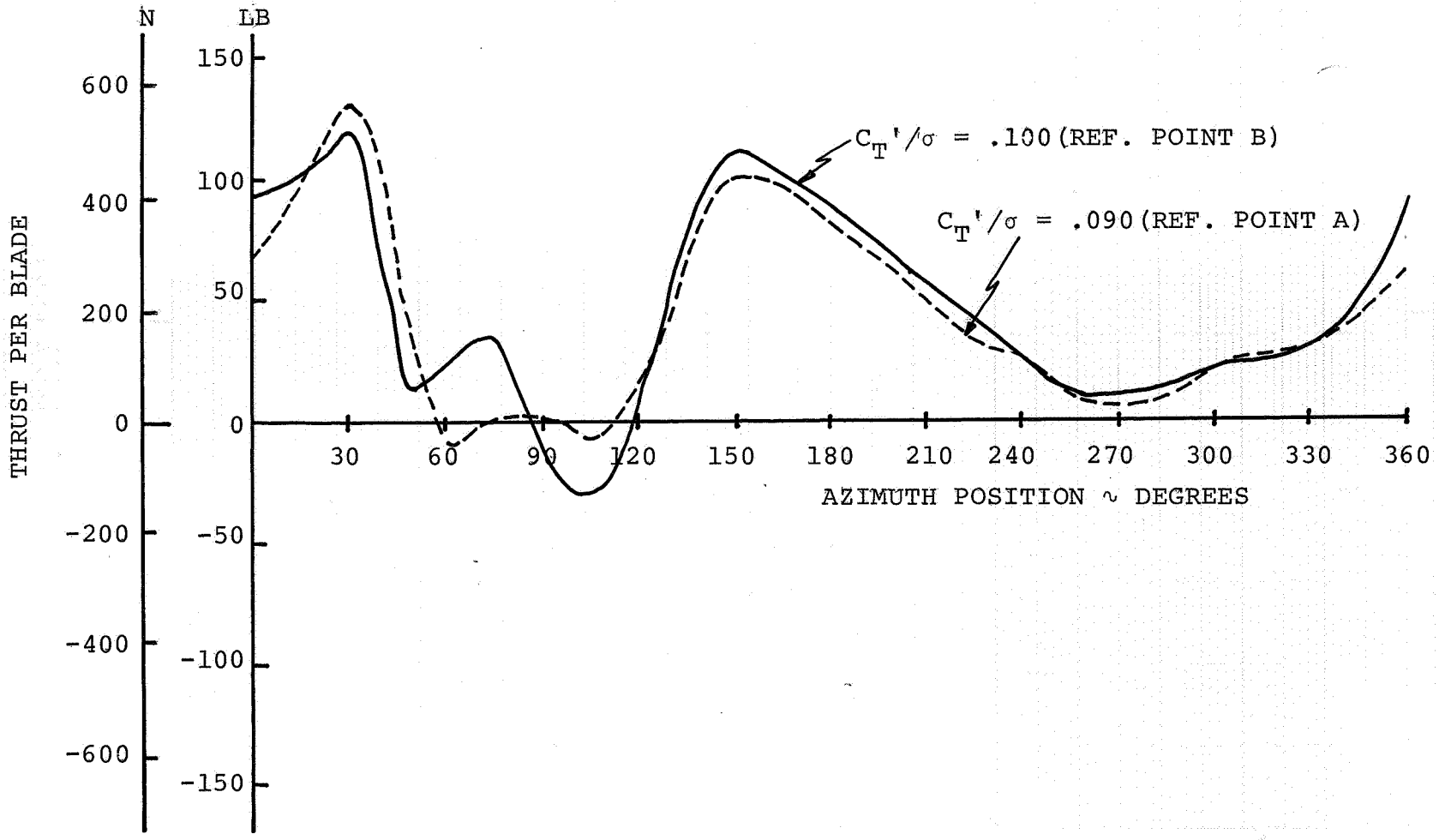

Figure 4.18 EFFECT OF TRIM ON STALL REGION NEAR 45° AZIMUTH

As a final verfication of our explanation for the behavior of the rotor at high lift and high speed we take another look at the azimuthal variation of flap bending and blade torsion. It was stated earlier in this section that the combination of high lift caused coning and the centrifugal restoring moment caused a downward bending of the blade as it approached stall. Refer again to Figure 3.3.2 and note how at $\psi = 45^{o}$ there is a rapid decrease in flap bending which is evidence of the downward deflection of the blade. This effect is amplified as the lift is increased. It was also stated that the high drag acted on this downward deflection to produce a nosedown twist at $\psi = 45^{o}$. As the blade unstalled it would twist back to its former position until $\psi = 90^{o}$, where the longitudinal cyclic and higher inplane velocity would produce a large negative section angle of attack. Looking again at Figure 3.3.12 clearly shows this effect. At the higher levels of lift there is a nosedown twist evident at $\psi = 45^{o}$. The blade starts to twist back again until $\psi = 90^{o}$ where a rapid decrease in twist to a large negative value is indicated. Thus there is strong support for the explanation of the rotor behavior at high speed near the lift limit.

5.0 MODEL AND FULL SCALE PERFORMANCE PREDICTION

The wind tunnel testing provided the data that defines the capability and the limits to the model rotor operation. Reference 1 presented a limited correlation of a rapid preliminary design performance program with this test data. The prediction program, SRIBR, is used primarily for preliminary design studies of various rotor configurations since it has numerous options and has a computational time of 10 to 15 seconds of machine time. SRIBR is a strip-theory analysis with an assumed tip loss and an induced velocity calculated as a function of the local loading to approximate the nonuniform downwash. The equations are written in the tip-path-plane axis system which eliminates the requirements for iterating on blade flapping and the airfoil characteristics are approximated with a series of equations.

An expanded correlation of the SRIBR predictions of rotor lift coefficient (C_T'/σ) and rotor power coefficient with test data is presented in Figures 5.1 and 5.2 at advance ratios of 0.2, 0.4, 0.45, 0.5, 0.53, and 0.57. The resulting correlation is good for the basic level of performance but the maximum lift predicted is significantly higher than actually obtained by the model at advance ratios up to 0.45. From μ = 0.50 the maximum lift predicted is approximately the same as test data. A summary of the performance is presented in Figure 5.3 as the maximum lift to effective drag ratio for the model. The prediction is slightly low up to an advance ratio of 0.4 and is slightly high at advance ratios beyond 0.4; but the overall performance prediction capability of SRIBR is acceptable.

The prediction method can be used to scale the test data up to full scale by using full scale airfoil characteristics to define the performance increments from the model predictions and adding them to the test data. Figures 5.4 and 5.5 present the comparison of the full scale and model scale performance, in terms of rotor lift coefficient (C_T'/σ) and rotor power coefficient (Cp/σ), at advance ratios of 0.2, 0.4, 0.45, 0.50, 0.53 and 0.57. There is a slight reduction in rotor power required at the lower levels of rotor lift coefficient at $\mu = 0.20$. As the advance ratio increases, the improvement in rotor power coefficient also becomes greater between full scale and model scale. There is no difference in the maximum lift between the full scale and model scale predictions; therefore the maximum lift defined by model test should be representative of full scale. Utilizing this difference in performance level and the model maximum lift to effective drag ratio, an estimate of the full scale maximum lift to effective drag ratio was defined and is presented in Figure 5.6. The full scale maximum cruise performance is achieved at an advance ratio of 0.4 with an L/DE of 9.8.

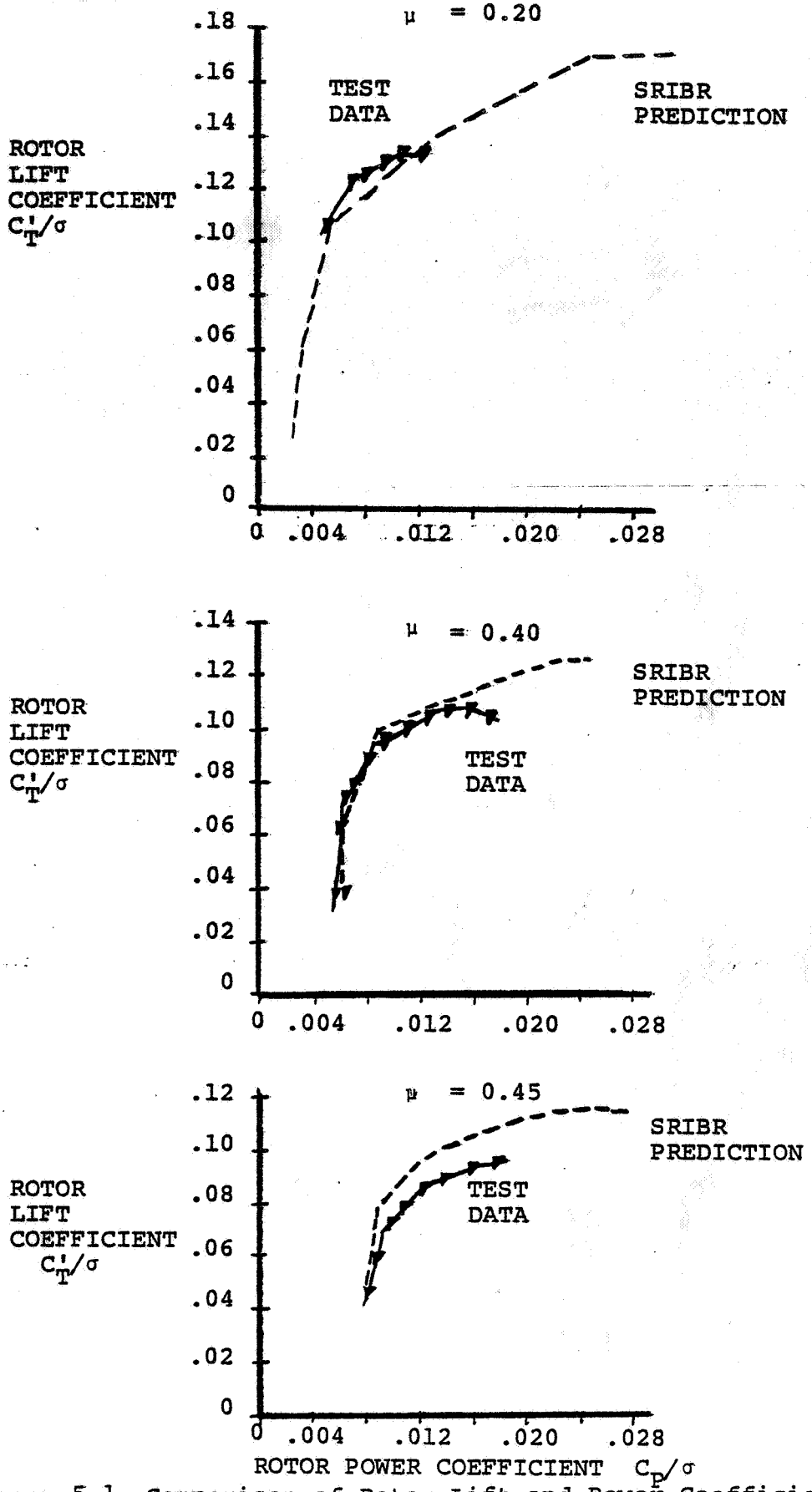

Figure 5.1. Comparison of Rotor Lift and Power Coefficient Prediction with Test Data

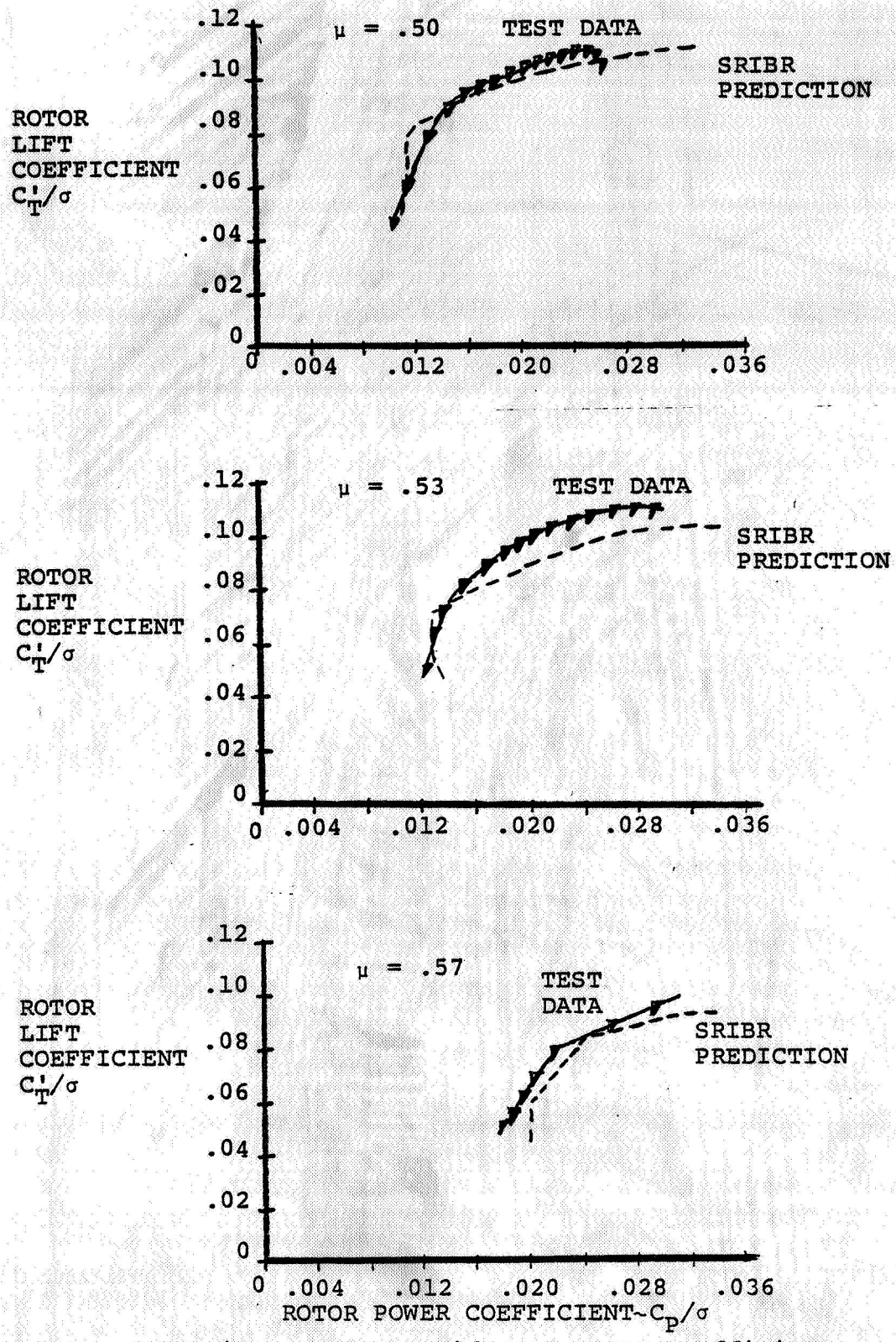

Figure 5.2. Comparison of Rotor Lift and Power Coefficient Prediction with Test Data

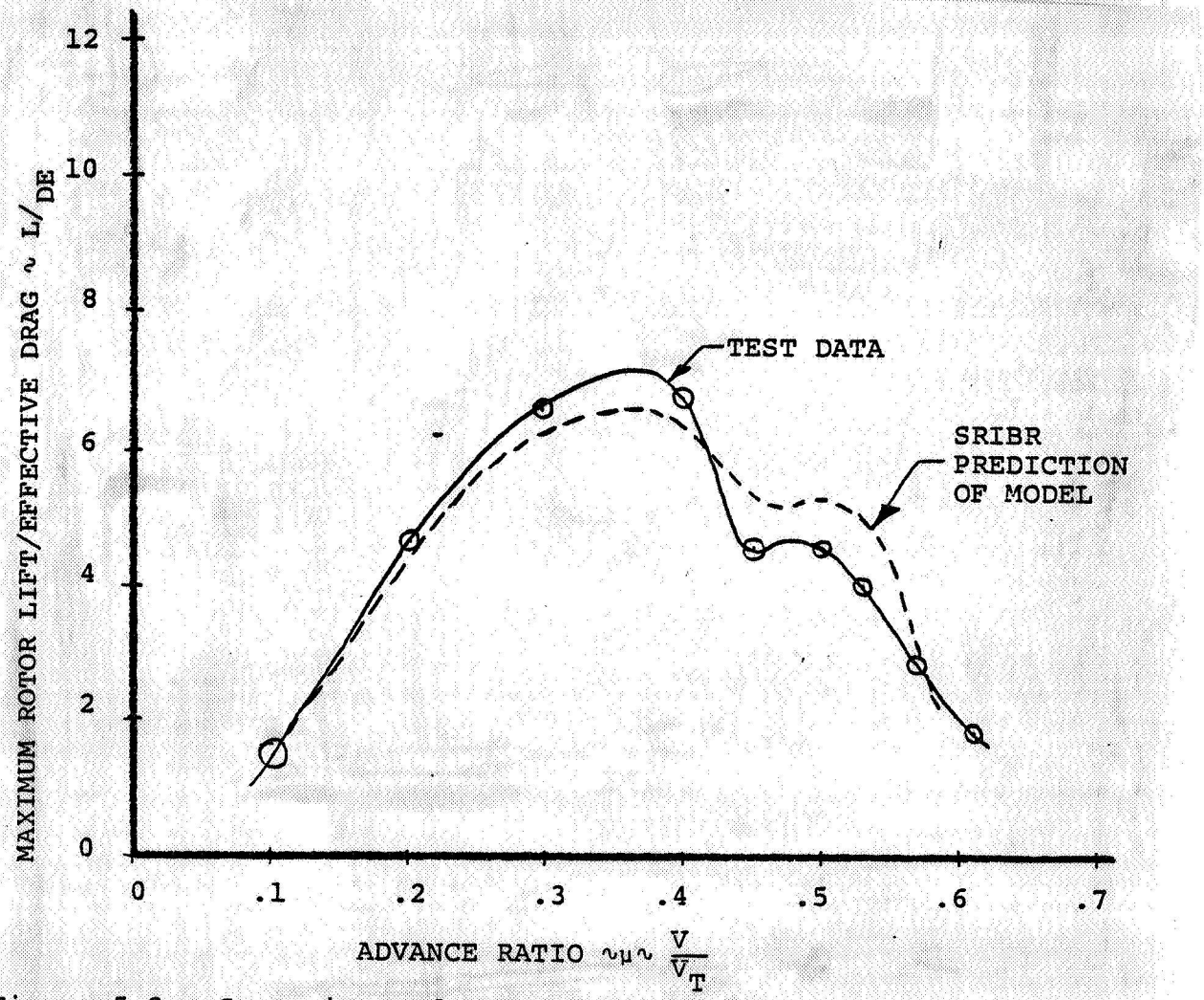

Figure 5.3. Comparison of SRIBR Prediction with Test Data - Maximum Rotor Lift/Effective Drag Ratio

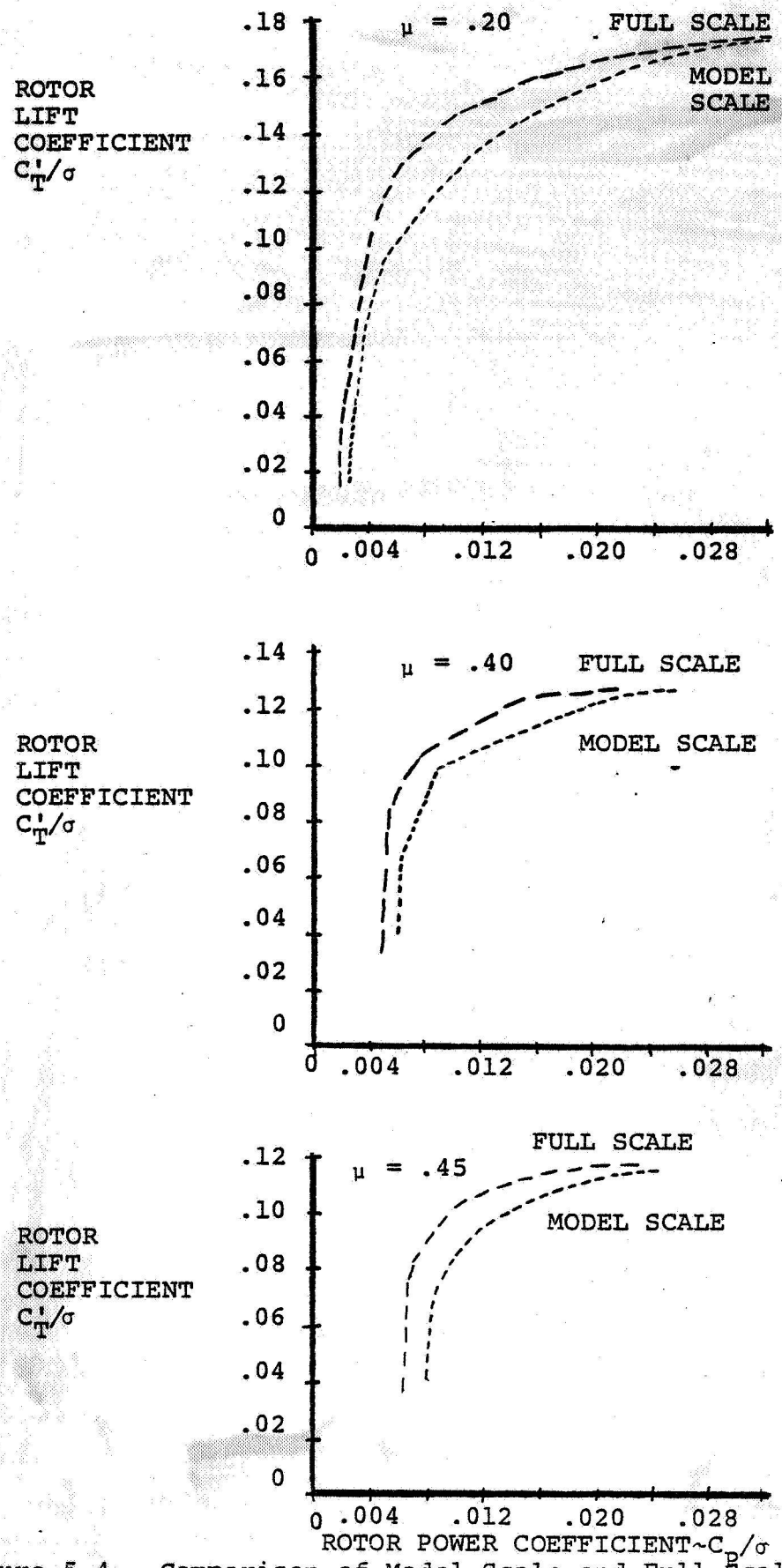

Figure 5.4. Comparison of Model Scale and Full Scale Performance Prediction (μ = .20, .40, and .45)

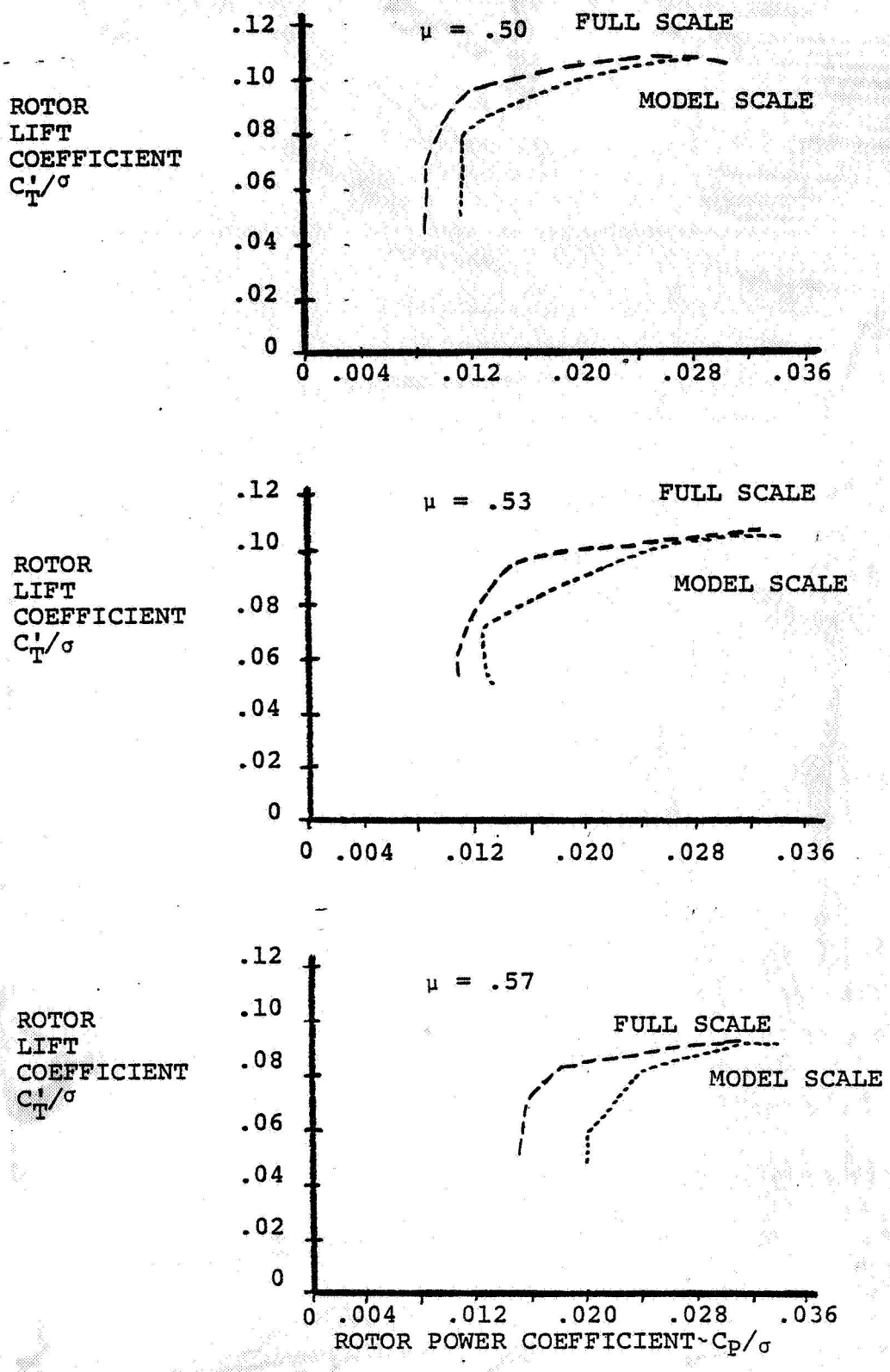

Figure 5.5. Comparison of Model Scale and Full Scale Performance Prediction (μ = .50, .53 and .57)

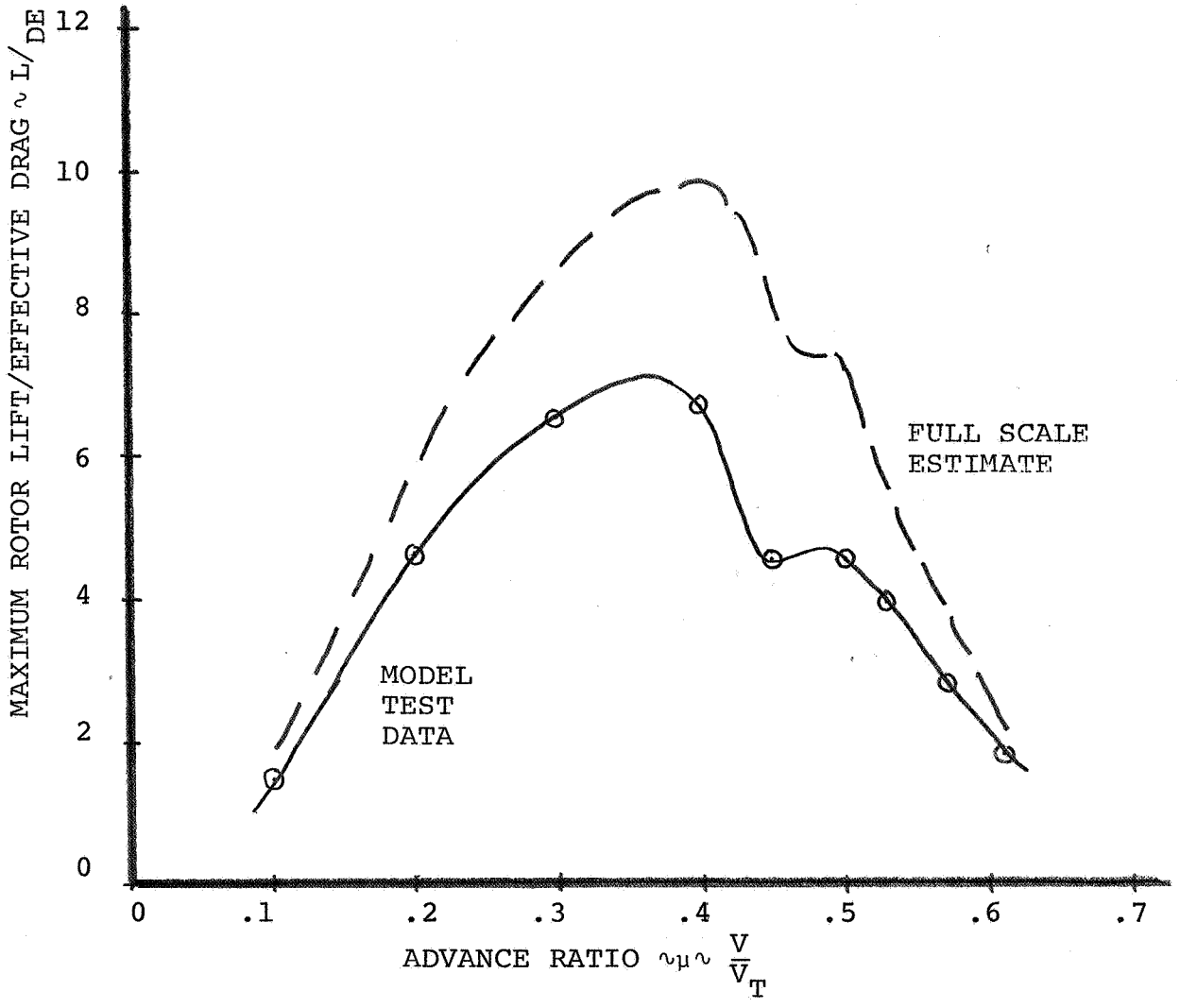

Figure 5.6. Estimated Full Scale Performance and Model Test Data - Maximum Rotor Lift/Effective Drag Ratio

6.0 CONCLUSIONS

1. The Aeroelastic Rotor Analysis Program, C-60, predicts a similar variation in rotor power with thrust at each advance ratio and propulsive force as compared to test data, but underpredicts the level of rotor power.

2. The C-60 analysis adequately predicts the lift limit variation with advance ratio.

3. The midspan flap bending loads correlation is good, while the root and midspan torsion loads correlation is fair.

4. The lift limit is defined by the rotor behavior in the fore and aft region of the rotor disc, particularly by the region of stall around $\psi = 30^{o}$.

5. The region of stall is a result of the nonlinear aerodynamic loading acting on the elastically deformed blade at high lift levels. The high drag loading acts on the downward deflection of the elastic blade to produce a nosedown twist causing the blade to unstall at $\psi = 45^{o}$.

6. The preliminary design performance prediction program, SRIBR, adequately predicts the maximum lift/effective drag ratio.

7.0 RECOMMENDATIONS

Since the lift limit is due to a torsion-flap coupling induced by high drag loads, it is proposed that a means of eliminating or delaying this effect could be investigated by:

1. Tailoring the blade flap stiffness to alter the elastically deflected shape of the blade.
2. Tailoring the blade torsional stiffness to alter the flap-torsion coupling and reduce the induced nosedown twist.
3. Analytically defining the airfoil pitching moment effect to determine its effect on the stall region and experimentally substantiating this.

REFERENCES

1. McHugh, Frank, Clark, Ross and Soloman, Mary, Wind Tunnel Investigation of Rotor Lift and Propulsive Force at High Speed, NASA CR 145217-1, October 1977.

2. LeNard, John M., and Boehler, Gabriel D., Inclusion of Tip Relief in the Prediction of Compressibility Effects on Helicopter Rotor Performance, USAAMRDL TR73-71, December 1973.